UNIVERSITY OF OKLAHOMA

GRADUATE COLLEGE

DESIGN, FABRICATION, AND DEVELOPMENT OF GETE PHASE-CHANGE SWITCHES FOR RECONFIGURABLE RF APPLICATIONS

A DISSERTATION

SUBMITTED TO THE GRADUATE FACULTY

in partial fulfillment of the requirements for the

Degree of

DOCTOR OF PHILOSOPHY

By

NEDA BATHAEI
Norman, Oklahoma
2023

DESIGN, FABRICATION, AND DEVELOPMENT OF GETE PHASE-CHANGE SWITCHES FOR RECONFIGURABLE RF APPLICATIONS

A DISSERTATION APPROVED FOR THE
SCHOOL OF ELECTRICAL AND COMPUTER ENGINEERING

BY THE COMMITTEE CONSISTING OF

Dr. Hjalti Sigmarsson

Dr. Yan Zhang

Dr. Jorge L. Salazar Cerreno

Dr. Binbin Weng

Dr. Bin Wang

© Copyright by NEDA BATHAEI 2023
All Rights Reserved.

This dissertation is dedicated to the hero of my life, my MOTHER,

the memory of my FATHER,

and to all brave Iranian people who fight for FREEDOM!

WOMAN, LIFE, FREEDOM

Acknowledgments

First and foremost, I would like to sincerely thank my research adviser Professor Hjalti Sigmarsson, for his continuous support and patience during my Ph.D. research. His immense knowledge and positive thinking encouraged me even though all hope was lost. He made me a better student, engineer, and human being. I am forever grateful for his guidance.

In addition, I want to express appreciation to the other committee members, Professor Yan Zhang, Professor Jorge Salazar-Cerreño, Professor Binbin Weng, and Professor Bin Wang. They continuously demonstrated a vested interest in my success and provided feedback on my research throughout the project.

I would like to extend my thanks to all my friends who supported me during tough times, Shila Shams, Soren Shams, Delaram Nematollahi, Shahrokh Saeedi, Hadi Saeidi-Manesh, Sattar Atashbahar, Solmaz Shamsadini, Taha Yekan, and for most my partner and my love Mehrdad Arjmandi.

Finally, I would like to thank my mother and sisters, Azita, Anahita, and Aida Bathaei, to whom I greatly miss and owe a lot, for boundless love, encouragement, and sacrifice. None of this work would have been possible without them.

Table of Contents

Acknowledgments **v**

Abstract **xiv**

1 Introduction **1**

1.1 Motivation 1

1.2 Problem Statement 2

1.2.1 Semiconductor-Based Switches 3

1.2.2 MEMS Based Switches 7

1.2.3 Comparison Between Current State-of-the-Art RF Switches 9

1.3 Literature Review 10

1.4 Proposed Research 12

1.5 Contribution 14

1.6 Dissertation Overview 15

2 Chalcogenide Phase Change Material **17**

2.1 History 17

2.2 Phase Change Physics 18

2.3 Literature Review 20

2.3.1 Phase Change Memory 20
2.3.2 Phase Change Switch 22
2.4 Conclusion 23

3 PED Growth Technique of GeTe Thin Film 25
3.1 Motivation 25
3.2 Pulsed Electron-beam Deposition Physics 26
3.3 Pulsed Electron-beam Deposition of GeTe 27
3.3.1 Pulse Energy Measurements 29
3.3.2 Plume Range Measurements 30
3.3.3 Material Composition 34
3.4 XRD Results 36
3.5 Conclusion 37

4 Crystallization Kinetics of GeTe Phase Change Thin Film 40
4.1 Motivation 41
4.2 Post Thermal Annealing Process 41
4.2.1 Furnace Annealing 45
4.2.2 Hot Plate Annealing 50
4.2.3 Annealing Summary 53
4.3 Conclusion 55

5 RF Switch Fabrication and Results 56
5.1 PCM RF Switch Design 56
5.1.1 Direct Heating Switch 57
5.1.2 Indirect Heating Switch 58

5.1.2.1 Device Structure 60
5.2 RF Switch Fabrication 66
5.2.1 Material Deposition 67
5.2.1.1 Heater 67
5.2.1.2 Dielectric 71
5.2.1.3 Phase Change Material 74
5.2.1.4 RF Electrode 76
5.2.1.5 Passivation 77
5.3 Electrical and RF Testing 77
5.4 Device Model 80
5.5 Results and Discussion 85
5.5.1 Circuit Model 87
5.6 Summary 95

6 Conclusions and Future Directions 97
6.1 Conclusions 97
6.2 Future Research Directions 99
6.2.1 Fabrication Process Improvements 99
6.2.2 GeTe Atomistic Structure Analysis 100
6.2.3 PCM RF Switches Enhancement 100

References 102

Appendix A Direct Heating Switch 114

Appendix B List of Acronyms and Abbreviations 118

List of Tables

1.1 Qualitative comparison between some RF switch technologies (from [15]). 10

3.1 PED deposition parameters. 39

4.1 Atomic% ratio of Germanium, Telluride, and Oxygen in four samples handled differently. The remaining percentage is Si, which comes from the substrate. 55

5.1 Dielectric material properties and parameters. 72

5.2 Summary of issues and solutions for the fabricated RF switches. 81

List of Figures

1.1 Physical cross-section of (a) MESFET and (b) CMOS. 5

1.2 Schematic of a stacked-FET switch with resistive gates [13]. . 6

1.3 The two configurations in RF MEMS switches (a) cantilever beam and (b) air bridge [21]. 8

1.4 Insertion loss and isolation performance of current state-of-the-art RF switch technologies [40]. 13

2.1 $Ge_1Sb_xTe_1$ films' (a) resistivity as a function of temperature for heating ramp to 300–450°C at 5°C/min and subsequent cooling back to room temperature, (b) recrystallization times along isoelectronic tie line in the Ge-Sb-Te ternary diagram [41]. 19

2.2 Top: Atomic structure Layouts of GeTe at different states. Smaller red and larger blue spheres represent Ge and Te atoms. Bottom: Temperature profiles of reset and set pulses for chalcogenide phase change materials to achieve phase transitions between the crystalline and amorphous states. 20

2.3 Schematic cross-section of PC memory cell [54]. 21

2.4 Schematic cross-section of (a) Directly heated and (b) Indirectly heated RF switch. 23

3.1 Schematic of the PED system [64]. 27
3.2 Inside the PED chamber. 29
3.3 Growth rate dependence on the applied PEBS at pressure 5.5 mTorr and target-to-substrate distance 8 cm. 31
3.4 Growth rate dependence on the target-to-substrate distance at pressure 5.5 mTorr and PEBS 15 kV. 31
3.5 Top SEM view of GeTe thin films deposited at (a) 3 cm, (b) 5 cm, and (c) 8 cm target-to-substrate distances at pressure 5.5 mTorr and PEBS 15 kV. 32
3.6 Surface roughness as a function of target-to-substrate distance at pressure 5.5 mTorr and PEBS 15 kV. 33
3.7 Top SEM view of GeTe thin films deposited at (a) 15 kV and (b) 17 kV PEBS potentials at pressure 5 mTorr and target-to-substrate distance 8 cm). 34
3.8 Growth rate dependence on the background pressure at PEBS 15 kV and target-to-substrate distance 8 cm. 35
3.9 Germanium and Telluride ratio dependence on the background pressure at PEBS 15 kV and target-to-substrate distance 8 cm). 36
3.10 XRD pattern of the as-deposited GeTe film. 37

4.1 Top row: The RF switch configuration with the initial amorphous PCM thin-film (OFF state). Activation pulse results in the ON state. Bottom row: The ideal configuration, with an initial crystalline thin-film of PCM (ON state). Activation pulse results in the OFF state. The Dash arrow in both cases shows the portion of the PCM layer that needs to transform. . 42
4.2 RTP-1000D4 by MTI rapid thermal annealer. 43
4.3 (a) Normalized XRD spectra, (b) FWHM value and calculated grain size from the crystalline plane (202) as a function of annealing temperature, and (c) resistivity of annealed GeTe films as a function of annealing temperature. 46
4.4 (a) Normalized XRD spectra and (b) resistivity of annealed GeTe films as a function of chamber gas. 48
4.5 Top SEM view of GeTe thin-films (a) as-deposited, annealed at (b) Ar, and (c) forming gas (80%N_2+20%H_2). 49
4.6 The two-probe setup is used to measure the real-time resistance changes on a hot plate. 51
4.7 Measured electrical resistivity ($\mu\Omega$·m) of GeTe while heating from hot plate to approximately 250°C. 52
4.8 Top SEM view of GeTe thin-films annealed at air (hot plate) and related elements' atomic percentage. 54

5.1 Direct heating switch design (a) cross-section view, (b) top view, and (c) fabricated switch. 59
5.2 Order of layers to fabricate PCM switch (from bottom to top). 60

5.3 Two RF switch structures were designed (left), and the top view of the fabricated switches (right). 61
5.4 A 3D view of the designed RF switch. 62
5.5 (a) and (b) show the RF switch relation to the heater width. (c) and (d) display the RF gap impact on the RF performance. 63
5.6 (a) Wide RF gap design, (b) fabricated switch with wide RF gap, (c) narrow RF gap design, and (d) fabricated switch with narrow RF gap. 64
5.7 Simulated insertion loss of the switch in the (a) ON-state and (b) OFF state for different RF gap and GeTe thicknesses. . . . 66
5.8 Fabrication process flow of the PCM RF switch, deposition and patterning of (a) heater layer, (b) dielectric layer, (c) PCM (GeTe) layer, (d) RF electrodes layer, (e) passivation layer, and (f) metal contacts layer. 68
5.9 RF switch with NiCr heater melted and deformed after applying reset pulse. 69
5.10 XRD results for W thin films deposited at different power and pressure and after annealing at 850°C for 1 hour. 71
5.11 Top SEM view of AlN thin films deposited by (a) PED and (b) DC sputtering. 73
5.12 (a) Top view of the switch before testing, (b) oxidized GeTe after pulse applied. 77
5.13 RF measurement setup. 78
5.14 Switch with DC and RF probes are connected under the test. . 79
5.15 Indirect heating switch actuation circuit diagram. 80

5.16 Structures and two-port network models of the (a) GeTe switch, (b) open, and (c) short circuit. 83
5.17 Measured, simulated, and de-embedded the GeTe RF switch (a) insertion loss at the ON state and (b) isolation at the OFF state. 88
5.18 Schematic of the GeTe switch and lumped-element model (a) cross-section, (b) top view. 89
5.19 Equivalent lumped-element model of a GeTe switch in the (a) ON state, (b) OFF state. 90
5.20 Measured and the model RF responses of the GeTe RF switch (a) reflection coefficient (S11) and (b) insertion loss (S21) in the ON state. 92
5.21 Measured and equivalent model RF response of the GeTe RF switch (a) reflection coefficient (S11) and (b) insertion loss (S21) at the OFF-state. 94
5.22 Switch schematic in (a) the initial state GeTe poly-crystalline, (b) GeTe amorphous in the RF gap after applying reset pulse. 96

A.1 Direct heating switch design (a) top view, (b) cross-section, and fabricated switch (c) after RF electrodes fab, and (d) finished fab. 115
A.2 Direct heating switch actuation circuit. 116
A.3 Direct heating switch RF results. 117

Abstract

This research is devoted to studying the chalcogenide phase change material (PCM) properties and their potential capability in RF switching applications. The goal of RF switches would be to realize the reconfigurability and adaptability of RF and microwave systems. The current RF switches are primarily based on solid-state and, more recently, micro-mechanical technologies. Each has limitations like integration compatibility, cost, reliability, or power handling. In the beginning, PCM was employed almost exclusively in non-volatile memory usage. However, PCMs exhibit properties that can improve the current state-of-the-art RF switches, like high contrast between electric conductivity in their two stable states. This means switches with low loss and high isolation subsequently translate to high cutoff frequency (f_{CO}). Another feature that is very suitable for RF systems is PCM switches' very low power consumption. They require power only during state changes and can keep their state since both crystalline and amorphous phases are stable at room temperature. Among all chalcogenide PCM compounds, germanium telluride (GeTe) has features like fast switching speed and low resistivity in the crystalline state, which makes it the best candidate for RF applications.

This work presents the study of GeTe growth, crystallization, and design of RF switches utilizing it. A novel, physical vapor deposition (PVD) method

called pulse electron-beam deposition (PED) was experimentally studied to investigate the requirements for the ablation of GeTe. It will be discussed that the as-grown GeTe is amorphous and why the initial crystalline state is preferred. In order to convert the GeTe thin film into a crystalline formation, post-treatment annealing was performed. To optimize the post-annealing procedure, several annealing parameters were experimentally investigated. The thin film resistivity dropped by six orders of magnitude upon the crystallization process. The crystallized GeTe thin films were investigated by contemplating the crystallite quality and the electrical conductivity performance. In the following, the design and fabrication of RF ohmic switches, as well as the challenges and solutions, are discussed in detail. Also, PCM-based RF switches are modeled to perceive their behavior better.

Chapter 1

Introduction

1.1 Motivation

Wireless communication is a familiar concept, and most people encounter it daily. Our lives widely depend on data transition between our phones, computers, cars, and household appliances utilizing wireless communication. Wireless communication systems employ radio frequency (RF) modules to transmit and receive wireless data. The coexistence of diverse wireless communication standards resulted in frequency-band switching is usually needed in RF front ends. The future of microwave systems, such as wireless communications and radar systems, requires added reconfigurability to operate in an ever-crowded spectrum and dynamic spectral environments. This means the RF front-end hardware must be configured to operate at multiple frequencies and possibly with multiple functionalities. Particularly tunable filters, antennas, amplifiers, and matching networks are required for the operation of RF systems. One approach to reconfigurability is using RF switches to select between specified circuit blocks. Employing tunable elements and switches enable the reconfigurability of RF circuits. Microwave switches are

critical components that provide the ability of RF modules to accommodate multiple frequencies and functionalities.

Utilizing a high-frequency switch enables the reconfigurability of RF circuits to overcome a limited-frequency spectrum. State-of-the-art switches in current RF systems are almost exclusively silicon-based [1], [2]. Solid-state-based RF switches have been developed utilizing different semiconductor strategies such as silicon on insulator (SOI) [3], or gallium arsenide (GaAs) based integrated circuitry [4]. Nonetheless, these strategies have limitations, like needing a constant power supply to maintain a state. One category of chalcogenide materials proposes opposite electrical and optical properties in each of their stable phases. This group of materials, which is called Phase change materials (PCM), have been used in the memory industry based on their optical features and recently interested the RF community in using them based on electrical properties in high-frequency systems [5]. The advantage of the PCM-based switch over its silicon counterparts is that it does not require external power to maintain any of its states. Power is only needed during the transition from one phase to another. In addition, PCM switches offer lower loss, essential for realizing the next generation of RF and wireless systems.

1.2 Problem Statement

In a multi-band system, RF switches are commonly used to select between the transmitter and receiver modules or for band selection. Therefore, RF switches are essential in wireless RF modules, and the system performance

depends on their efficiency. The essential RF switches' qualifications are low signal transmission in the ON state and high isolation in the OFF state. Other demands are high switching speed and high power handling. Switching speed expresses how fast the state of the switch can be changed. Power handling capability indicates the RF power level the switch can carry out without degrading its performance. In addition to those performance criteria, ease of fabrication and integration compatibility of RF switches in RF circuits and modules implies the simplicity and cost of fabrication, which are essential. The two primary categories of RF switches are solid-state and electromechanical. Some of the most utilized solid-state switching technologies in the RF/microwave industry were recounted and compared in section 1.2.1. These switches suffer from nonlinearity and leakage. On the other hand, electromechanical technology, introduced in section 1.2.2, offers good RF performance, but it is bulky and not compatible with integration [6]. The following sections present a close look at each dominant technology and its associated constraints.

1.2.1 Semiconductor-Based Switches

Switching components mostly rely on solid-state technology and are divided into three general categories: PIN diodes, field-effect transistors (FET), and hybrid (FET and PIN diode) switches. The two-terminal PIN diode is typically less expensive and complected than transistors. From the 1950s, they were the most used in the early stage of switching devices. They can handle high power levels but require an elaborate biasing network and consume relatively high DC power [7]. Also, PIN diodes' bandwidth is narrower com-

pared to transistors' due to their biasing circuitry. PIN diodes are available in Si [8], GaAs [9], and gallium nitride (GaN) [10] technologies. As a two-terminal device, the RF and programming signals share the same path in a PIN diode. The other drawback of PIN diode in RF switching applications is they need a constant current while the switch is ON. These narrowed down their use in this application.

Field effect transistors are one of the most developed solid-state-based RF switches. It is due to their fabrication compatibility with semiconductor-based components [11]. They operate in the passive mode, and control voltage is applied through the gate terminal, which is isolated from the RF path. So, unlike PIN diodes, FET switches do not need an expensive high-performance RF choke. Also, FET switches are voltage-controlled devices, so they consume less current compared to PIN diode switches.

FET application in microwave devices has been substantially improved since the 1970s, and various switches based on FET technology have been designed and implemented for microwave applications. The two types of FET transistors primarily utilized in the switching industry are metal oxide semiconductor field effect transistors (MOSFETs) and metal-semiconductor field effect transistors (MESFETs) [12]. MESFETs are commonly fabricated in GaAs and GaN technologies, while CMOS are mostly silicon-based. Figure 1.1 shows a cross-section view of a switching MESFET and n-type complementary MOS (CMOS). Silicon-based analog devices are prevalent, so CMOS RF switches are privileged due to the lower cost of integration and assembly. However, standard CMOS switches suffer from coupling, high insertion loss, and low isolation due to a low-resistive substrate, and break-

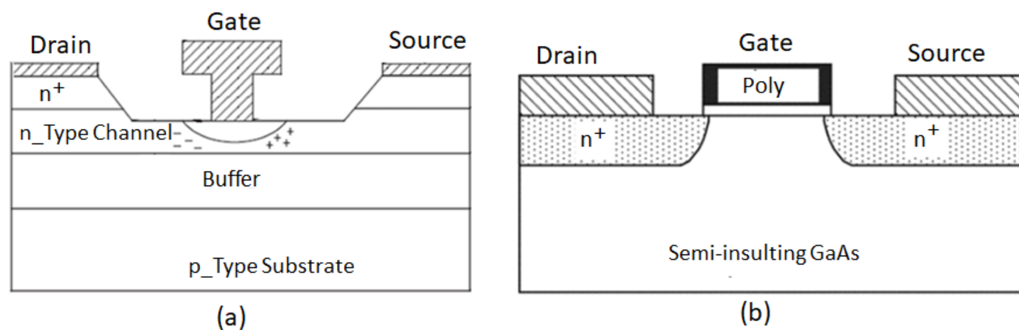

Figure 1.1: Physical cross-section of (a) MESFET and (b) CMOS.

down voltage is typically low. These reasons were used to prevent CMOS from using in high-frequency applications. However, it has been overcome by altering the base silicon substrate with a high-insulating one. Silicon-on-sapphire (SOS) and, more recently, Silicon-on-insulator (SOI) are two technologies that were implemented in RF and microwave applications by exchanging a low resistive substrate for a high resistive one and enhancing the loss and isolation [7]. In SOS technology, a thin layer of silicon epitaxially grown on top of a sapphire (Al_2O_3) substrate. Compared to standard silicon, SOS technology provides less parasitic capacitances by reducing the substrate conductivity [2]. On the other hand, SOI is the technology with a similar approach to increase substrate insulation, but it is more compatible with RF integrated circuits. SOI has a buried oxide layer on a silicon wafer, which facilitates reducing parasitic capacitances and improving the cut-off frequency by improving the substrate insulation. Low breakdown voltage is a common issue with all Si, SOS, and SOI FET switches. The standard method to overcome this limitation is stacking multiple FET devices in series to distribute the voltage across the FETs, and a higher voltage can be han-

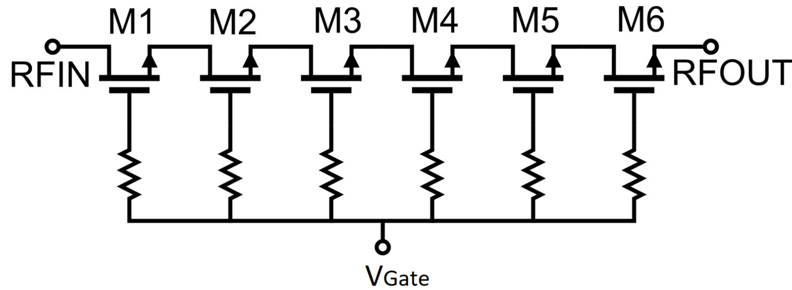

Figure 1.2: Schematic of a stacked-FET switch with resistive gates [13].

dled [2], [13]. Figure 1.2 shows a structure with six FET switches stacked in series. The specified applied power determines the number of stacked switches. While the breakdown issue under a high level of power is solved by this method, another trouble of non-linearity would be initiated. In a structure of multiple stacked FET switches, the current leakage causes an unbalanced current to flow through each device, resulting in an unbalanced distributed voltage across each device [14].

HEMT, which stands for high electron mobility transistor, has a structure close to the FET transistor with some differences. The channel is narrower, and rather than a doped region, it integrates a junction between two materials with different band gaps (heterojunction). The GaN HEMT has excellent performance for high-power, high-voltage applications at millimeter-wave frequencies [15]. GaN HEMTs are available on sapphire, silicon, and SiC, while the last one exhibits some benefits over others, like high thermal conductivity and high electrical resistivity, which enable SiC-based GaN HEMTs to deal with significantly high power signals that devices on GaAs or Si cannot tolerate [16].

Microwave switches based on GaAs are one of the popular approaches be-

cause of their low bias power and high power handling [17]. They have been the primary technology used since the 1980s owing to the feasibility of monolithic microwave integrated circuit (MMIC) circuits [15]. However, GaAs FET switches in RF/microwave applications have some constraints like high level of distortion [18]. So, they have been replaced by another version of GaAs-based switches called pseudomorphic high electron mobility transistors (pHEMTs). The critical advantages of pHEMTs are utilizing material with lower electrical resistivity, leading to lower ON resistance. Also, they have smaller OFF capacitance due to their optimized gate configurations and high resistivity substrate. The main drawback of HEMTs and pHEMTs switches is they need their own fabrication process, and to be employed in CMOS RF systems requires heterogeneous integration. This process is costly and contradicts their advantages.

1.2.2 MEMS Based Switches

Micro-electromechanical systems (MEMS) switches employ mechanical contacts as the switching mechanism and are an alternative procedure to overcome the issues like power handling and linearity associated with solid-state switches; however, they are bulky and not a good choice for integration [19]. There were concerns about their reliability in the first stages of MEMS in RF switching applications, but the next generations could overcome those limitations and become very reliable [7]. MEMS switches utilize a mechanical element, usually a cantilever beam or a bridge, that makes electrical contact and realizes switching [20], [21]. Figure 1.3 illustrates the two main structures of RF MEMS-based switches. Due to the metal connection or sep-

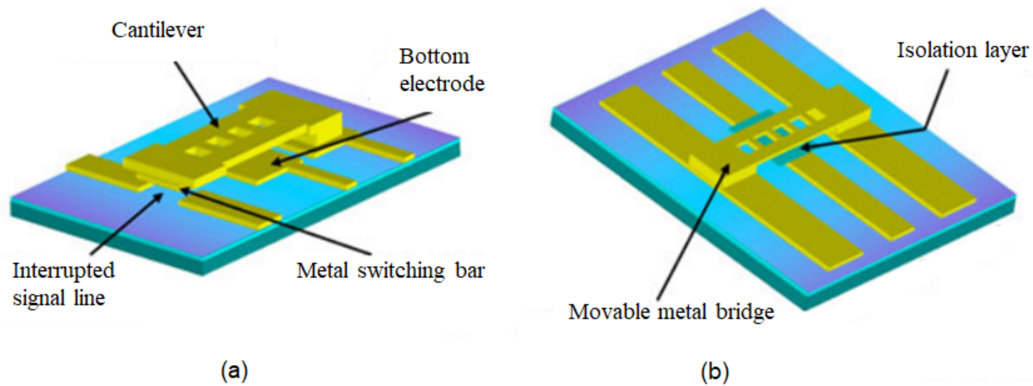

Figure 1.3: The two configurations in RF MEMS switches (a) cantilever beam and (b) air bridge [21].

aration, MEMS switches show very low insertion loss in the on state and a high isolation level in the off state. The applied DC bias generates the required electrostatic force to move the cantilever or bridge and achieve switching. In the absence of this DC bias, the moving element separates and turns the MEMS switch off [22]. As a result, MEMS switches demand large DC voltages to actuate the mechanical lever, typically 20-80 volt [23]. Other disadvantages of a MEMS switch are their complicated and non-compatible fabrication process with other RF components in the system and their considerably large sizes, typically a few hundred microns, which is much larger than a solid-state diode or transistor [24]. MEMS switches have been the significant technologies used in RF applications in the past decade. However, concerns like power consumption, switching speed, and size have led to research on the next generation of RF switches [25].

1.2.3 Comparison Between Current State-of-the-Art RF Switches

All the technologies discussed here and more are provided by various commercial foundries. The main criteria that are highly considered in RF switching performances are:

- Transmission and isolation,
- switching speed,
- power handling,
- actuation and power consumption, and
- integration and packaging compatibility.

Semiconductor-based RF switch technologies are compatible with other front-end RF modules, and their fabrication is relatively low-cost. Still, suffer from low power handling, high transmission loss at mmWave frequencies, and unsatisfactory linearity [26]. FET-based RF switches (CMOS, HEMT, pHEMT) are voltage-controlled devices and require simple actuation circuits. On the other hand, PIN diodes are current-controlled and involve a more completed actuation circuit which increases power consumption. While MEMS RF switches have excellent RF performances, their size and power consumption limit their applications. Also, considering their micro membrane mechanical movement, MEMS-based components' reliability degrades over time [19]. A qualitative comparison between popular RF switch technologies is provided in Table 1.1. All these indicate that the next gener-

Table 1.1: Qualitative comparison between some RF switch technologies (from [15]).

Technology	**Si PIN Diode**	**GaAs PIN Diode**	**GaAs pHEMT**	**GaN/SiC HEMT**	**CMOS**	**MEMS**
Insertion loss	*Low*	*Moderate*	*Moderate*	*Moderate*	*High*	*Low*
Isolation	*Good*	*Good*	*Excellent*	*Good*	*Good*	*Excellent*
Power handling	*Very high*	*Moderate*	*Moderate*	*High*	*Low*	*High*
Switching speed	*Low*	*High*	*Very high*	*High*	*High*	*Low*
Power consumption	*High*	*High*	*Low*	*Moderate*	*Low*	*Very high*
Integration capability	*Limited*	*Good*	*Good*	*Good*	*Excellent*	*Limited*
Size	*Large*	*Small*	*Small*	*Very small*	*Very small*	*Very large*

ation of RF switch technology is necessary for the high demand for reconfigurability in RF systems.

1.3 Literature Review

As discussed, solid state-based switches have been the most used type in RF applications. However, based on Moore's law, the number of transistors on integrated circuits (IC) would be doubled relatively every two years. It has been true in the last decades. However, by physically reaching the limits of transistor miniaturization physically, it is becoming harder to follow Moore's law. As a result, the inventions of new devices and materials for

switching applications have become more and more demanding [11], [27]. Devices based on PCM and metal-insulator transition (MIT) are two candidates that show reassuring properties in RF and millimeter-wave (mmWave) applications [28], [29]. Vanadium dioxide (VO_2) is an MIT material that has been utilized in RF switching from DC to 280 GHz with superior performance [30]. Also, VO2-based RF switches have been reported in tunable filters [31], [32] and reconfigurable antenna [33]. The main constraint that limits the VO_2 application is its low transition temperature (68°C). In commercial and high RF power applications, the temperature can potentially pass 68°C transition point, and self-actuation happens.

Another promising technology to the RF community is the PCM-based switch, which offers excellent high-frequency electrical properties [5], [34]. Phase change materials are chalcogenide compounds with two stable phases at room temperature, crystalline and amorphous. The transformation from one phase to another is realized through thermal actuation. The most significant difference between these two phases is their electrical resistivity, which makes PCM an exciting element for switching applications. The chalcogenide materials consist of compounds from germanium (Ge), tellurium (Te), and/or antimony (Sb), sometimes with doping elements like indium (In), selenium (Se), etc. Germanium telluride (GeTe) is one of the most exciting chalcogenides family due to its fast crystallization speed [35] and low electrical resistivity in the crystalline state [36], [37]. Furthermore, GeTe exhibits a significant resistivity difference, a factor of 10^6, between its two stable phases [38], [39]. These features make GeTe highly desirable for RF switching applications. RF switches are evaluated based on the low inser-

tion loss in the ON-state and high rejection in the OFF-state [25], which translates to low electrical resistivity in crystalline and high electrical resistivity in amorphous phases, respectively. The insertion loss and isolation of some of the recently reported solid-state, and MEMS RF switches are compared with the PCM-based switch in Figure 1.4. The PCM switch performs better in both states than its counterparts regarding lower insertion loss and wider operation frequency.

The quality of PCM plays an important role in the performance of PCM-based RF switches, and growing high-quality PCM is a prerequisite for their applications in RF systems. The reported GeTe-based RF switches are mostly prepared by sputtering deposition technique [41], [42]. The current techniques for deposition PCM have some constraints like complications, low growth rate, range of material that can be deposited, and cost. A novel growing technique for PCM thin films would be pulsed electron-beam deposition (PED). PED shows the capability to overcome the limitations of the ongoing deposition methods for PCM and result in a high-quality PCM thin film. PED was successfully established to grow materials like GaN [43], CeO_2 [44], SnO_2 [45], ZnO [46], and complex oxides [47].

1.4 Proposed Research

Properties of the GeTe, like the resistivity, crystallization temperature, and crystallization speed, highly depend on its deposition method and conditions. This dissertation is devoted to GeTe-based switches development utilizing a novel growth technique of PCM. The main application of the grown

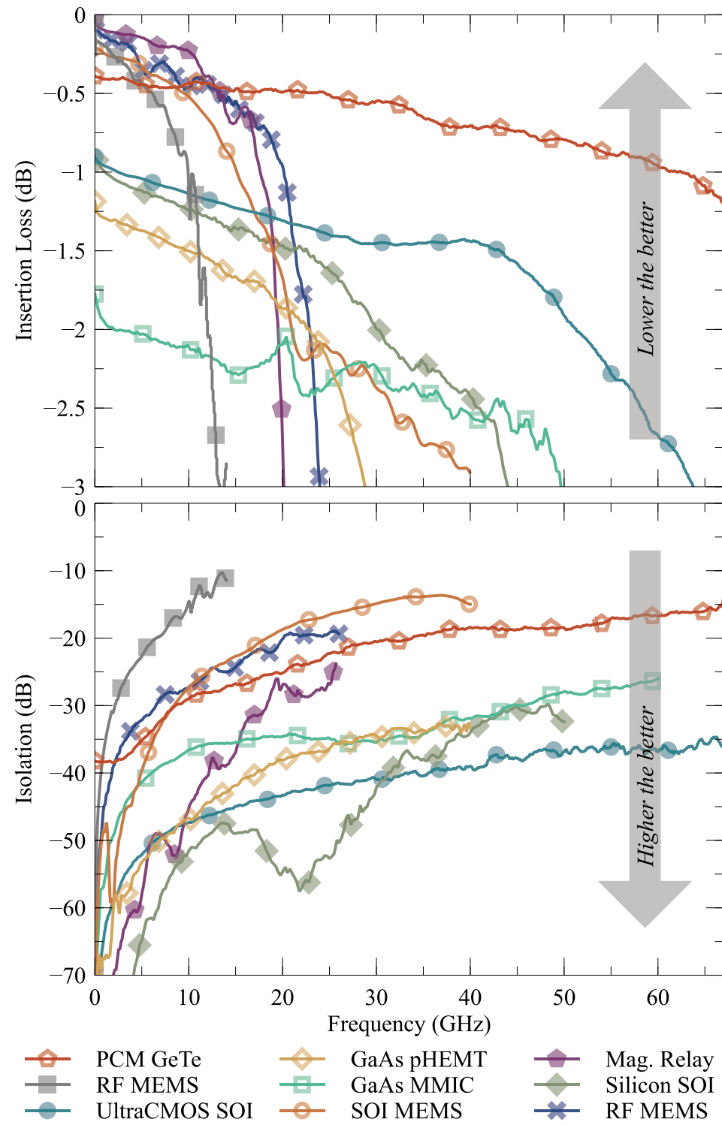

Figure 1.4: Insertion loss and isolation performance of current state-of-the-art RF switch technologies [40].

GeTe thin films studied in this research is reconfigurable RF and microwave applications. Different perspectives have been discussed, including the GeTe properties, the novel technique to grow PCM, and RF switches based on GeTe. Utilizing PED as a physical deposition method, which will be deliberated in Chapter 3, has the advantage of controlling the atomic structure of the grown material. This supervision of the GeTe thin film features gives the ability to manipulate the electrical properties of the deposited material in favor of the RF switching requirements. The current deposition techniques of GeTe, which have been used for RF switch fabrication, do not offer this ability. In order to acquire the PED ability, lots of development efforts were carried out to realize the relationship between elemental GeTe properties and its electrical properties in high-frequency applications. The GeTe performance in the RF switch application highly depends on the thin-film deposition method and conditions. This research focuses on developing the PED to control the GeTe crystal structure and improve the efficiency of RF switches.

1.5 Contribution

The primary goal of this study is to demonstrate the capability of the PED method for growing complex composite thin-film materials like PCM. The first experimental study using PED to grow chalcogenide materials has been reported in this research. GeTe thin film, the most motivating PCM in high-frequency applications, is targeted to demonstrate the PED capabilities. The following detailed contributions are determined based on the proposed research:

1. The growth parameters of PCM thin film using PED are investigated to find the efficient conditions which result in a high-quality PCM thin film with a smooth surface and a specific atomic ratio, which are required for employing PCM in RF and microwave applications. The optimization of microfabrication technique parameters is essential to enhance the RF performance of the switch.

2. A crystallization procedure is accomplished on the amorphous as-grown GeTe thin film. The crystallization parameters are characterized to achieve a high contrast resistivity ($R_{Amorphous}/R_{crystalline}$ ratio) which translates to high isolation to the insertion loss of the RF switch in the OFF and ON states.

3. An RF switch based on the deposited GeTe thin film is designed and fabricated. The design other than the GeTe layer contains different layers to provide the required functions, including thermal, isolation, and RF signal carrying. The material properties, as well as the pattern and dimensions of each layer, are studied and optimized to improve the RF switch performance.

The reported PCM-based RF switch is the first demonstration of utilizing the PED technique to grow PCM thin film and contributes to a better perception of the developed RF switch.

1.6 Dissertation Overview

Following, the structure of each chapter is introduced briefly. In Chapter 1,

introduction, The current RF switch technologies and their limitations have been introduced, and the background of PCM and the motivation for developing novel RF switches using PCM are discussed. This chapter covers the literature review and the structure of the dissertation. Following the Introduction, Chapter 2 provides an overview of the chalcogenide phase change materials concept and the differences between each state (amorphous versus crystalline). Phase transitions between amorphous and crystalline and the history of PCM in RF switching applications have discoursed in this chapter. Chapter 3 discusses the novel deposition technique called PED to grow GeTe thin film. The advantages of utilizing this technique for PCM over the other deposition techniques and The optimization process of PED for high-quality thin-film PCM have been deliberated with details. Chapter 4 first discusses why pre-crystallization of GeTe material in RF switches application is critical. Then the annealing parameters required for a high-quality crystalline are described. Chapter 5 debates PCM-based RF switches and their structure. The design procedure, fabrication process, principle of operation, and performance evaluation are discussed in detail. Chapter 6 concludes all the research and experiment results and suggests possible applications for PCM as the direction of future research in this field.

Chapter 2

Chalcogenide Phase Change Material

Phase-change materials have been attracting significant attention due to the possibility of substantially changing their electrical and optical properties. PCMs relate to the chalcogenide compounds family that have two stable states at room temperature, crystalline and amorphous. The PCM can be repeatedly switched between these two phases and behave oppositely in both electrical and optical manners. Reversed behavior derives from structural contrast in the disciplined crystalline and disordered amorphous states.

2.1 History

In 1968, the first report on phase change material claimed that a special category of materials could change resistance drastically by applying an electric field [48]. Phase change material was first used commercially in the 1990s for digital information storage, exploiting the material's optical reflectivity difference between the amorphous and crystalline phase [49], [50]. Ever since the first article on PCM-based memory was published, researchers in this field have actively been working to discover new series of PCM materi-

als and new ways to use their bi-stable characteristics for memory applications. Another noteworthy difference between the two states of PCM is the considerable change in electrical resistivity, which can be several orders of magnitude. In the last couple of years, a new exciting application of PCM, low-loss and low-power switching, has been investigated [38], [51].

2.2 Phase Change Physics

An interesting type of PCM is GST or GeSbTe family. GST identifies chalcogenide materials combining Ge, Sb, and Te. Typically $Ge_xSb_yTe_z$ with various numbers or percentages of (x, y, z) represent the compound formula, and they dominate most electronics applications due to their high contrast between each state and speed of switching between those states. Among all GST families, $Ge_1Sb_xTe_1$ (x<1) has the lowest resistivity, which is critical for RF switch and defines the loss in the ON state. Figure 2.1(a) shows the resistivity versus temperature for five different x values. As can be seen, GeTe (x=0) has the lowest resistivity and crystallization temperature, and both of them increase with Sb incorporation. The other factor that plays an essential role in PCM application is how quickly it can be recrystallized. The re-crystallization time for some $Ge_1Sb_xTe_1$ compositions is specified in Figure 2.1(b). The fastest re-crystallization times belong to those with a high level of Sb (6 in this case) or nothing Sb, or pure GeTe [41].

The PCM in the amorphous state has low optical reflectivity and high electrical resistivity, which function close to a semiconductor or dielectric. The GeTe in an amorphous state can be considered as a p-type semiconductor

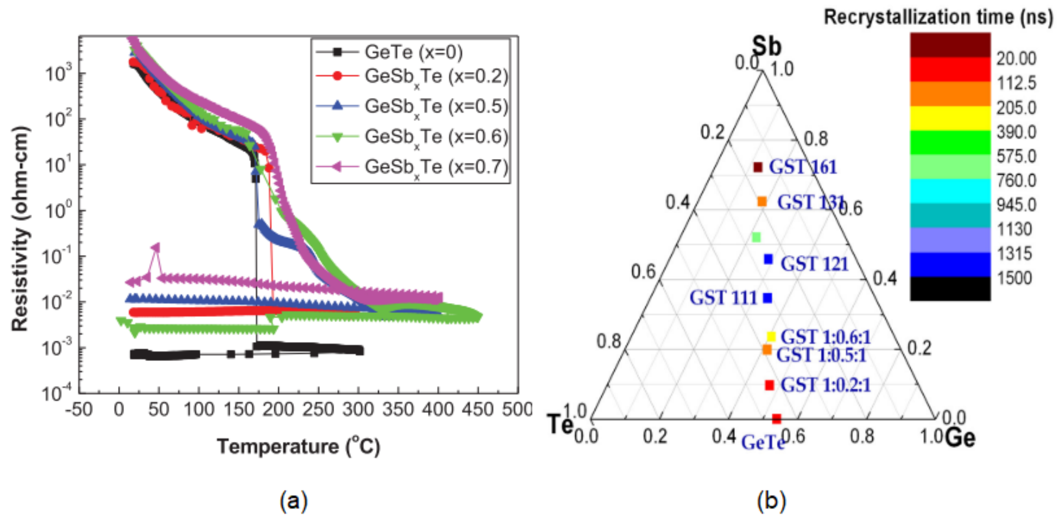

Figure 2.1: $Ge_1Sb_xTe_1$ films' (a) resistivity as a function of temperature for heating ramp to 300–450°C at 5°C/min and subsequent cooling back to room temperature, (b) recrystallization times along isoelectronic tie line in the Ge-Sb-Te ternary diagram [41].

with a bandgap energy of 0.8 eV. Nevertheless, in the crystalline state behaves very similarly to a metal with a narrow band-gap (∼0.1–0.2 eV) [52]. The transformation between amorphous and crystalline states is accomplished by specific heating profiles; above crystallization temperature and beyond melting temperature. Figure 2.2 shows an example of the two stable states as well as melted and glass transition states. The high rate of electric or laser pulses (based on the application) can provide the required heat for the transformation. A slower cooling profile lets atoms form in a crystalline structure (SET pulse). On the other hand, rapid heating and quenching result in atoms forming a disorganized amorphous structure (RESET pulse).

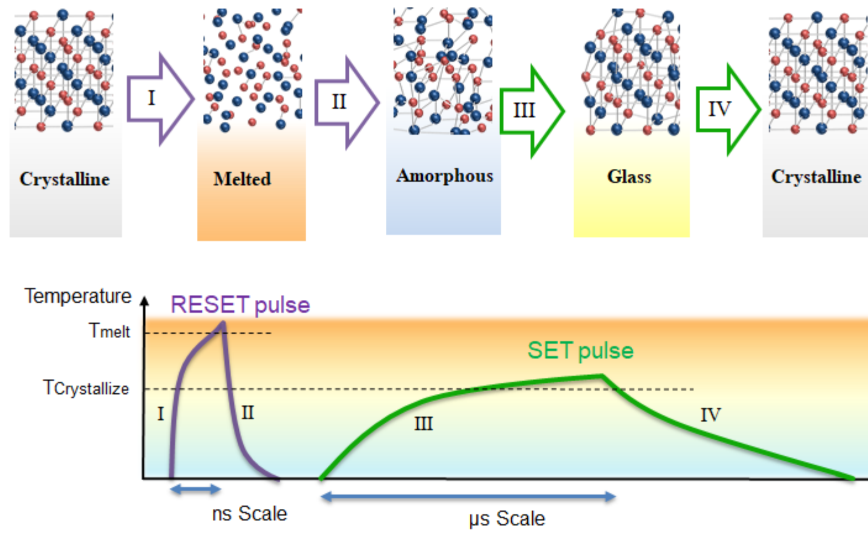

Figure 2.2: Top: Atomic structure Layouts of GeTe at different states. Smaller red and larger blue spheres represent Ge and Te atoms.
Bottom: Temperature profiles of reset and set pulses for chalcogenide phase change materials to achieve phase transitions between the crystalline and amorphous states.

2.3 Literature Review

PCM is a class of materials in which the transitioning back and forth between crystalline and amorphous states is possible with heating pulses. These two states offer a high contrast in optical reflectivity and electrical conductivity. The memory industry has utilized the former for making non-volatile memories, and the latter enables low-loss and low-power switching in radio frequency (RF) applications.

2.3.1 Phase Change Memory

The contrast in reflectivity between the amorphous and crystalline states is employed to store bits of data as 1 or 0. In 1986, thin films of Te-Ge-Sn-

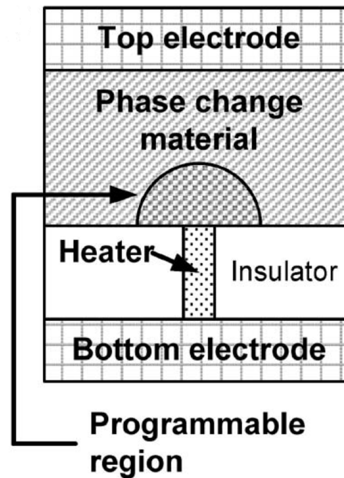

Figure 2.3: Schematic cross-section of PC memory cell [54].

Au exhibited use in rewritable memory applications [53]. Optical memory cells exploit the high reflectivity difference in two states of PCM to store data. To amorphize the PCM, a fast pulse is utilized. On the other hand, a longer, lower power pulse is served to crystalize the PCM. The type of accusation pulses can be either laser or electric current. Figure 2.3 shows the schematic cross-section of a PCM mushroom memory cell, which uses the electric current. The PCM, sandwiched between the top electrode and heater, switches between the two states by crowding the current at the heater. Passing through PCM results in a programmed region illustrated by the mushroom boundary [54]. In the case of laser operation, laser pulses' energy is used to create amorphous spots in the PCM for use in RW-DVDs [55]. To provide the appropriate heat to melt/quench by 0.2 μs, 6 mW or recrystallization using a 1 μs, 2 mW laser pulses.

2.3.2 Phase Change Switch

The noteworthy change in electrical resistivity in the two stable states of chalcogenides material, which can be several orders of magnitude, facilitated the switching application. The low-loss and low-power PCM switches have been investigated in the last decade [38], [51]. The exciting property of PCM, which makes them suitable for switching applications, is the inherent non-volatility of the material. This implies that they can retain their state till hit by external energy. As a result, contrary to a semiconductor switch, no power is required to hold the current state. The heating profile to turn the device OFF/ON (RESET/SET) is shown in Figure 2.2(b).

There are two configurations of PCM switches based on the ways of applying the electrical pulse to generate the required heat:

- Directly heated
- Indirectly heated

Both have four terminals, two for the RF signal and two for the actuation current. The difference is for the directly heated switch, the current passes through the PCM region, while for indirectly heated, there is a dielectric layer that serves as an insulator between RF and thermal actuation signals. Figure 2.4(a) and (b) illustrate the cross-sectional schematic of directly and indirectly heated, respectively. There is a lateral RF signal path connected through the PCM layer and a vertical thermal signal path also connected through the PCM layer. Heating pulses are applied to heater terminals, and the actuation is realized by the current drawn from PCM via [56]. Although this structure functions, the shared via between thermal actuation and RF

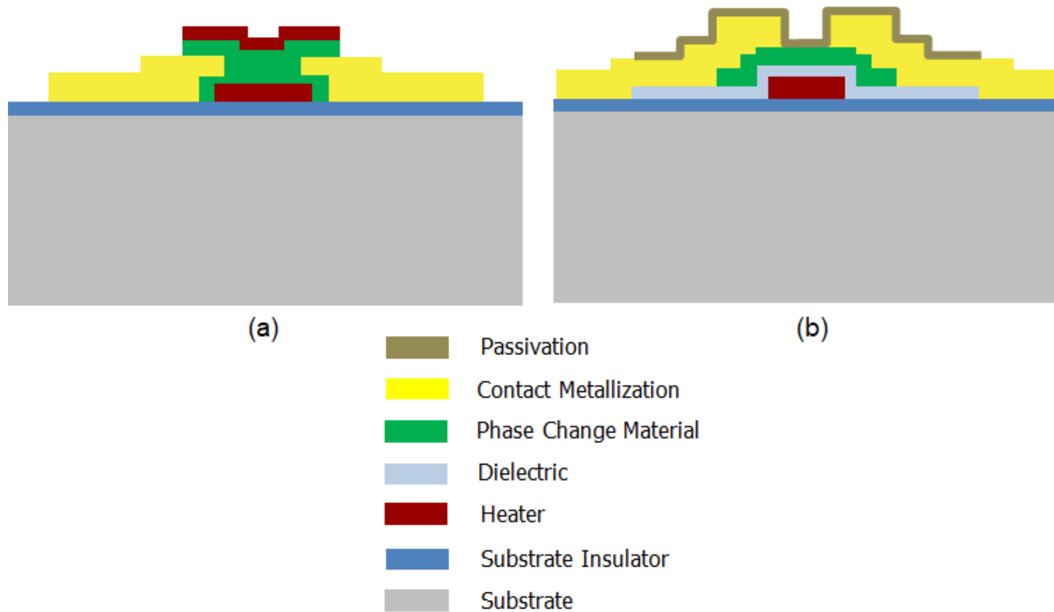

Figure 2.4: Schematic cross-section of (a) Directly heated and (b) Indirectly heated RF switch.

signal reduces the isolation and limits its application. The indirectly heated structure has good isolation between heating and RF signals owing to the dielectric layer separating them. This structure was used for the PCM switch designed and fabricated, which will be discussed in depth in Chapter 5.

2.4 Conclusion

Chalcogenide phase change materials are alloys of group *VI* elements with a unique property of reversible switching between amorphous and crystalline states. The transformation between two stable states occurs by applying a distinct heat treatment using electrical pulses. The large electrical resistivity between these two phases encourages their utilization in RF switching appli-

cations. Among all chalcogenide materials, GeTe shows the best properties for RF switching applications, like fast switching speed and high dynamic range. Due to the great potential of PCM and its successful application in the non-volatile memory industry, RF switches based on GeTe PCM propose a promising solution to reconfigurability for RF systems. In the next chapters, the growth, characterization, and application of GeTe thin film in an RF switch design will be discussed.

Chapter 3

PED Growth Technique of GeTe Thin Film

This chapter discusses the common growth technology for PCM, their weaknesses, and the advantages of using pulsed electron-beam deposition (PED) as an alternative. The focus is on the GeTe deposition as the most promising of the chalcogenide family for RF applications.

3.1 Motivation

Thin film growth of chalcogenides composition is an exciting field, owing to their interesting optical and electrical properties. The most popular deposition technique for growing GST and GeTe thin films is sputtering [51], [57], [58]. Molecular beam epitaxy (MBE) [59] and pulsed laser deposition (PLD) [60]–[62] are two other commonly used growth methods. Nevertheless, each has limitations such as low growth rate, complexity, and ability to ablate a limited selection of materials. Pulsed physical vapor deposition (PVD) methods can precisely control the growth rate (sub-monolayer per pulse). Compared to sputtering, there is no need to consider the electrical properties of target materials, and smaller targets of expensive and

highly pure material are required [60]. MBE uses distinct elemental targets to grow compound materials and an ultra-high vacuum (UHV) chamber ($<10^{-9}$ mTorr), both increasing the complexity and cost. Still, PVD methods utilize one compound target and do not need UHV for operation [59]. Moreover, both sputtering and MBE suffer from low deposition rates. PLD is the most studied and frequently used pulsed PVD methods that have been used to deposit GeTe thin-film layers. However, it has limitations regarding the laser beam reflection due to the plasma optically shielding the target. The shielding results in a lower growth rate, which becomes even worse with the expansion of the plasma over time.

This research reports a first-time demonstration of a novel method for growing GeTe thin films. This growth method is called pulsed electron-beam deposition (PED). The ablation mechanism in PED is similar to PLD, where a concentrated electron beam replaces the laser beam. While PLD suffers from optical shielding of the target surface, the plasma does not reflect the electron beam in PED, which results in improved efficiency. Also, there is no need for large, expensive excimer lasers and optical setups that are necessary for PLD [47]. GeTe thin film, the most motivating PCM in high-frequency applications, is targeted to demonstrate the PED capabilities.

3.2 Pulsed Electron-beam Deposition Physics

The schematic of the PED process is presented in Figure 3.1, in which a high-power electron beam (1000 A, 15 kV) produces pulses with 80-100 ns duration and focus of relatively 1 μm of the target. As a result, the target ma-

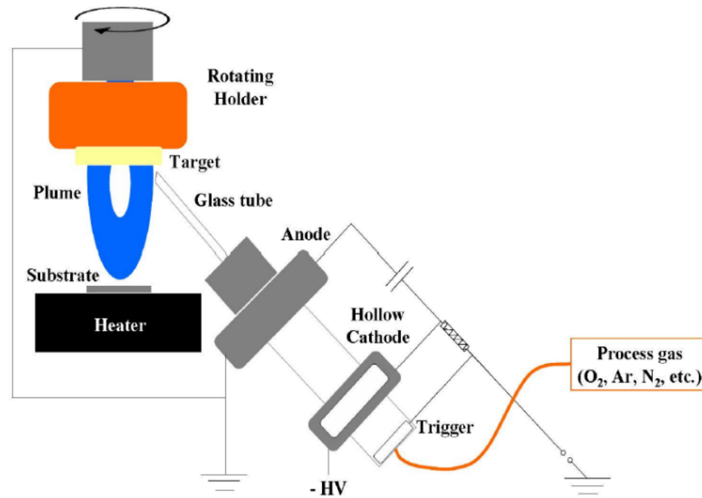

Figure 3.1: Schematic of the PED system [64].

terial will be evaporated and produces plasma [63]. The PED system at the University of Oklahoma uses a Neocera PEBS-21 electron gun, which uses the channel spark technique. A high potential difference between the hollow cathode and the target holder, which acts as a ground, accelerates the electrons. In the hollow cathode, a variable number of ceramic capacitors store the electrical energy and discharge it with pulses. The high current density ($\sim 10^6$ A/cm^2) that is realized serves as a very high peak power during the spark.

3.3 Pulsed Electron-beam Deposition of GeTe

GeTe thin films were deposited on (100) silicon substrates at room temperature using pulsed electron-beam deposition using a single 1 inch, 99.99% GeTe target. The deposition process was carried out in an ultra-high vacuum system equipped with a channel-spark source (PEBS-20) from Neocera, Inc.

Figure 3.2 Shows a close look inside the PED chamber. Before starting the deposition process, the substrate was ultrasonically cleaned in acetone and isopropyl alcohol. After that, the wafer was placed underneath the GeTe target at a target-to-substrate distance varying from 3 to 8 cm. In the growth process, the deposition chamber was vacuumed down to a base pressure of around 1×10^{-6} Torr. The growth was conducted in an Argon environment with the background pressure varying from 2.6 to 5.5 mTorr. Since Argon is an inert gas and well suited for background deposition purposes [65], it was used as the background gas during deposition. The pulsed electron-beam source (PEBS) was operated from 11 to 17 kV at 5 Hz frequency with a total number of $\sim$20,000 pulses. During the growth, both the target and the substrate were rotated to avoid damage to the target and to improve the thickness uniformity of the films, respectively. The growth factors, including E-beam generating voltage, target-to-substrate distance, background gas pressure, and the growth temperature, were investigated to find optimized growth conditions. After the growth, the thin films were systematically characterized using a KLA Tencor D500 stylus profiler and a high-resolution Zeiss Neon EsB FESEM for the surface morphology. Energy-dispersive X-ray spectroscopy (EDX) was employed to study the material composition of the GeTe films. Correspondingly, a Rigaku powder X-ray diffraction (XRD) system was employed for the crystal structure analysis.

During the PED growth process, both the E-beam parameters, such as PED voltage and plume range, as well as the deposition parameters, including background gas pressure and substrate temperature, control the quality of the deposited thin films. The impact of these factors on the GeTe thin film

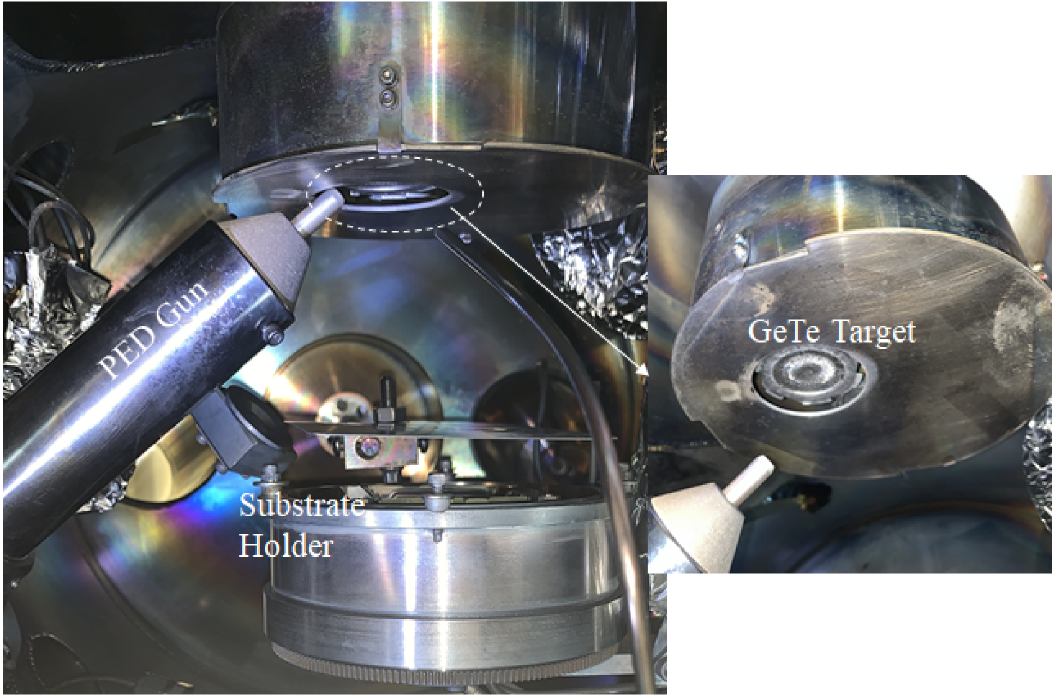

Figure 3.2: Inside the PED chamber.

and growth rate was investigated, and the results are presented in this section. Higher throughput and lower fabrication cost are the results of a higher deposition rate. More importantly, a higher deposition rate results in a lower impurity concentration in the deposited material [66].

3.3.1 Pulse Energy Measurements

First, the energy required to ablate the GeTe target was optimized experimentally. The energy should be higher than the minimum energy that can penetrate the target and less than the energy that causes the plume range to be longer than the target-to-substrate distance. PED is a channel-spark discharge system in which the applied voltage defines the electron beam energy

emitted to ablate the target material [67]. Figure 3.3 presents the growth rate as a function of PEBS voltage. Although higher beam energy results in a higher growth rate and enhanced throughput, the surface morphology is determined by the energy the target material requires for evaporation. If the applied voltage is lower than the optimum, it leads to a low growth rate due to the lack of energy to ablate the material. This was found when 11 and 13 kV potentials were applied to the PED gun. To increase the growth speed, the voltage was increased to 15 kV, which resulted in a growth rate of 0.04 Å/pulse or 1.2 nm/min. This is a reasonable rate for GeTe deposition compared to PLD [59]. Raising the voltage to 17 kV resulted in a higher growth rate but poor film quality in terms of the number and the size of particulates formed on the surface. These particulates are common in pulsed PVD methods [67]–[70]. The possible sources are emissions from the target and extraction after ablation in the gas phase [67]. Nevertheless, the size and number of these particulates drop when the substrate is placed at the end of the plume range. This is because the optimal target-to-substrate distance is adjacent to the plume range [71]. The plume range was measured by its effects on the deposited film regarding surface smoothness and non-zero growth rate. Overall, the optimized E-beam voltage was found to be 15 kV.

3.3.2 Plume Range Measurements

The plume range is an important E-beam parameter during growth. The key features that define the plume range are the applied PED voltage and the

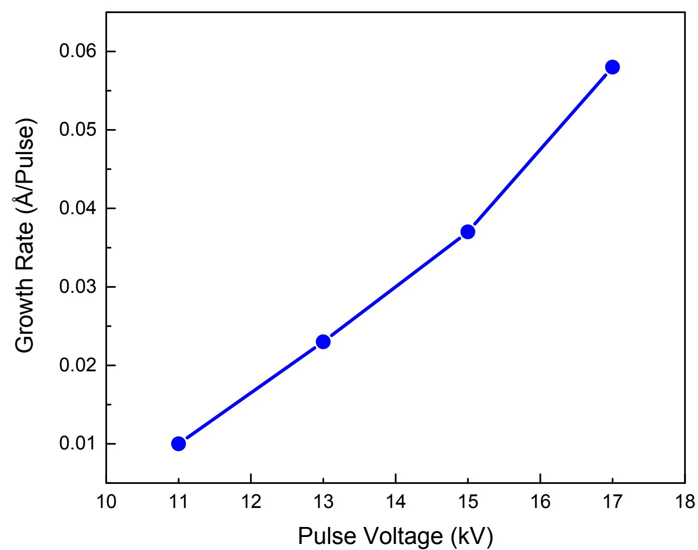

Figure 3.3: Growth rate dependence on the applied PEBS at pressure 5.5 mTorr and target-to-substrate distance 8 cm.

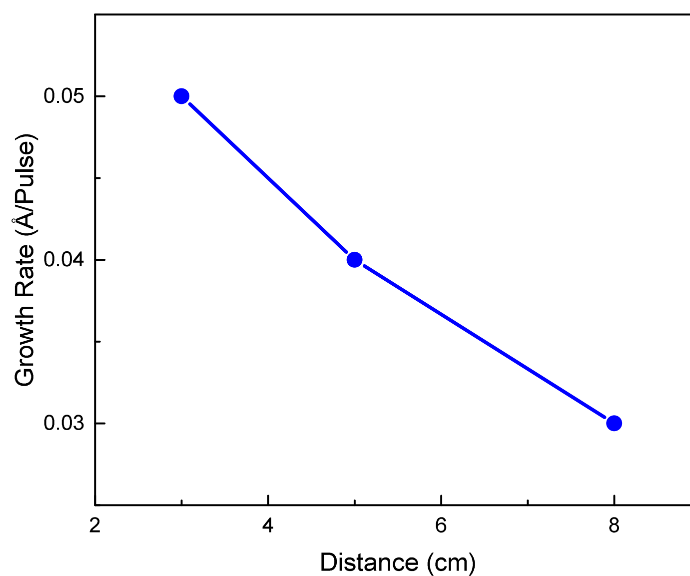

Figure 3.4: Growth rate dependence on the target-to-substrate distance at pressure 5.5 mTorr and PEBS 15 kV.

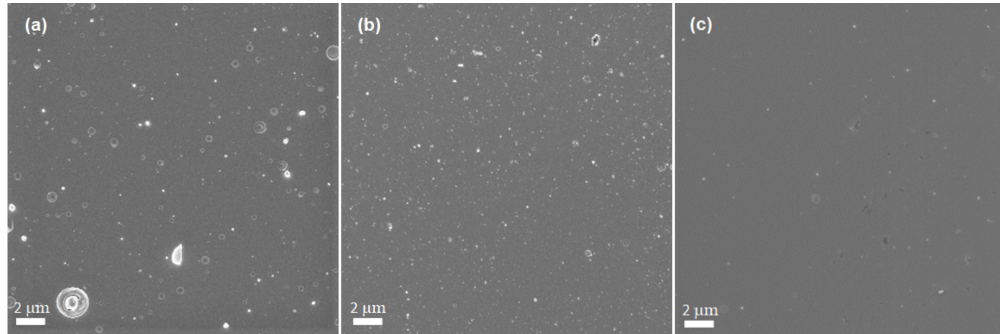

Figure 3.5: Top SEM view of GeTe thin films deposited at (a) 3 cm, (b) 5 cm, and (c) 8 cm target-to-substrate distances at pressure 5.5 mTorr and PEBS 15 kV.

target-to-substrate distance. In our experiments, three different target-to-substrate distances were tested. The highest distance from the target that the chamber allows is 8 cm. Two extender substrate holders were used to grow thin films at 3 and 5 cm as well as 8 cm. Figure 3.4 shows the average growth rate as a function of the target-to-substrate distance. The top view morphology results of 3, 5, and 8 cm are shown in Figure 3.5 (a) to (c), respectively. In Figure 3.4, the average growth rate has a linear and negative dependency on the target-to-substrate distance. Figure 3.5 shows that, by decreasing the target substrate distance, some irregular particulates are formed on the deposited films. Although a closer target resulted in a higher growth rate, the surface roughness was increased, and subsequently, the film quality was reduced drastically. Lower the target-to-substrate distance resulted in larger particulates' sizes and densities. The arithmetical mean deviation surface roughness, R_a, was calculated from the films' height profile, was measured by an alpha-step profilometer. The results are shown in Figure 3.6, confirming that the larger the distance, the smoother the sur-

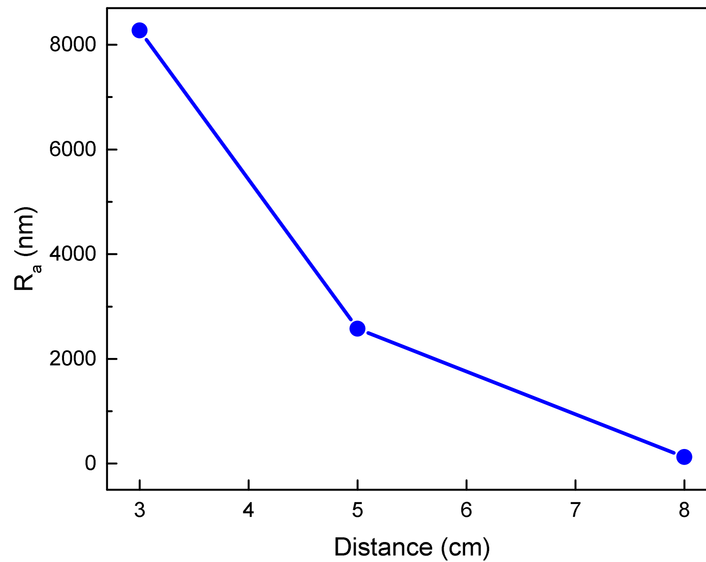

Figure 3.6: Surface roughness as a function of target-to-substrate distance at pressure 5.5 mTorr and PEBS 15 kV.

face. By increasing the target-to-substrate distance, a drastic reduction in the number and size of the particulates in the deposited film was observed, and a smoother surface was obtained. Since the 8 cm distance resulted in the best surface morphology, and it is the largest distance that the chamber allows, the rest of the experiments were conducted at this distance. A higher PEBS potential (17 kV) was tested to confirm that 15 kV was the optimum PEBS voltage. Figure 3.7 (a) and (b) show the morphology of the as-deposited GeTe films, grown at 15 and 17 kV, respectively. The results confirm that the 15 kV is the optimum potential needed for ablating the GeTe target using the PED tool. 15 kV PEBS voltage was used for the rest of the experiments.

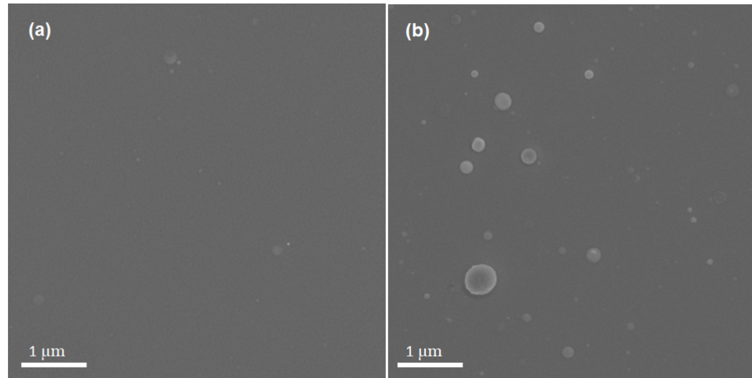

Figure 3.7: Top SEM view of GeTe thin films deposited at (a) 15 kV and (b) 17 kV PEBS potentials at pressure 5 mTorr and target-to-substrate distance 8 cm).

3.3.3 Material Composition

A background gas pressure of Ar between 2.6 to 5.5 mTorr was investigated for the GeTe thin-film quality. The PEBS requires at least some pressure for generating and sustaining the E-beam propagation. This pressure for GeTe is at least 2.5 mTorr. Pressures higher than 6 mTorr showed unbalanced materials compositions as well as low growth rates. Figure 3.8 shows the average growth rate as a function of the background pressure. Decreasing pressure results in higher growth rates, which are dramatically increased from 3.5 to 2.6 mTorr to 0.1 Å/pulse or 3 nm/min. The cause is an increase in the mean free path at lower pressures. This higher growth rate results in improved purity in the grown material. Highly pure chalcogenide materials are required for less sheet resistance in the crystalline state, which is essential for high-frequency applications [58]. Oxidation of PCM during deposition is a common issue [58]. In the absence of ultra-high vacuum (UHV), increasing the growth rate prevents PCM from oxidizing. The oxygen content in the as-

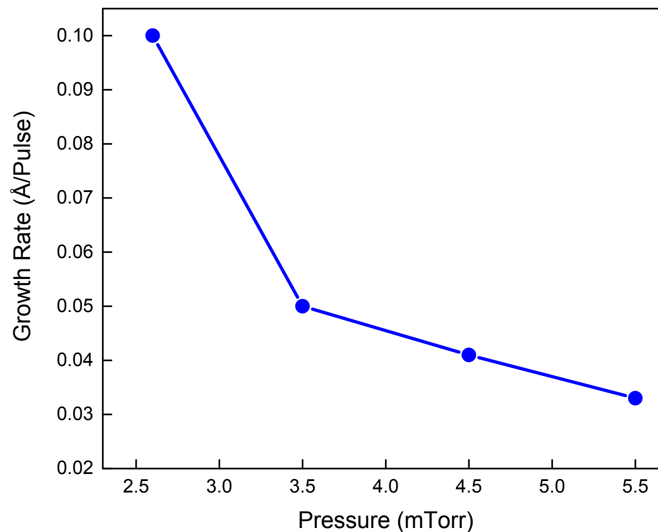

Figure 3.8: Growth rate dependence on the background pressure at PEBS 15 kV and target-to-substrate distance 8 cm.

deposited GeTe films decreased from 3.5 to 0.6 by increasing the deposition rate at lower pressure (2.6 mTorr).

Another challenge in the PCM thin film growth, which determines the sheet resistance, is reaching the proper ratio between material concentrations in the deposited thin film [72]. GeTe (50:50) has the lowest sheet resistance of the GST family of PCM. Previous research on GeTe materials showed that a slight change in the ratio of the elements does not have a considerable variation in the PCM properties [73]. Figure 3.9 illustrates the impact of the background pressure on the ratio between Ge and Te in the deposited material. Higher pressures result in telluride-rich, thin films. This occurs because telluride-rich clusters like $GeTe_2$ are formed and present in the plasma. These molecules can be deposited on the substrate at higher pressures [59]. The ratio between elements in the composition of Ge:Te can be controlled

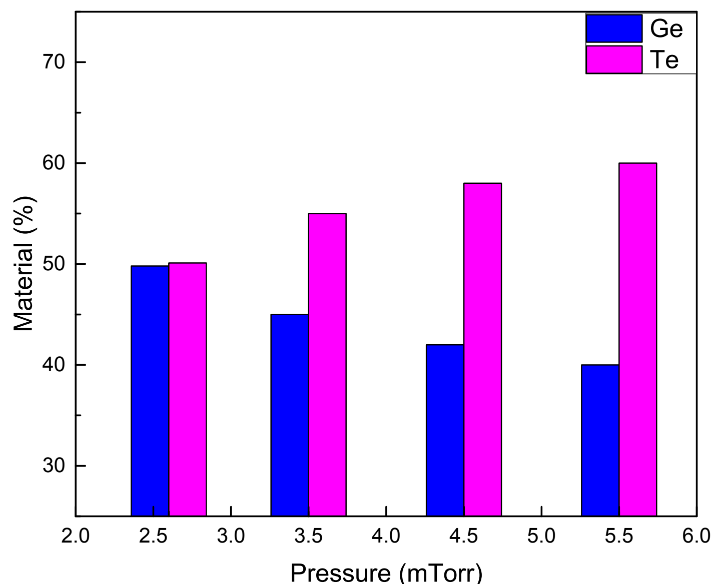

Figure 3.9: Germanium and Telluride ratio dependence on the background pressure at PEBS 15 kV and target-to-substrate distance 8 cm).

by reducing the pressure. Based on the trend of decreasing telluride and increasing germanium, the 2.6 mTorr provides $Ge_{50}Te_{50}$, which is the exact 50:50 stoichiometric composition.

3.4 XRD Results

Amorphous and crystalline are two stable phases of PCM at room temperature. Epitaxial growth of materials can be performed at high temperatures to reach single crystalline thin-film material [74]. On the other hand, PVD methods are generally used to deposit PCM thin films at room temperature [75], [76]. In this study, the growth of the GeTe thin films, us-

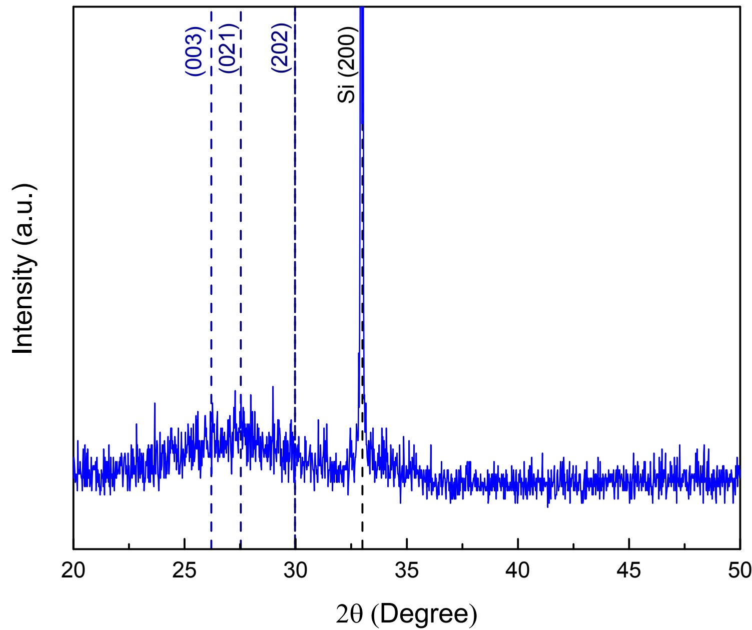

Figure 3.10: XRD pattern of the as-deposited GeTe film.

ing the PED method, was performed at room temperature. Figure 3.10 shows the XRD pattern for the GeTe thin film as deposited. The broad crest on the three-major crystalline GeTe materials' peaks ((003), (021), and (202)) verifies the amorphous structure of the as-deposited GeTe thin film. Post-annealing methods are commonly used to transform the amorphous as-deposited PCM material to a crystalline state [77], [78].

3.5 Conclusion

The pulsed electron-beam deposition has been employed to grow thin films of chalcogenides composition, and its capability to grow high-quality PCM

thin films was investigated in this chapter. GeTe thin films, the major PCM in high-frequency utilization, have been successfully grown on silicon (100) substrates at room temperature. The quality of the deposited film was defined by the desired physical properties, such as smoothness and uniformity of the surface and the fundamental elements ratio of the material. The surface roughness of the films was defined by the plume range, which itself depends on the PEBS and target-to-stage distance. Background gas pressure determines the growth rate and the ratio between the two elements (Ge and Te). XRD profile was used to show that the as-grown GeTe thin film at room temperature was amorphous in configuration. The advantages of PED over other deposition methods, such as sputtering and PLD, make it a suitable alternative growth method for amorphous chalcogenides, as demonstrated by the growth of high-quality GeTe thin films. The optimized growth parameters for depositing thin-film GeTe with the PED system are summarized in Table 3.1. These conditions lead to smooth and uniform GeTe thin films deposited with the PED method. The necessity of having a crystalline GeTe layer for RF switching application and the crystallization procedure will be discussed in the next chapter.

Table 3.1: PED deposition parameters.

Parameter	**Value**
Voltage	15 kV
Target-to-substrate distance	8 cm
PED frequency	5 Hz
Chamber base pressure	1 μTorr
Deposition pressure	2.6 mTorr
Deposition temperature	room temperature

Chapter 4

Crystallization Kinetics of GeTe Phase Change Thin Film

In this chapter, the technique for crystallization of GeTe thin films was experimentally studied. The GeTe thin films have been grown by pulse electron-beam deposition (PED). To evaluate the qualifications of the PED method, high-quality GeTe thin films have been investigated by contemplating the crystallite quality and the electrical conductivity. Chapter 3 discussed that the GeTe thin film was amorphous as grown. In order to convert the GeTe thin film into a crystalline formation, post-treatment annealing was performed. To optimize the post-annealing procedure, several annealing parameters were experimentally investigated. The thin-film resistivity dropped by six orders of magnitude upon crystallization. X-ray diffractometry (XRD) spectrum and resistivity were used to evaluate the crystal quality. Alternative material characterization methods, like field emission scanning electron microscope (FESEM) and energy-dispersive X-ray spectroscopy (EDX), were used to explore the crystallization parameters further.

4.1 Motivation

Important factors that affect the RF switch's performance are the loss in the ON state and the isolation in the OFF state. These translate to a high ratio of R_{off}/R_{on}, where R_{off} and R_{on} are the PCM thin-film resistance in amorphous and crystalline states, respectively. The GeTe thin film deposited by PED at room temperature is amorphous. The electrical resistivity of amorphous GeTe is on the order of 10^6 $\mu\Omega$·m. The analysis of the XRD shows a broad and weak peak between 26 and 30° in the 2θ range, which indicates that the GeTe thin-film is amorphous. These two criteria (electrical resistivity and XRD diffraction peaks) were taken into consideration to analyze the crystallization quality of the GeTe thin films. Figure 4.1 shows the basic concept of PCM-based RF switches. The thin-film resistor underneath the PCM layer produces the required heat for a phase transition. Metal contacts on top of the PCM layer carry the RF signal. The initial Amorphous case shows the condition that the switch has been made with as-grown amorphous PCM. The initial crystalline state demonstrates the switch based on the annealed and crystallized PCM layer. In both cases, the dashed lines show the sizes of the channel that need to change phase during actuation.

4.2 Post Thermal Annealing Process

Germanium Telluride thin films were deposited by PED at room temperature. A single GeTe target was used to grow the GeTe thin film on a high-resistivity silicon wafer with a natural oxide layer [79]. The GeTe films were 80 nm

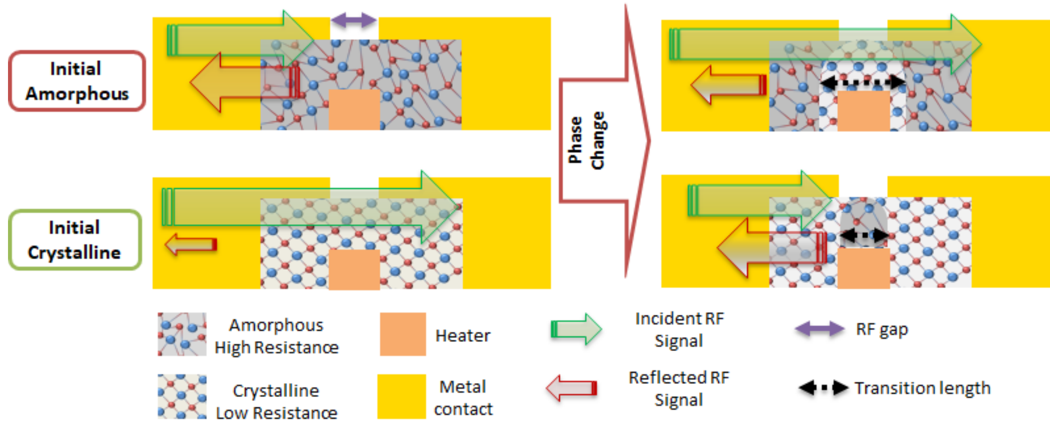

Figure 4.1: Top row: The RF switch configuration with the initial amorphous PCM thin-film (OFF state). Activation pulse results in the ON state.
Bottom row: The ideal configuration, with an initial crystalline thin-film of PCM (ON state). Activation pulse results in the OFF state. The Dash arrow in both cases shows the portion of the PCM layer that needs to transform.

thick and were in an amorphous state as grown. The GeTe samples that were used for the experiment were deposited at the same time, and all have smooth surface morphology. Two techniques were employed to crystallize the amorphous GeTe thin films. In the first technique, the amorphous GeTe samples were annealed in two different rapid thermal annealers (RTA) furnaces under different gas atmospheres to validate the application of both furnaces. The impact of the annealing temperature T_A and the annealing time have been studied. In order to investigate the effects of other conditions on the GeTe crystallization, the ramping speed, gas type, and pressure variation results were examined. In all cases, the air was vacuumed from the furnace chamber and filled with the study's gases. The first RTA used for the phase transition to crystalline was RTP-1000D4 by MTI (shown in Figure 4.2), and the other RTA was AG ASSOCIATEs HEATPULSE 610 rapid

Figure 4.2: RTP-1000D4 by MTI rapid thermal annealer.

thermal processor. The difference between these furnaces is that the former has a pump to vacuum the furnace chamber, which is then filled with desired gas, while the latter employs a high-pressure gas injection, which forces the air out of the chamber. So the pressure inside the chamber is tractable for the RTP-1000D4, whereas for the AG-610 it is always around atmospheric pressure.

In the second technique, the GeTe thin film was grown with two metal electrodes on two sides to measure the in-situ GeTe resistivity change during the

crystallization. With this technique, the crystallization time and speed are measurable as well. Figure 4.6 illustrates this measurement setup, which includes a GeTe thin film on a silicon substrate and two metal contacts of gold on two sides of it. Two probes, separated by a constant distance, were used to measure the resistance as the substrate sat on a hot plate, and the temperature was increased gradually by a fixed ramp rate of 10°C/min. From the measured resistance, the electrical resistivity is extracted to take out the impact of the gap and thickness of the material. The GeTe thin film electrical resistivity, as well as surface morphology and material composition, analyzed using scanning electron microscope (SEM) and energy-dispersive X-ray spectroscopy (EDX), were the parameters that revealed the quality of GeTe thin film crystalline. All samples were polycrystalline with one dominant crystalline plane (202). Further investigation about the effects of the presence or absence of oxygen during the crystallization was performed at the end. Important factors that affect the RF switch's performance are the loss in the ON state and the isolation in the OFF state. These translate to a high ratio of R_{off}/R_{on}, where R_{off} and R_{on} are the PCM thin film resistance in amorphous and crystalline states, respectively. The GeTe thin film deposited by PED at room temperature is amorphous [79]. The electrical resistivity of amorphous GeTe is on the order of 10^6 $\mu\Omega\cdot$ m. The analysis of the XRD shows a broad and weak peak between 26 and 30° in the 2θ range, which indicates that the GeTe thin film is amorphous. These two criteria (electrical resistivity and XRD diffraction peaks) were taken into consideration to analyze the crystallization quality of the GeTe thin films.

4.2.1 Furnace Annealing

First, the crystallization temperature ($T_{Crystallize}$ in Figure 2.2) was ascertained by annealing multiple GeTe thin-film samples at different peak temperatures in an Ar environment. For this experiment, an RTP-1000D4 furnace was pumped down to 400 mTorr and filled with Ar gas at one atmospheric pressure. The annealing time was 10 min, and the heating and cooling rates both were 10°C/min. The XRD results for four annealing temperatures are presented in Figure 4.3(a). The peak at 32.9° corresponds to the silicon substrate, and all the results were normalized to that peak. Figure 4.3(b) shows the resistivity of the annealed GeTe thin films at the same annealing temperatures. Although the sample was annealed at 180°C did not show a visible XRD peak related to GeTe, its electrical resistivity dropped by 10^5 $\mu\Omega\cdot$m compared to amorphous GeTe. By increasing the annealing temperature to 220°C, the broad XRD peak changed to three prominent diffraction peaks at 26.1, 27.5, and 29.9° in the 2θ range, which are associated with the (003), (021), and (202) lattice planes of rhombohedral GeTe, respectively. Also, its resistivity decreased compared to the sample annealed at 180°C. These results show that the GeTe crystallization started at temperatures above 180°C. Increasing the annealing temperature to 260°C resulted in the maximum intensity of all XRD peaks, even a peak at 43.4° related to (220) lattice plane appeared as shown in Figure 4.3(a). The full width at half maximum (FWHM) gained from the XRD plot for (202) crystalline plane as the dominant peak is plotted in Figure 4.3(b) (left axes) as a function of annealing temperature. The grain size was determined using the

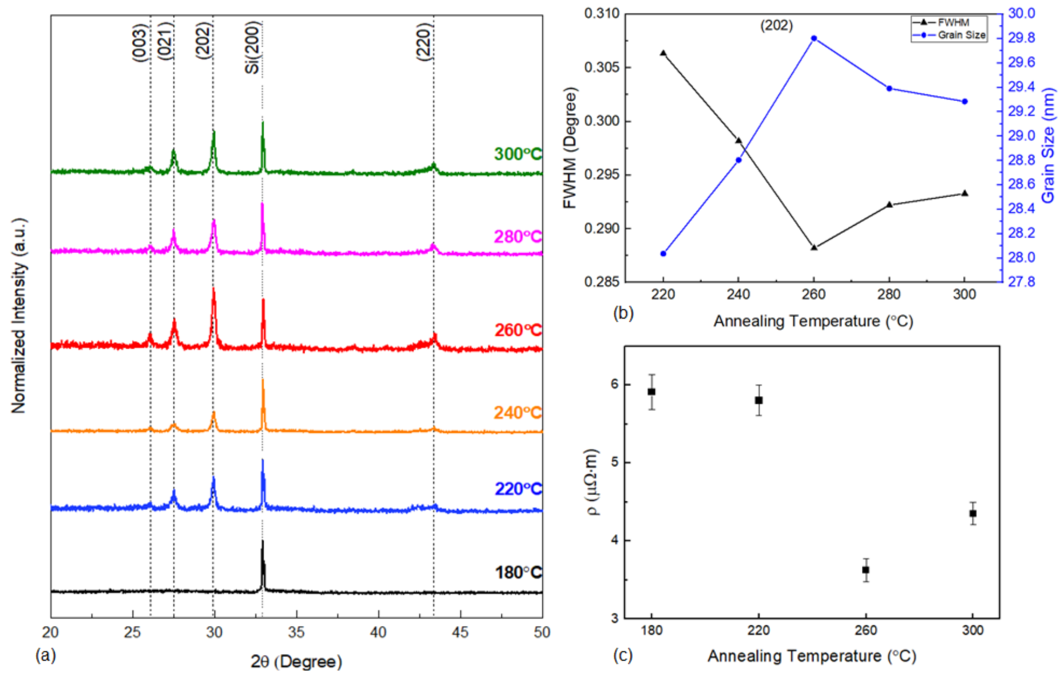

Figure 4.3: (a) Normalized XRD spectra, (b) FWHM value and calculated grain size from the crystalline plane (202) as a function of annealing temperature, and (c) resistivity of annealed GeTe films as a function of annealing temperature.

Scherrer-formula Equation 4.1 [80],

$$D = \frac{k\lambda}{w \cos\theta} \tag{4.1}$$

where $k = 0.9$, λ is the wavelength of measured X-ray (1.54 $\mathring{A}$), w is the full width at half maximum (in radians), and θ is the half diffraction angle of crystalline orientation peak. The average grain sizes of (002) crystallite plotted in Figure 4.3(b) (right axes). The crystalline grain size has an inverse relationship to the FWHM value, increasing from 28 to 30 nm as the annealing temperature increases from 220 to 260°C. The lowest FWHM and the largest grain size are related to 260°C of these discrete examined annealing temperatures from 180 to 300°C. Moreover, the lowest electrical resistivity was measured from this sample. The magnitude of all XRD peaks gradually decreased by raising the annealing temperature from 260 to 300°C. This indicates that the peaks become weaker when the temperature rises beyond 260°C. This agreed with the increased electrical resistivity, shown in Figure 4.3(c); both imply a more inferior crystal quality of the GeTe thin films that were annealed at 300°C. These results indicated that the best GeTe crystalline thin film was obtained from the 260°C annealing temperature out of the investigated temperatures in this dissertation.

In the next step, the GeTe thin films were annealed in an AG-610 RTA furnace. This furnace offered the additional benefit of using two other types of gases. This was utilized to investigate the gas-type effects on the GeTe crystallization. These two gases were nitrogen and forming gas (80%N_2+20%H_2, limited to 20% H_2 due to laboratory safety requirements). A comparison be-

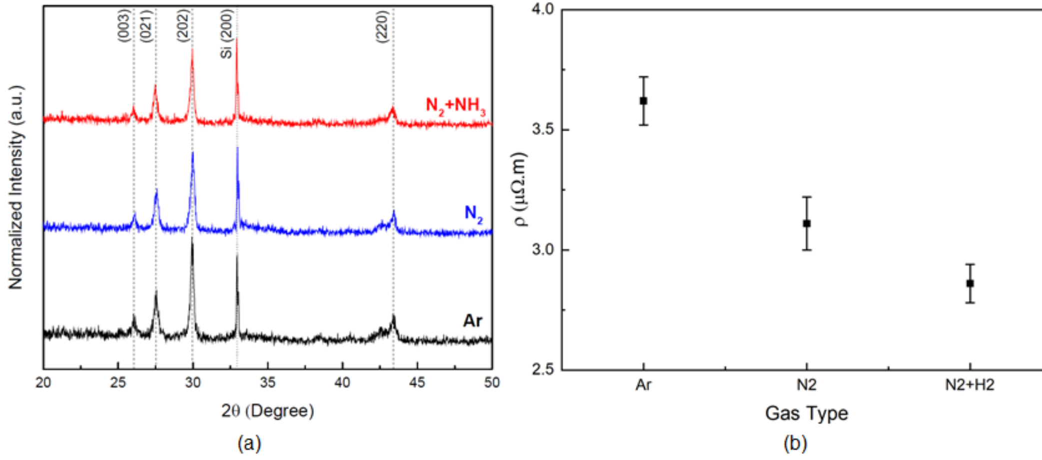

Figure 4.4: (a) Normalized XRD spectra and (b) resistivity of annealed GeTe films as a function of chamber gas.

tween the intensity of the XRD peaks and the resistivity results of this experiment is shown in Figure 4.4. The annealing temperature and time were the same for these three samples, and the XRD peaks were normalized to the silicon peak at 32.9°, just like they were in the previous experiment. The XRD peaks had almost the same intensity. However, the film resistivity dropped slightly from 3.6 $\mu\Omega$·m for Ar to 2.8 $\mu\Omega$·m where forming gas was utilized to fill the furnace chamber. This will be discussed further in the section 4.2.3 Annealing Summary. The top surface morphology of as-deposited GeTe and those annealed in Ar and forming gas environments are illustrated in Figure 4.5(a)-(c), respectively. Both amorphous and crystalline GeTe thin-films have a smooth surface morphology and homogeneous structure as shown in Figure 4.5. The crystallization led to GeTe thin films revealing dim regions between the poly-crystalline zones as the grain sizes were increased. Accumulation of nano-sized voids during PCM crystallization has been previously observed [81]. The crystallite coarsening intensifies slightly from the Ar en-

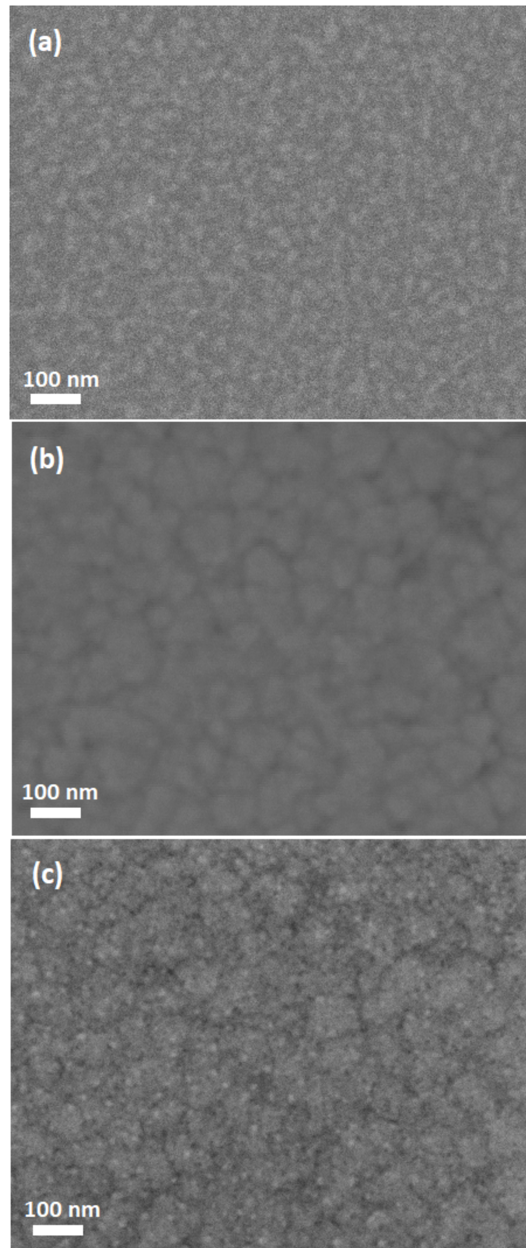

Figure 4.5: Top SEM view of GeTe thin-films (a) as-deposited, annealed at (b) Ar, and (c) forming gas (80%N_2+20%H_2).

vironment to the forming gas environment. This agrees with the resistivity outcomes, which are lower for the forming gas. The introduction of hydrogen in the forming gas reduces the oxide in the GeTe crystal film and thus results in an overall better electrical performance.

4.2.2 Hot Plate Annealing

The real-time resistance changes were tracked by patterning GeTe thin films on a Si substrate. A 100 nm thick GeTe thin film was deposited by PED, then two metal pads of copper and gold (Cu/Au) were deposited on either side with varying gap distances and shapes. Two test probes from Harwin P13-0123 were installed in a fixture with constant distance and made contact with metal pads for real-time resistance measurements while the substrate was on a hot plate. The hot plate temperature was increased gradually, and the resistance between the two pads was monitored. An illustration of the measurement, with the GeTe film in amorphous and crystalline states, is shown in Figure 4.6. The gap between the two metal pads determined the resistance during the experiment. The thin-film resistivity in $\mu\Omega{\cdot}$m is calculated and reported in Figure 4.7. The results are consistent with what was shown in the previous section. The GeTe resistivity, which is an indication of GeTe crystallization, decreased while the temperature was increased. Still, around the crystallization temperature, 210°C, the resistivity dropped drastically from around $2{\times}10^4$ to less than 10 $\mu\Omega{\cdot}$m. One of the primary purposes of this experiment was to see if the crystallization occurs at a specific temperature or if it happens gradually over a range of temperatures. These results, repeated for several samples with different shapes and gaps, showed that

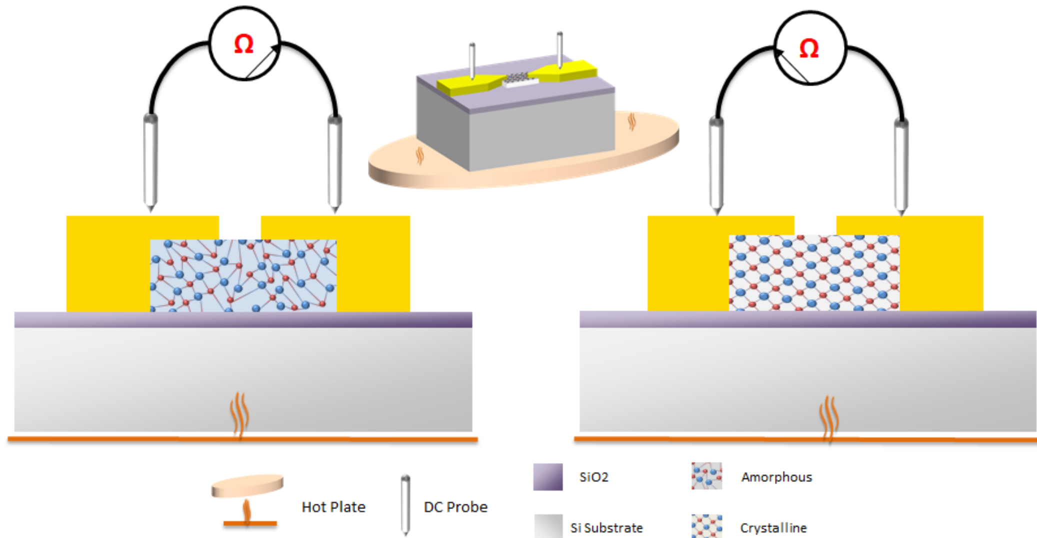

Figure 4.6: The two-probe setup is used to measure the real-time resistance changes on a hot plate.

the phase transformation to conductive mainly happens around crystallization temperature. This abrupt change in resistivity makes GeTe a desirable material for RF switches. This feature has been used in both RF and Memory applications where a short thermal pulse is used to change between the states of the PCM [82].

Figure 4.7 illustrates the real-time thin-film resistivity changes as a function of the hot plate temperature. The drop in resistivity occurs in two steps. There is a minor resistivity drop around 100°C followed by a significant drop at the GeTe thin-film crystallization temperature of 210°C. This temperature is 50°C lower than what was investigated earlier in the absence of air. This crystallization-temperature decrease is a direct result of oxidation of the PCM [83], [84]. GeTe thin-film surface oxidizes naturally in the presence of oxygen in the atmosphere [85]. This process is expedited when heat is applied. In the furnace annealing in the absence of oxygen, this phenomenon

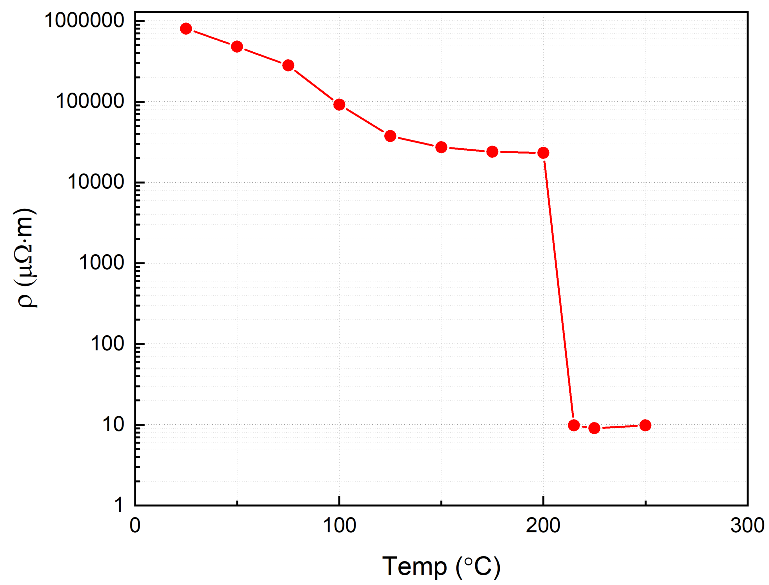

Figure 4.7: Measured electrical resistivity ($\mu\Omega{\cdot}$m) of GeTe while heating from hot plate to approximately 250°C.

has a negligible effect. The first resistivity reduction is due to the natural thin oxide on the surface crystallizing at lower temperatures [86]. The nucleation process is followed by a homogeneous crystallization inside the volume, which requires more energy and occurs at higher temperatures [84]. The GeTe thin film, in this experiment, did not have a capping layer to protect it from oxidation during the annealing. Subsequently, the whole GeTe thin film was exposed to air, and the molecules below the natural surface oxide layer followed the heterogeneous surface nucleation. Also, the crystallized oxide GeTe has a porous structure that increases the surface area and allows more Ge and Te atoms to be exposed to air [87]. This process will continue, and most of the GeTe thin film will oxidize during the crystallization. As a result, the resistivity in the crystalline state is higher than for the GeTe annealed in the furnace, and it has a rough surface morphology. The top SEM view is shown in Figure 4.8 illustrates the formation of voids, which supports this argument. The amount of oxygen directly affects the properties of PCM. In the case of GeTe, these properties include crystallization temperature, electrical resistivity, and optical reflectivity [88]. The atomic percentage of the elements of this sample is shown in Table. 4.1.

4.2.3 Annealing Summary

Crystallization of GeTe thin-film samples utilizing post-thermal annealing was investigated in this experiment. The purpose of the furnace annealing was to determine the best crystallization conditions, which resulted in the GeTe thin film with the lowest resistivity in the crystalline state. One crucial factor that increases PCM resistivity is the presence of oxygen. As-deposited,

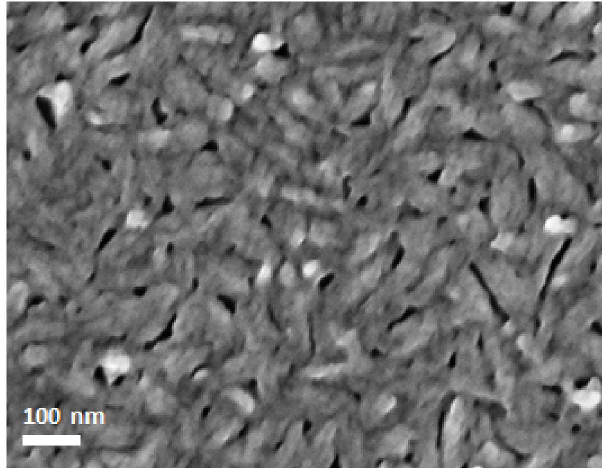

Figure 4.8: Top SEM view of GeTe thin-films annealed at air (hot plate) and related elements' atomic percentage.

GeTe thin films contain very little oxygen, which comes from the tendency of GeTe to oxidize when it is in contact with air [58]. The related elements' atomic percentages for samples in this study are reported in Table 4.1. The oxygen elimination is different for furnace annealing in the absence of air, based on the gas ambient type used for annealing. It is reduced to almost zero when forming gas is utilized. These results are in agreement with the resistivity outcomes. Alternatively, when annealing was performed on a hot plate in an oxygen-rich environment, the amount of oxygen in the film grew by one order of magnitude. This rapid increase in the amount of oxygen, compared to as-grown GeTe thin-film, validates the high tendency of GeTe material to oxidize during crystallization. As a result, PCM RF switches require a passivation layer to protect them from contacting air while nucleation.

Table 4.1: Atomic% ratio of Germanium, Telluride, and Oxygen in four samples handled differently. The remaining percentage is Si, which comes from the substrate.

Sample		**Element%**		
		Ge	**Te**	**O**
As-Deposited		1.9	1.9	4
Annealed at/on	Ar	3.9	4.5	3.2
	Forming Gas	4.1	4.7	0.1
	Hot Plate	1.8	2.3	43.8

4.3 Conclusion

This chapter investigated the crystallization of amorphous GeTe thin films deposited by PED. The effects of different parameters like temperature and environmental conditions were examined to reveal the optimum conditions for crystallization. The crystal quality was evaluated by structural and electrical properties. The as-deposited amorphous GeTe thin film has a smooth surface with a 50-50 Ge and Te ratio. GeTe thin films with a smooth and uniform surface and equal elements ratio lead to a high-quality crystalline structure with low electrical resistivity. It was shown that the post-thermal annealing environment is critical for the crystal quality, and it is essential to protect the GeTe thin film surface with a passivation layer. The high contrast in electrical resistivity in the two stable states is the high-frequency switching applications foundation. The next chapter will utilize crystallized GeTe thin film to make an RF switch based on PCM.

Chapter 5

RF Switch Fabrication and Results

The PCM RF switch performance is sensitive to each element. This means that not only the high efficiency but also the functioning of the PCM switch relies on the design and fabrication of all elements. The last two chapters thoroughly discussed the deposition and crystallization of the PCM layer. In this chapter, the fabrication process of other layers, which serve as the heater, dielectric, electrodes, and passivation, will be investigated. The limitation for improving their performance will be explained. Subsequently, the step-by-step switch fabrication process and the test setup are presented. Finally, the results are discussed.

5.1 PCM RF Switch Design

The PCM-based RF switch has been designed and implemented using a coplanar waveguide (CPW) transmission line (T-line). The substrate was a high-resistive silicon wafer with natural oxide on top. The GeTe RF switch includes two RF terminals connected by the GeTe via. The PCM switch element is placed in the middle of a 50 Ω CPW line. The switching section is

a T-line discontinuity filling with GeTe material and the heating pulse structure. The best GeTe crystalline quality was achieved by furnace annealing crystallization (chapter 4), with an electrical resistivity as low as 2.8 $\mu\Omega\cdot$m, which translates to 3.5×10^{5} S/m electrical conductivity. The copper electrical conductivity (5.8×10^{6} S/m) is more than two orders of magnitude higher than the best achieved for GeTe. The difference between the electrical conductivity of metal and GeTe in the crystalline state resulted in a higher impedance of the T-line in the switch location. To tackle this mismatch in the CPW line, a tapering strategy close to GeTe via has been used. This tapering was designed based on the simulation results for 100 nm thickness of the GeTe layer with electrical conductivity of 3×10^{5} S/m and RF gap of 1 μm. Changing the PCM state requires applying thermal pulses to it. The heat would be applied through a short actuation pulse. The first strategy for applying heat pulse is utilizing the same technique used in PCM memory, in which a bias signal penetrates into the GeTe layer. On the other approach, the heat pulse is isolated from the RF path by a dielectric layer with good thermal conductivity, and thermal energy is coupled to the GeTe layer. The first strategy is direct heating, and the second is indirect heating. Each of these will be introduced further in the following sections. This research focuses mainly on the indirect heating switch, which will be discussed in detail.

5.1.1 Direct Heating Switch

In this strategy, the heating pulses pass through the GeTe layer and change its state. Figure 5.1 (a) and (b) illustrate the schematic cross-section and top view of the direct heating switch, respectively. The fabricated direct heat-

ing switch is shown in Figure 5.1 (c). The problem with this technique is the RF signal and the heat pulse shares the same path, causes introducing noise to the RF signal. The biasing pulses have a very short duration, so their introduced noise can be problematic in RF applications. Several critical parameters need to be considered to make this design work. For instance, the heater material must have high resistance to provide enough isolation between RF and thermal paths. In the meantime, it has to have suitable impedance matching with GeTe to pass most of the thermal pulse with a very low duration. Considering all the direct-heating switch design complications, the project's main goal specified the indirect heating structure. The challenges and results of the direct heating approach are discussed in Appendix A.

5.1.2 Indirect Heating Switch

The RF switch in the indirect heating approach has four terminals, two for RF signal connected through GeTe via, and two for applying heat pulses, connected with a resistive heater underneath GeTe via and covered with a dielectric material. The heater layer is a narrow thin film conductor with good electrical conductivity and a high melting point material for applying direct biasing. The heater creates the required thermal energy from electrical energy. This heater has two pads to apply the actuation pulse. A dielectric layer sits on top of the heater and makes electrical isolation to minimize the impact of the heating signal on the RF one. In this approach, the RF signal transmission path is electrically isolated from the heater path, while the dielectric layer provides a thermal coupling between them. The barrier

(a)

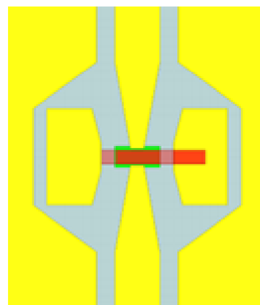

(b)

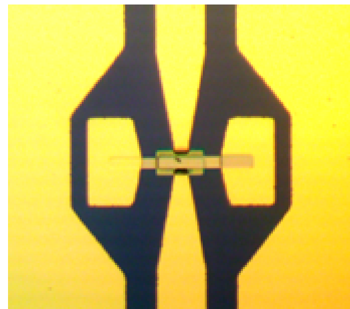

(c)

Figure 5.1: Direct heating switch design (a) cross-section view, (b) top view, and (c) fabricated switch.

material must have high thermal conductivity to deliver most of the thermal energy produced by the actuation pulse to the PCM layer. The PCM layer is deposited on top of the dielectric layer and plays the switching role. The PED deposition method is used to grow the GeTe. RF electrodes and bias electrodes are made from copper and coated with gold. There is a discontinuity in it which is called an ”RF gap.” The RF gap is between two RF electrodes that the GeTe fills, the essential parameter in the PCM switch. This section rejects or passes the RF signal based on the GeTe state. Finally, to stop GeTe from oxidizing during the switching, a thin passivation layer from a suitable dielectric material should be deposited on top of GeTe. A cross-sectional schematic of the order of the layers that the PCM switch requires is shown in Figure 5.2.

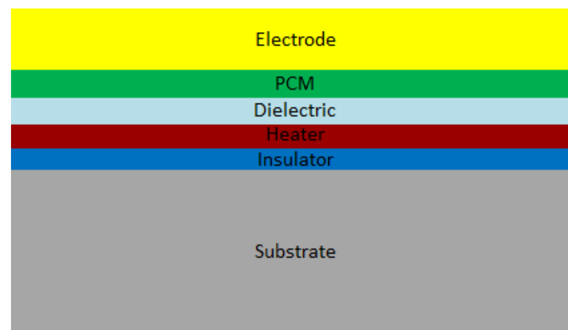

Figure 5.2: Order of layers to fabricate PCM switch (from bottom to top).

5.1.2.1 Device Structure

Two RF switch structures were designed for the experiment. The design schematics and the fabricated switches are shown in Figure 5.3. The heater architecture is the main difference between these two designs. The heater length in design *A* is shorter, and heat-biasing electrodes are located between

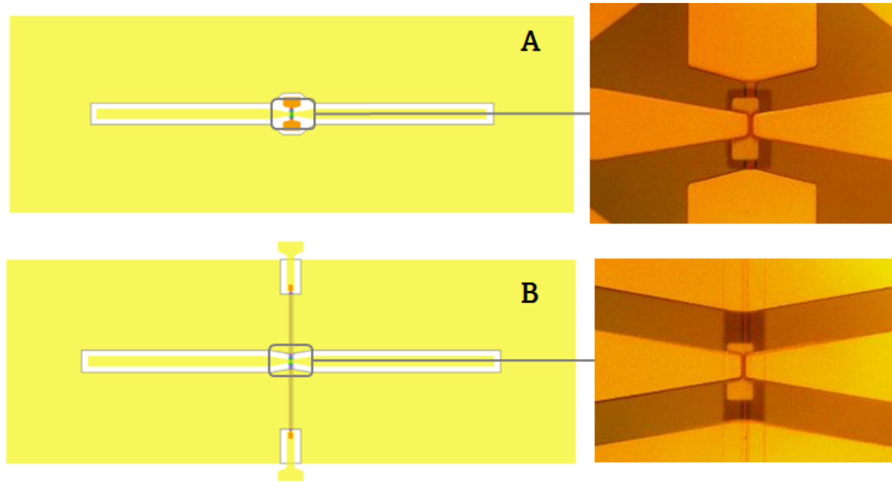

Figure 5.3: Two RF switch structures were designed (left), and the top view of the fabricated switches (right).

the RF signal line and the ground. On the other hand, design *B* keeps the CPW configuration the same for the entire length of the T-line, and the biasing pads are moved to the outside of the CPW's ground. Design *A* has a lower heat resistance, so less applied voltages can produce sufficient thermal energy, which is preferred. However, its RF performance will be poorer due to the parasitic capacitances in the switch via location. While in the design *B*, the heater is longer and requires higher biasing voltage to make the phase transition in the GeTe layer. Also, the produced heat would be distributed all over the heater length. As a result, the required electrical energy for the GeTe phase transform would be higher and produced thermal energy is less efficient compared to design *A*. Figure 5.4 illustrates a closer view of the switch via structure.

Heater shape and RF gap are critical parameters significantly impacting the device's performance. The heater's width and thickness define the required electrical energy to produce suitable heat bias. Although the heater

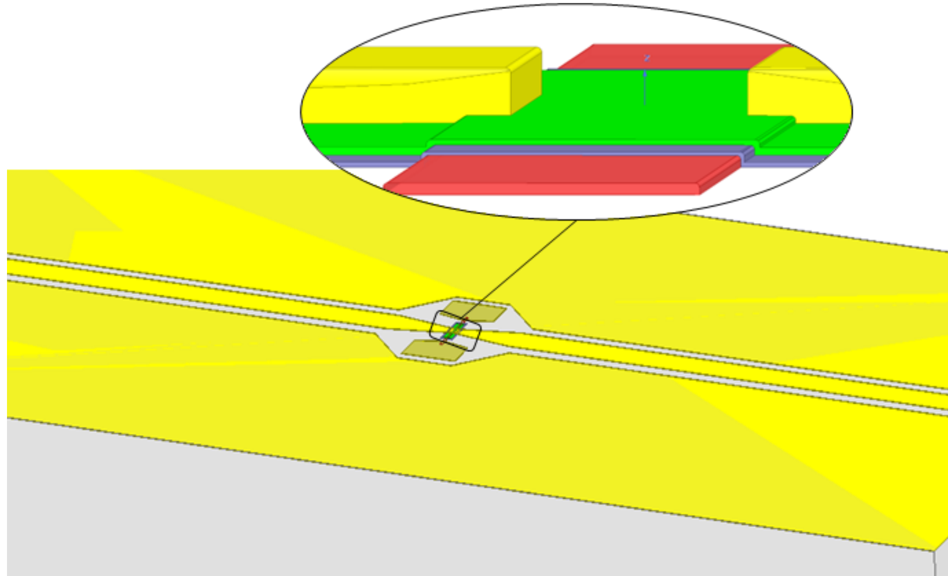

Figure 5.4: A 3D view of the designed RF switch.

width can decrease its resistance, which is preferred in terms of the required power to alter the switch state, the thermal energy efficiency will be affected as well. Figure 5.5 (a) and (b) show a sketch of a GeTe switch with two heater widths. In Figure 5.5 (a) with a wider heater, the produced heat was distributed over a larger area of the GeTe material, while in Figure 5.5 (b) with a narrower heater, the thermal energy is applied to a smaller amount of the PCM layer. As a result, the total volume of GeTe experience phase transitions during each cycle is reduced, and the switching speed will improve. Heater thickness affects the PCM layer profile and the switch performance. On the other hand, the thicker the heater layer, the lower its resistance and the lower the electrical voltage needed to generate the thermal energy. So, there is a trade-off between DC and RF efficiency. Based on the heater material's electrical properties (tungsten), a thickness of 100 nm would have low enough resistance for actuation purposes. So, the fabricated switches have

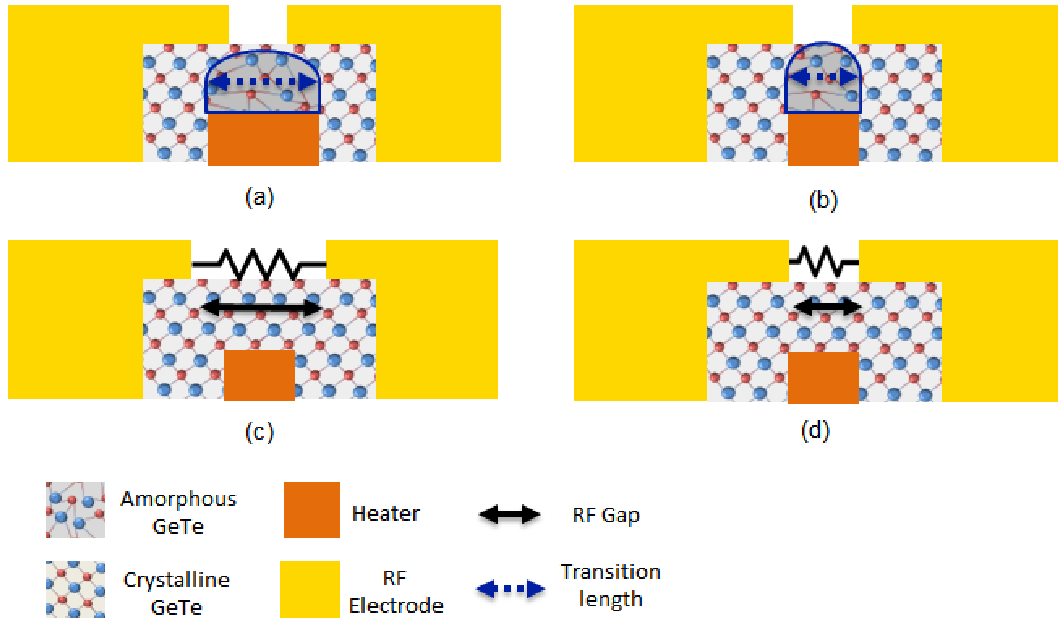

Figure 5.5: (a) and (b) show the RF switch relation to the heater width. (c) and (d) display the RF gap impact on the RF performance.

around 100 nm thickness.

The other crucial factor in the RF switch design is the RF gap. The RF gap is the distance between two RF electrodes, filling with switching PCM (GeTe). As mentioned before, copper's electrical conductivity is more than two orders of magnitude higher than that of GeTe in its low-resistance crystalline phase. This means that the less GeTe material in the RF signal path, the lower loss of the switch in the ON state. In other words, the narrower the RF gap, the lower the transmission loss. Figure 5.5 (c) and (d) show an illustration of a GeTe switch with two RF gaps; when the RF gap is larger, (a) RF signal has to pass through more material with higher resistance and therefore has higher loss compared to the case with shorter RF gap (b). Lower insertion loss in the ON state of an RF switch is a vital factor affecting its performance.

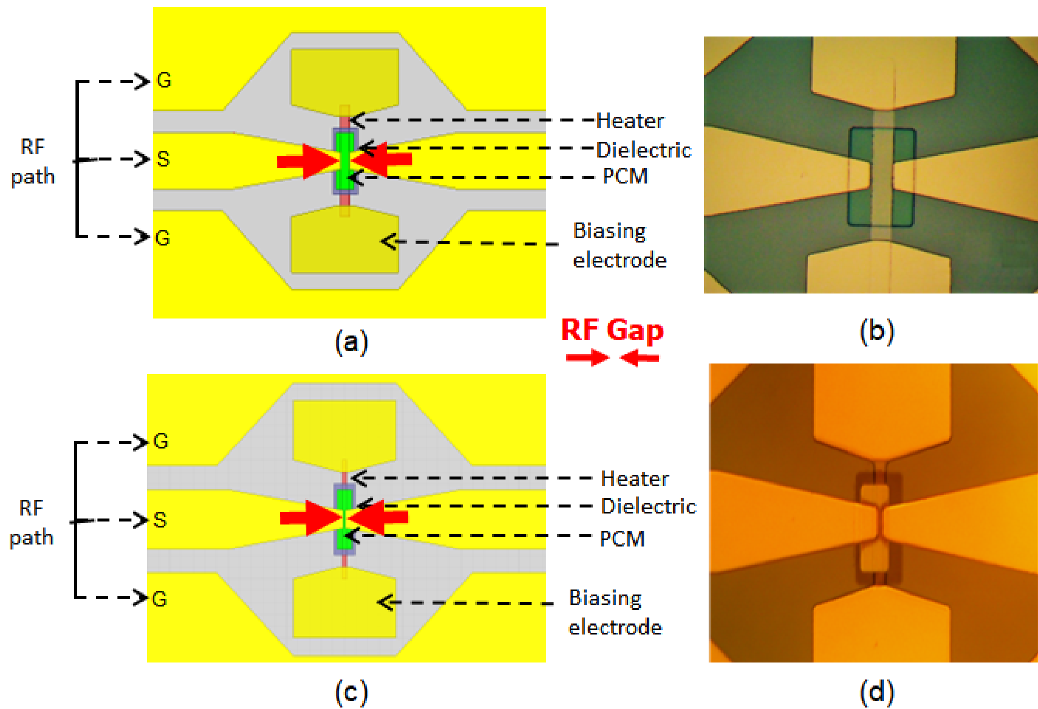

Figure 5.6: (a) Wide RF gap design, (b) fabricated switch with wide RF gap, (c) narrow RF gap design, and (d) fabricated switch with narrow RF gap.

A comparison between wide and narrow RF gaps in the PCM switch architecture is represented in Figure 5.6 (a) and (c), respectively. Figure 5.6 (b) and (d) show the actual fabricated RF switch for each of those two designs.

One approach for decreasing the PCM switch loss in the ON state would be increasing the GeTe thickness to minimize the RF gap's resistance. However, the thickness of the GeTe layer has a negative effect on the switch performance in the OFF state. Since the GeTe layer is initially in the crystalline phase, the phase change is only required in the RF gap. The GeTe in the RF gap section switches to amorphous and crystalline states, while the remaining GeTe film always holds the crystalline phase. The reset thermal energy produced by the heater must penetrate the entire thickness of the GeTe to

transform it into an amorphous state. By increasing the PCM layer thickness, the thermal energy should be distributed over a greater volume of GeTe material for transition between its phases. Otherwise, some portion of the GeTe layer on the top part remains in the crystalline state and provides a path for the RF signal in the OFF status. So, there is a trade-off between the actuation performance and the RF signal loss. The thicker the GeTe material, the more energy is required to transform its phase. Experiments demonstrated that the generated thermal energy by the designed heater is sufficient to penetrate to around 100 nm of GeTe thickness.

A 3D electromagnetic simulation using ANSYS HFSS was performed to design the CPW T-line and to estimate the GeTe via impedance and loss at the frequency band 1-20 GHz. The GeTe via impedance was derived by electromagnetic simulation for different GeTe thicknesses and RF gaps. Figure 5.7 (a) presents the simulation results for various RF gap and GeTe thicknesses while GeTe is in the crystalline state with the conductivity of 3.5×10^{5} S/m (2.8 $\mu\Omega\cdot$m resistivity). This plot indicates that the lowest loss relates to a shorter RF gap and a thicker GeTe layer. So, the PCM layer thickness was selected to 100 nm for fabrication. The designed switch structures had varied RF Gaps from 1 μm to 4 μm. Unfortunately, the minimum feature size with available material and equipment in the photolithography was larger than 2.5 μm, and switches with RF gaps smaller than 3 μm were short-circuited. So, the lowest RF gap that could be realized was 3 μm. This fabrication limitation greatly affected the RF switches' performance, which will be discussed in section 5.5. Figure 5.7 (b) shows the off-state isolation for the same RF gap and GeTe thicknesses assuming the GeTe conductivity is

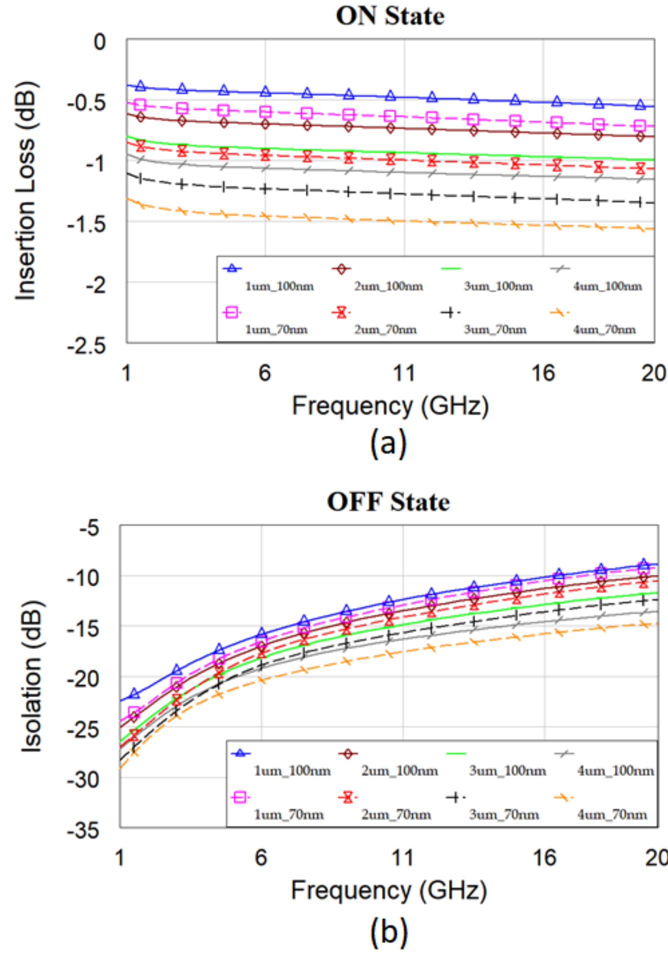

Figure 5.7: Simulated insertion loss of the switch in the (a) ON-state and (b) OFF state for different RF gap and GeTe thicknesses.

1×10^{3} S/m.

5.2 RF Switch Fabrication

The fabrication process included the deposition and patterning of thin-film materials for distinct purposes. The mask used for patterning each layer was designed with switch versions. Also, reference standards, like baselines

open-circuited and short-circuited switches, were included in the design. All layers in this work were patterned through lift-off. A negative photo-resist was used, and patterns were created by photo-lithography before the layer deposition followed by a lift-off process. After depositing each material (W, AlN, and GeTe), annealing was performed to enhance their crystal strictures.

5.2.1 Material Deposition

This section discusses the growth and patterning process for each material. The substrate used for this research was a 2 inch undoped high resistivity (100) silicon (Si) wafer. It had a thin layer of (3000 $\mathring{A}$) silicon dioxide (SiO_2) on it, purchased from WaferPro. High resistivity substrate improves the RF performance by reducing the coupling effects. The SiO_2 layer provides a boundary preventing DC current to leak into the substrate. All fabrications and experiments for this research were conducted in the University of Oklahoma's clean-room facility under the micro-fabrication research and education center. A process flow of the switch fabrication is shown in Figure 5.8.

5.2.1.1 Heater

The heater is the underlying layer that transforms electrical energy into thermal energy. The heater should be a good conductive material to decrease the expected electrical energy required to generate the appropriate thermal energy. In the early stages of fabrication, nickel-chrome (NiCr) was used for the heater layer. Although NiCr has good electrical conductivity and a straight-

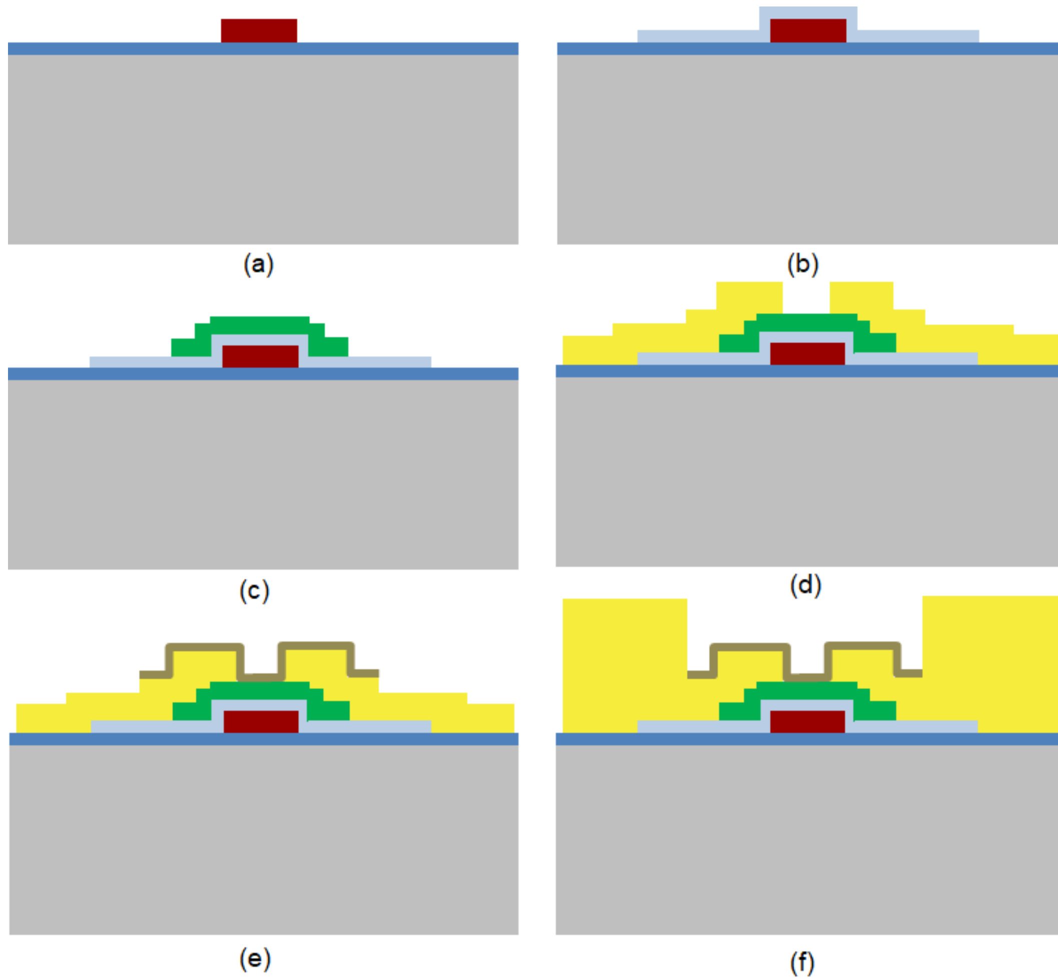

Figure 5.8: Fabrication process flow of the PCM RF switch, deposition and patterning of (a) heater layer, (b) dielectric layer, (c) PCM (GeTe) layer, (d) RF electrodes layer, (e) passivation layer, and (f) metal contacts layer.

forward fabrication process, its melting point is 1400°C, which is low for heater purposes. Since there is a barrier layer between the heater and PCM layers in the indirect heating structure, the heater temperature needs to increase higher than 1400°C to transfer enough heat to the PCM layer and increase its temperature to its melting point. This was tested experimentally to produce sufficient heat to melt GeTe during amorphization NiCr reached its melting point and deformed. A picture of the melted NiCr switch is shown in Figure 5.9. So, another important factor for selecting the material for the heater layer is its melting point should be much higher than the GeTe melting point. Considering both factors for heater material, The best candidates for the heater are Molybdenum (Mo) or Tungsten (W) with low bulk resistivity (53 nΩ·m = 5.3 $\mu\Omega$·cm), and high-temperature durability (melting points), 2900, and 3700°C respectively.

The first growth method tested for both Mo and W was E-beam deposition

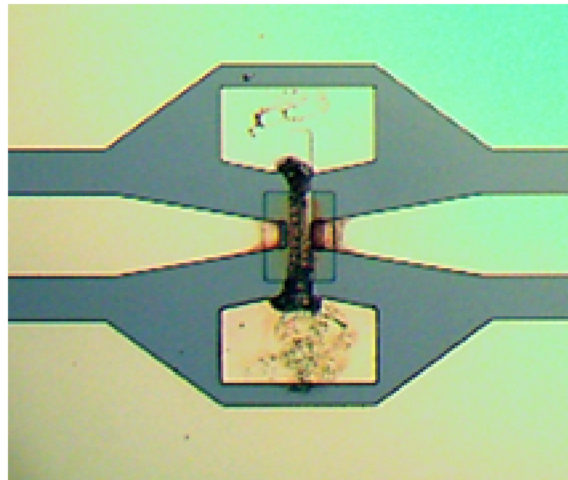

Figure 5.9: RF switch with NiCr heater melted and deformed after applying reset pulse.

and lift-off used for patterning. Due to the high temperature in the chamber

during deposition, the photo-resist (PR) was burnt. To solve this problem, wet chemical etching was tested for patterning W. The etchant type, ratio, and etch rate were found after several tests. However, the results were not so promising. The heater pattern was narrow compared to its thickness, and wet etching of the tungsten layer etched and removed either a large undercut or the tungsten had not been etched completely. The latter happened in one switch batch, and a skinny layer of W remained underneath all switches, resulting in all devices being short-circuited. As a result, the deposition method changed to sputtering. There are two phases of tungsten α and β, in which the low resistivity is related to the α one [89]. As-deposited W thin films can be either two phases or mixtures of both. Several sputtering depositions were conducted to find the thin-film tungsten with the lowest impurity and highest conductivity. The XRD results for some samples are shown in Figure 5.10. It has been revealed that the type of its phase is strongly related to the deposition parameters. Even though the higher sputtering power and higher pressure resulted in the appearance of α phase in the XRD results (Figure 5.10), still the β phase peak appears in the XRD results. Post-thermal annealing was performed on several samples to optimize the annealing parameters and reduce the resistivity. The thin-film resistivity is higher than the bulk resistivity and dependent on the thickness of the film [90]. The lowest W thin film resistivity reported was greater than 10 $\mu\Omega$·cm [91]. In this research, the best resistivity of as-grown W thin film, which has a combination of α and β phases, was $\sim$255 $\mu\Omega$·cm. Post-thermal annealing was operated in a vacuumed chamber and filled with Ar to 1 bar, resulting in its resistivity dropping to 49 $\mu\Omega$·cm. The annealing was conducted at 850°C for

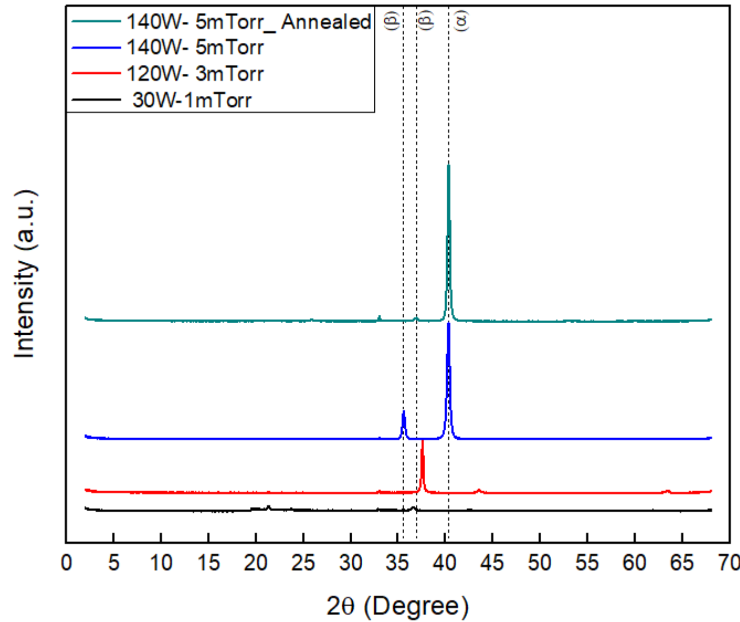

Figure 5.10: XRD results for W thin films deposited at different power and pressure and after annealing at 850°C for 1 hour.

60 min. This W thin-film was used for the heater, and lift-off patterning was performed between deposition and heat treatment.

5.2.1.2 Dielectric

The barrier layer that separates the heater and PCM layers has an important role by providing electrical insulation between the RF and actuation signals. The two critical criteria for this layer are high electrical insulation and thermal conduction. So, while providing good electrical isolation between RF and thermal paths, it conducts the most thermal energy from the heater to the PCM layer. At the early stages of fabrication, SiO_2 as an excellent dielectric material was used, providing good electrical insulation. However, it suffers from very low thermal conductivity (1.1 $Wm^{-1}K^{-1}$). The best

Table 5.1: Dielectric material properties and parameters.

Material	Thermal Conductivity (W/m.K)	Specific Heat Capacity (J/Kg.K)	Thermal Expansion Coefficient (1/K)
SiO_2	1.1	730	$0.5\times10^{-}6$
AlN	320	740	$4.5\times10^{-}6$

candidate for the dielectric layer with high electrical resistivity and thermal conductivity is aluminum nitride (AlN). Its thermal conductivity can be as high as 320 $Wm^{-1}K^{-1}$ [92]. Thermal properties of SiO_2 and AlN dielectric materials are compared in Table 5.1. The material properties depend on the material and crystalline qualities. The reported thermal conductivity in table 5.1 is the highest achieved for AlN and can be lower than these depending on material quality. As the PED deposition method was the concentration of this research for growing chalcogenide compositions, Also, it was tried to use PED to grow the AlN thin film. Several attempts were made, but depositing a smooth thin film of AlN by PED was unsuccessful. All the samples had a very high surface roughness. Figure 5.11 (a) shows the SEM picture of the top surface morphology of PED-grown AlN. Previous research on growing AlN using PED showed successful nano-wire AlN growth at low-temperature [64]. The smoothness of the AlN barrier layer is vital for the fundamental layer as it is underneath the GeTe layer. The PCM layer in an RF switch requires a smooth base underneath it. A smooth base is required for a high-quality PCM layer resulting in better crystallization. So, the PED-grown AlN thin film was unacceptable for the barrier layer.

After enhancing the PED chamber with the sputtering system, two different

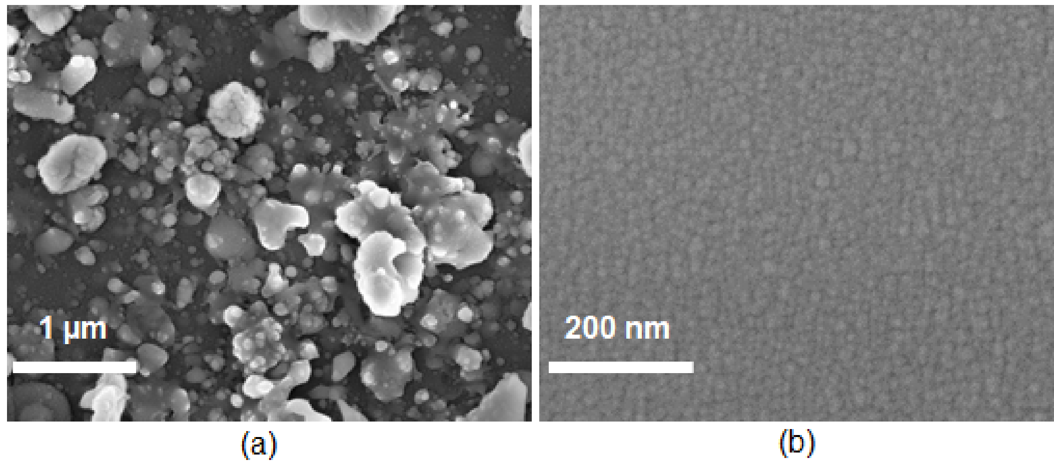

Figure 5.11: Top SEM view of AlN thin films deposited by (a) PED and (b) DC sputtering.

sputtering methods for AlN were investigated. RF sputtering using an AlN target, and DC sputtering with an Al target. The RF sputtering with insulator AlN target throughput was too low and hard to deposit. As a result, an alternative deposition method for AlN is the DC sputtering using an Al target in an Ar and N_2 gas combinations. Various parameters like the sputtering power, N2/Ar ratio, and pressure were tested to achieve the best film quality (surface morphology) with the highest electrical resistivity. Figure 5.11 (b) shows the top SEM view of the AlN thin film deposited with DC sputtering.

The essential factor for choosing AlN over other dielectric materials for the barrier layer was its reported high thermal conductivity. The thermal conductivity of AlN material tremendously depends on its crystal structure [93]. The reported thermal conductivity in Table 5.1 is for bulk AlN. The thin film AlN has lower thermal conductivity, reported between 25-120 $Wm^{-1}K^{-1}$ [94], [95] depending on the crystal structure and thickness. This is lower than bulk AlN but is still much higher than other available choices of dielectric

materials. The sputtered AlN thin film at low temperatures has a poor crystal quality, but post thermal annealing at a high temperature above 1600°C in N_2 ambient for about one hour can improve its crystal quality and therefore, its thermal conductivity [96], [97]. Unfortunately, the available furnace could not reach beyond 1000°C not more than 5 minutes. The sputtered and patterned AlN thin films were annealed at 850°C for 20 minutes to increase their crystallinity and, as a result, their thermal conductivity. XRD measurements were utilized to indicate AlN thin film crystal structure and quality. The post-thermal annealing conducted on AlN thin film helped to alter it towards the crystalline structure. Although a peak related to the crystalline plane (103) appeared in XRD results after annealing, this peak was weak and broad. One reason for poor crystalline quality can be the AlN thin film thickness, which is preferred to be thin due to the low barrier thickness required for RF PCM switch performance. The AlN layer thickness was 70 nm. The thermal and electrical characteristics of the achieved AlN thin film were sufficient for the purpose of the dielectric layer to isolate bias pulses from the RF signal.

5.2.1.3 Phase Change Material

The PCM layer in an RF PCM switch is the essential part, which changes between two phases and passes or rejects the RF signal. The early phase change RF switches were based on $Ge_2Sb_2Te_5$ composition, as it was investigated and used in memory application. However, the reported resistance of $Ge_2Sb_2Te_5$ in the crystalline state is around 5 kΩ [51]. This resistance is satisfactory for memory applications, but an RF switch requires much lower

R_{on} amount for acceptable performance in terms of insertion loss. Between all chalcogenides material compositions, GeTe offers the highest contrast between its two stable states regarding electrical resistivity [35], [36], [41]. More importantly, GeTe has the lowest resistance in the crystalline state, as well as the lowest crystallization temperature and very fast crystallization speed [41]. This means that a low-loss RF switch with minor actuation power can be realized using GeTe material.

The amorphous GeTe deposited with PED at room temperature. The deposition of GeTe thin film on a Si substrate was investigated in Chapter 3. The same deposition parameters were used to grow the GeTe layer in an RF switch configuration. Lift-off was the patterning method for GeTe. GeTe had poor adhesion to the AlN layer, and the lift-off process caused GeTe to peel off from the underneath layer (AlN). This problem was dealt with by post-thermal annealing of the AlN layer. However, other research showed that AlN is not a good candidate for GeTe as its crystallization depends strongly on the seed layer crystal quality and structure [98].

The GeTe thin film was crystallized through post-thermal annealing with the conditions discussed in Chapter 4. The exception was that the seed layer had been changed from Si to AlN. The realized GeTe had higher electrical resistivity compared to what was achieved before with Si substrate. As discussed, the AlN layer did not have a strong crystal quality, which resulted in lower crystal quality of GeTe on top of that. Respectively, the electrical conductivity of the GeTe was affected and decreased. The measured conductivity of crystallized GeTe in a switch configuration was 1×10^5 S/m which is more than three times lower than what was previously extracted (3.5×10^5 S/m).

Although it was presumed that the RF loss would be higher than what the switches were designed based on, the difference between GeTe electrical conductivity in its two phases is still high enough to be used in an RF switch.

5.2.1.4 RF Electrode

The RF electrodes should be an excellent conductor to transmit the RF signal with the lowest loss possible. The other important factor in high-frequency designs is skin depth, which implies the thickness of the conductor materials as well as the surface smoothness. The skin effect indicates the high-frequency current tendency to flow at the conductor's surface, and it is a function of frequency. The higher the frequency, the lower the skin depth. This means that the surface smoothness of the conductor is critical at RF frequencies. On the other hand, the conductor thickness should be at least five times the skin depth at the lowest frequency for good performance. The conductor material was copper (Cu), which was covered by a thinner layer of gold (Au) to protect it from oxidation. The Cu/Au thickness ratio was around 80/20%. Also, a 10 nm titanium layer was used below each for better adhesion and making better contact. The deposition method to grow metal (Ti/Cu/Ti/Au) was thermal evaporation, and lift-off was the patterning method.

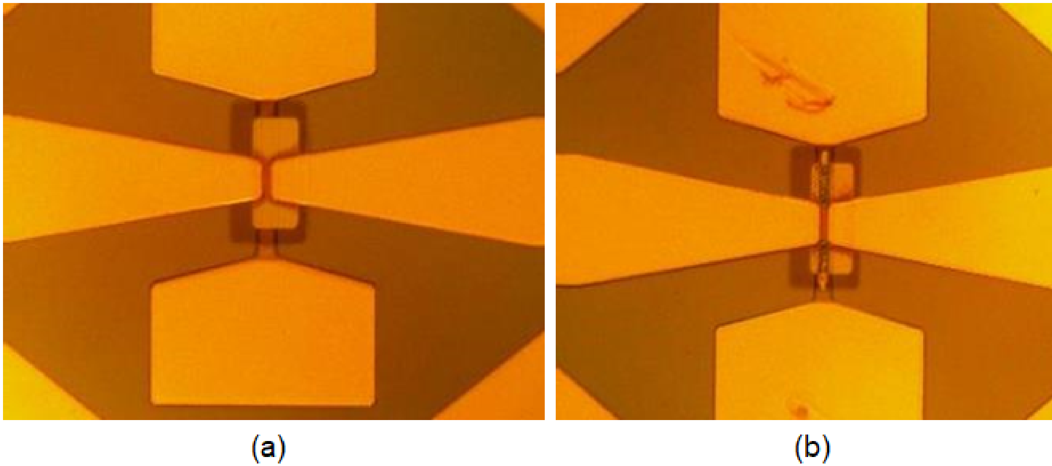

Figure 5.12: (a) Top view of the switch before testing, (b) oxidized GeTe after pulse applied.

5.2.1.5 Passivation

GeTe has a high tendency to oxidize. During switching and in the presence of heat, if it has not been protected from the air (O_2) and has contact with air, GeTe will oxidize and deform. Generally, a passivation layer to protect GeTe against oxidization is critical. The GeTe oxidation and deformation by applying the OFF pulse, without the passivation layer, is shown in Figure 5.12. A thin layer of dielectric material was deposited on top of the GeTe via and after electrode fabrication to tackle this problem. The materials tested for the passivation layer were SiO_2 and AlN, both deposited by sputtering.

5.3 Electrical and RF Testing

After designing and fabricating the RF switches, they have to be tested and checked for their performance. All measurements in this work were per-

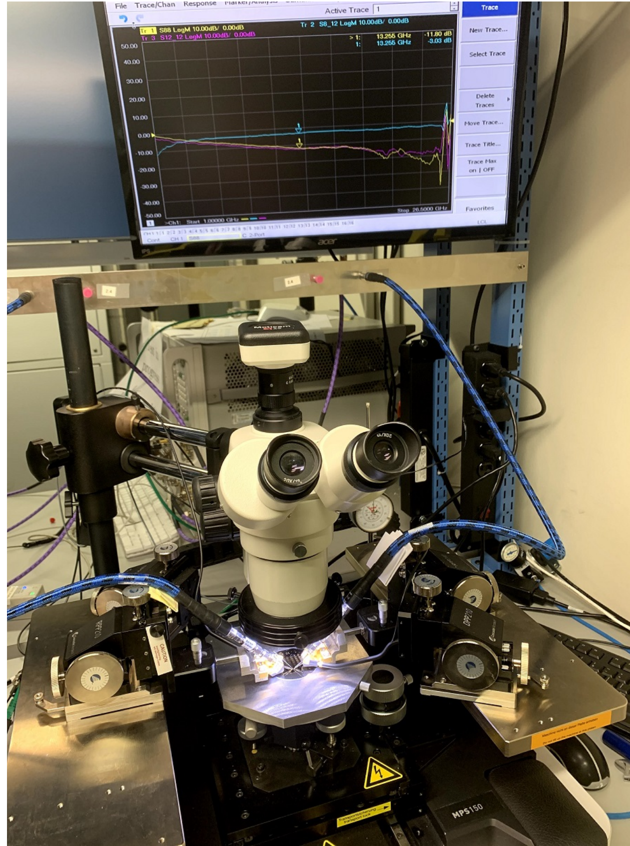

Figure 5.13: RF measurement setup.

formed at room temperature, and the devices were tested using a Cascade Microtech probe station with G-S-G air-coplanar probes. All measurements were conducted using an Agilent performance network analyzer (PNA). The PNA was calibrated with the short-open-load-through (SOLT) method with the Cascade calibration substrate. Two air-coplanar (ACP50) RF probes with the ground-signal-ground (GSG) configuration were used. The probe station and the measurement set-up are shown in Figure 5.13. A closer view of the switches under test, while RF and DC probes are connected, is shown in Figure 5.14. First, the reference standards were tested to verify that the con-

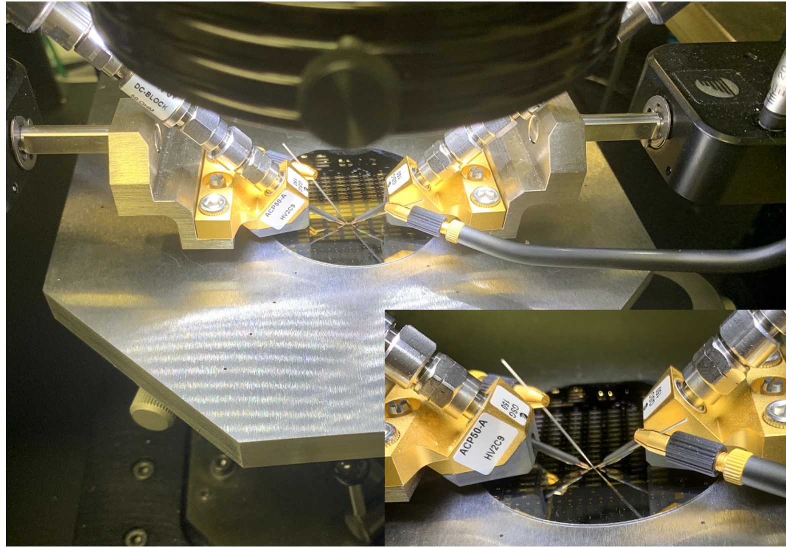

Figure 5.14: Switch with DC and RF probes are connected under the test.

ductor film quality was acceptable by testing the shorted reference. Also, the open reference provides insight into the performance of the silicon substrate and the maximum achievable isolation. Before applying any heat pulses, the initial resistance of GeTe between two RF electrodes was measured, and the GeTe conductivity was calculated based on it and the GeTe via size. The measured resistance was 20 Ω for 3 μm RF gap and 100 nm GeTe thickness. The switch width was 15 μm, which leads to 10 $\mu\Omega\cdot$m resistivity (ρ). The heater resistance for different switch structures was also measured, and the required pulse amplitude to produce sufficient heat was calculated. The RF measurements of the PCM switches followed this. Figure 5.15 shows the ideal set/reset electric pulses and the applied temperature profiles. The total duration of the set pulse was around 4.5 μs with an amplitude of 5.3 V. The reset pulse has around 10 ns and 11 V time and amplitude, respectively. So, the switching speed of the designed switch was 0.22 MHz. After

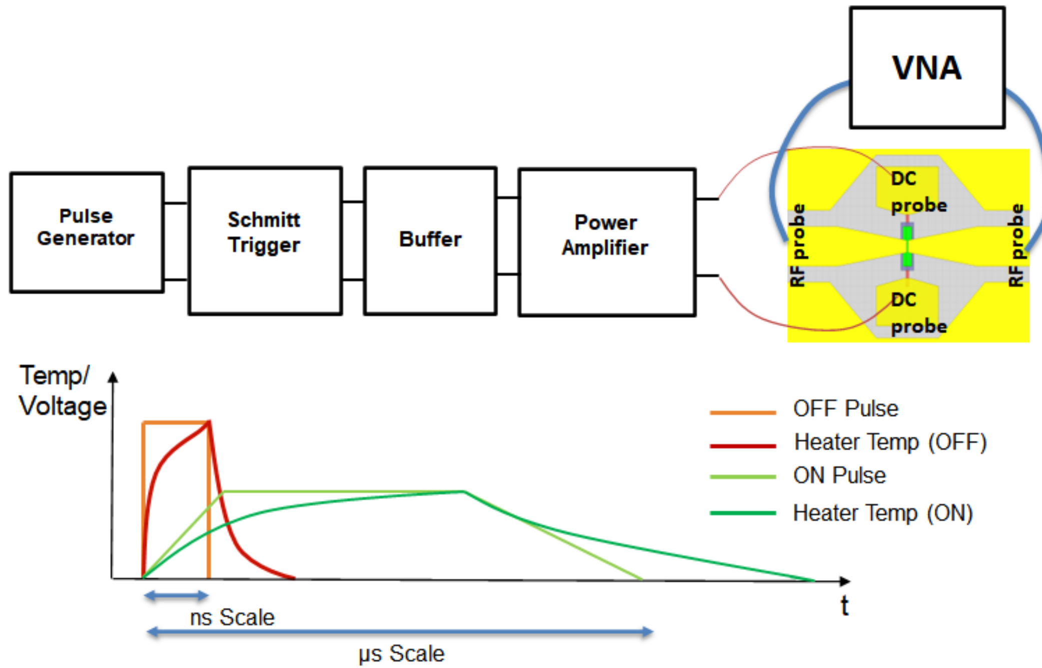

Figure 5.15: Indirect heating switch actuation circuit diagram.

the actuation pulse was applied, DC probes were disconnected during the RF measurements. Some issues were discovered during the fabrication and measurements of the switches, and the switch fabrication process and the material quality were modified after each run to improve the RF and switching responses. However, there was some limitation on the available equipment, which will be discussed later. Some of these issues are summarized in Table 5.2.

5.4 Device Model

Since fabrication and testing are the only approaches to demonstrate the RF switches' performances, a proper model can facilitate understanding the

Table 5.2: Summary of issues and solutions for the fabricated RF switches.

Switch Type	**Problem**	**Solution**
Indirect Heating Switch	Large RF gap	Design new mask
	Etching W layer	Revise the W sputtering and replace etching with lift-off
	GeTe oxidation during actuation	Add passivation layer
	Passivation layer quality	Replace SiO_2 with AlN as passivation layer
	Producing short enough pulse for OFF pulse	Revise test equipment

effects of each parameter on the design. The model for an ideal RF switch would be a resistor in the ON state (R_{ON}) and a capacitor in the OFF state (C_{OFF}). The GeTe resistivity in the crystalline state specifies the switch R_{ON}. C_{OFF} is the total capacitance of GeTe via in the amorphous state. These two parameters are essential to determine the cut-off frequency (f_{CO}) as the Equation 5.1 shows:

$$f_{CO} = \frac{1}{2\pi R_{ON} C_{OFF}} \tag{5.1}$$

A two-port network model of the switch has been generated to de-embed the parasitic elements' effects. Figure 5.16 (a) displays the designed GeTe switch structure and its equivalent network model. In this model, the parasitic effects of the pads and traces of the device under test (*DUT*) were

modeled as a parallel admittance (Y_p) and a series impedance (Z_s) on each side of the switch section and labeled as *I* and *II*. The switch (*Sw*) is modeled as three parallel admittances, including the heater structure (Y_h), GeTe via (Y_{GeTe}), and admittance between RF traces above the GeTe layer (Y_t). The admittance of *Sw* is equal to the sum of these three admittances (Equation 5.2).

$$Y_{Sw} = Y_t + Y_{GeTe} + Y_h \tag{5.2}$$

The *DUT*'s transmission (ABCD) matrix can be extracted from the measured scattering parameters (S-parameters). As three sections of *I*, *Sw*, and *II* are cascaded, the product of their ABCD parameters' matrices equals ABCD parameters of the *DUT* as shown in Equation 5.3.

$$ABCD_{DUT} = ABCD_I \times ABCD_{Sw} \times ABCD_{II} \tag{5.3}$$

Two structures of the designed RF switch with eliminating GeTe layer have been fabricated and measured to de-embed the parasitic elements. The RF gap in the first one is zero, and the RF traces make a short circuit. Also, the heater and barrier layers have been omitted. The short circuit configuration and related two-port network are shown in Figure 5.16 (b). The measured S-parameter of the short circuit configuration was converted to the equivalent Y-matrix. Similarly, Equation 5.4 presents the Y-matrix of the short circuit network model illustrated in Figure 5.16 (b). Comparing these two, Y_p and

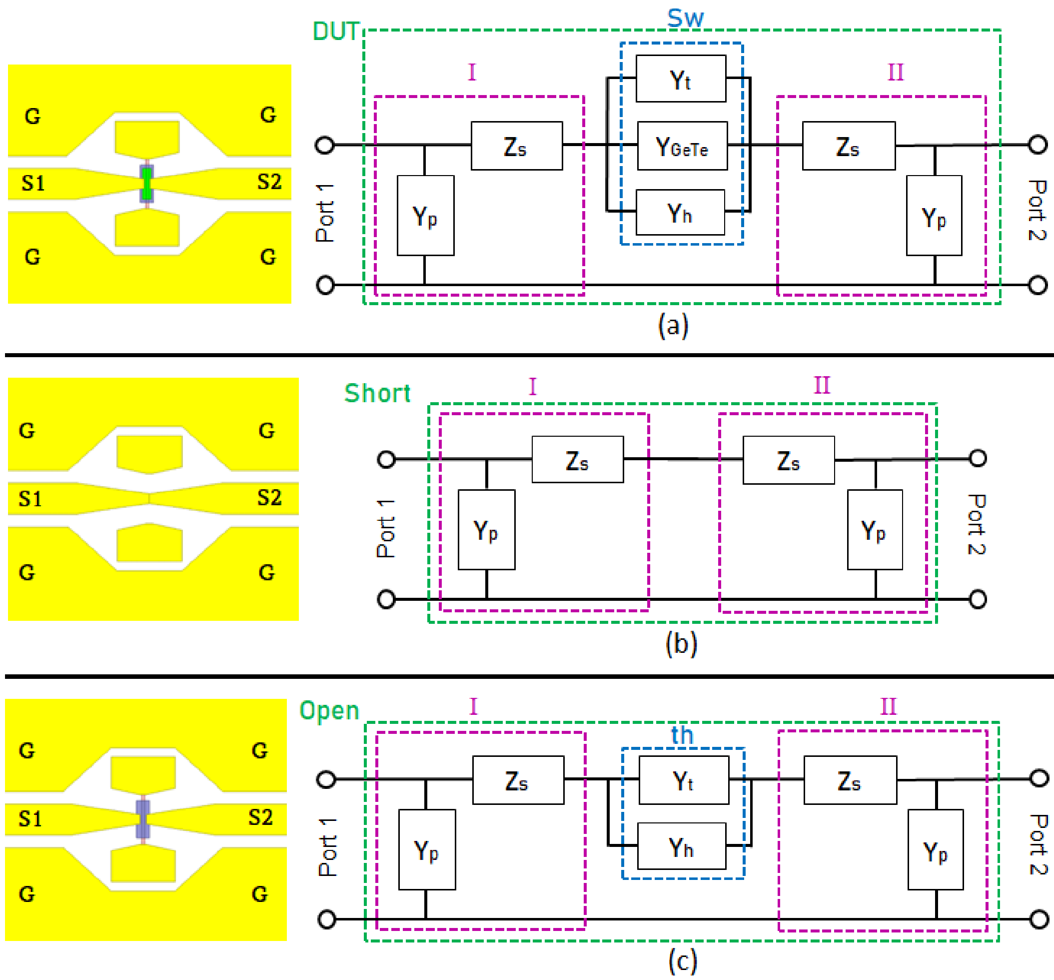

Figure 5.16: Structures and two-port network models of the (a) GeTe switch, (b) open, and (c) short circuit.

Z_s can be calculated from Equations 5.5 and 5.6, respectively.

$$Y_{Short} = \begin{bmatrix} Y_p + \frac{1}{2Z_s} & \frac{-1}{2Z_s} \\ \frac{-1}{2Z_s} & Y_p + \frac{1}{2Z_s} \end{bmatrix} \tag{5.4}$$

$$Y_p = Y_{11-Short} + Y_{21-Short} \tag{5.5}$$

$$Z_s = \frac{-1}{2Y_{21-Short}} \tag{5.6}$$

The second architecture is an open circuit, while the RF gap has not filled with GeTe material, but it contains heater and barrier layers. Figure 5.16 (c) shows this structure and the related two-port network. The open circuit network is cascaded from three sections, *I*, *th*, and *II*, in which "*th*" denotes the RF gap and heater admittances ($Y_{th} = Y_t + Y_h$). The ABCD parameters of sections *I* and *II* are shown in Equations 5.7 and 5.8, respectively.

$$ABCD_I = \begin{bmatrix} 1 & Z_s \\ Y_p & 1 + Y_p Z_s \end{bmatrix} \tag{5.7}$$

$$ABCD_{II} = \begin{bmatrix} 1 + Y_p Z_s & Z_s \\ Y_p & 1 \end{bmatrix} \tag{5.8}$$

So, $ABCD_I$ and $ABCD_{II}$ were derived from Equations 5.5 to 5.8. Also, by converting measured S-parameters from the open structure to ABCD param-

eters, $ABCD_{Open}$ was determined. Equation 5.9 shows the ABCD parameters for the open configuration, which leads to the $ABCD_{th}$ matrix from Equation 5.10.

$$ABCD_{Open} = ABCD_I \times ABCD_{th} \times ABCD_{II} \tag{5.9}$$

$$ABCD_{th} = ABCD_I^{-1} \times ABCD_{Open} \times ABCD_{II}^{-1} \tag{5.10}$$

Converting the ABCD matrix to Y matrix gives Y_{th}. Also, $ABCD_{Sw}$ can be derived from Equation 5.3 as:

$$ABCD_{Sw} = ABCD_I^{-1} \times ABCD_{DUT} \times ABCD_{II}^{-1} \tag{5.11}$$

Finally, Y_{GeTe} will be derived from Equation 5.12.

$$Y_{Sw} - Y_{th} = Y_{GeTe} \tag{5.12}$$

Considering the switch model as an ideal switch with a resistor (R_{ON}) in parallel with a capacitor (C_{OFF}), these values and cutoff frequency can be determined from Y_{GeTe}. This de-embedding strategy was used to extract R_{ON} and C_{OFF} to find the cut-off frequency.

5.5 Results and Discussion

The GeTe layer was crystallized by post-thermal annealing during the switch production. Therefore, all switches were initially in the ON state. Before

applying any pulses, the resistivity of the GeTe via was calculated based on the switch dimensions and its measured resistance. The measured resistivity is around 10 $\mu\Omega \cdot m$, three times higher than the GeTe thin film resistivity achieved on top of the silicon wafer. The growth and crystallization parameters of the GeTe material for both experiments were the same. Their seed layers' are the main difference between the GeTe film in the RF switch configuration and the studied one in chapter 4. A 100 Si wafer was used to grow the GeTe layer for the crystallization study, while in the switch structure, AlN was the underneath layer. The purpose of the AlN layer as the barrier was to provide electrical isolation between RF and actuation heat paths while delivering the thermal energy produced heat by the heater to the GeTe layer fast and efficiently. The quality of GeTe film has a vital role in the RF switches' performance, and specifically, its crystal quality depends on its seed layer crystal quality [99], [100]. One major issue during fabrication was the poor adhesion of the GeTe thin film to the AlN layer, which caused the GeTe film to peel off during the lift-off process. As discussed, the AlN layer was amorphous as deposited, and the equipment to supply proper heat treatment for crystallization was unavailable. The crystallization AlN temperature is around 1600°C in a vacuumed furnace filled with N_2 for over one hour. In comparison, the feasible thermal annealer can not reach the required temperature. The heat treatment for the AlN layer at 850°C for 20 min improved the quality, and the GeTe adhesion problem has been solved. Also, one of the associated peaks for crystalline AlN appeared in the XRD measurements after annealing. However, this peak was weak and broad, which means that the AlN layer was not fully crystallized. Ex-

periments showed that the composed AlN material's thermal conductivity is high enough to transfer the required heat to the GeTe layer. Still, the crystallized GeTe on top of the AlN has around three times more resistivity than the one on top of Si. Other research indicated that AlN is a poor choice as an underlying layer for GeTe [98]. Besides, due to the large RF gap from the minimum feature size from the photolithography, the achieved switches' insertion loss is higher than the designed switches.

The RF performance of the switches was measured, and the de-embedding mechanism discussed in section 5.4 was used to extract the GeTe via RF performance and eliminate the parasitic elements' effects. Measured, de-embedded, and related simulation results in the ON and OFF states of switches are displayed in Figure 5.17. Figure 5.17 (a) shows the switches insertion loss in the ON state. While the higher frequency performance agrees with the simulation data, the low-frequency results show more loss which has a reverse relation to frequency. Deriving the lumped element model of the switch can facilitate understanding the switch's behavior and evaluating its performance. Figure 5.17 (b) presents the GeTe switch OFF state isolation between input and output for measured, de-embedded, and simulation data. The OFF state RF performance is good and below -18 dB for 1-20 GHz bandwidth. The next section will propose the lumped circuit model of the GeTe RF switch, and the switch's performance will be characterized.

5.5.1 Circuit Model

The physical PCM switch with the biasing pads, heater structure, and traces connecting to the switching element (GeTe via) affect the RF switch perfor-

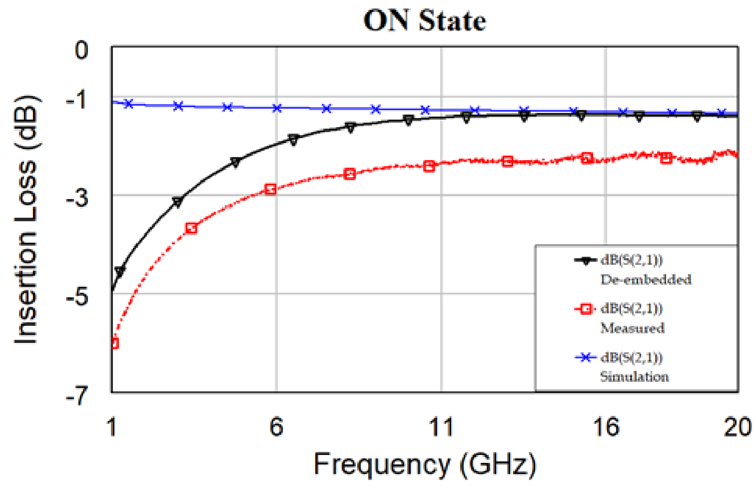

(a)

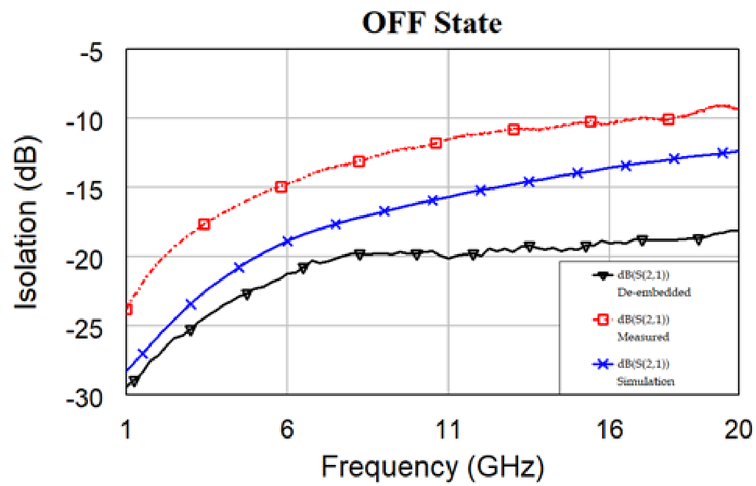

(b)

Figure 5.17: Measured, simulated, and de-embedded the GeTe RF switch (a) insertion loss at the ON state and (b) isolation at the OFF state.

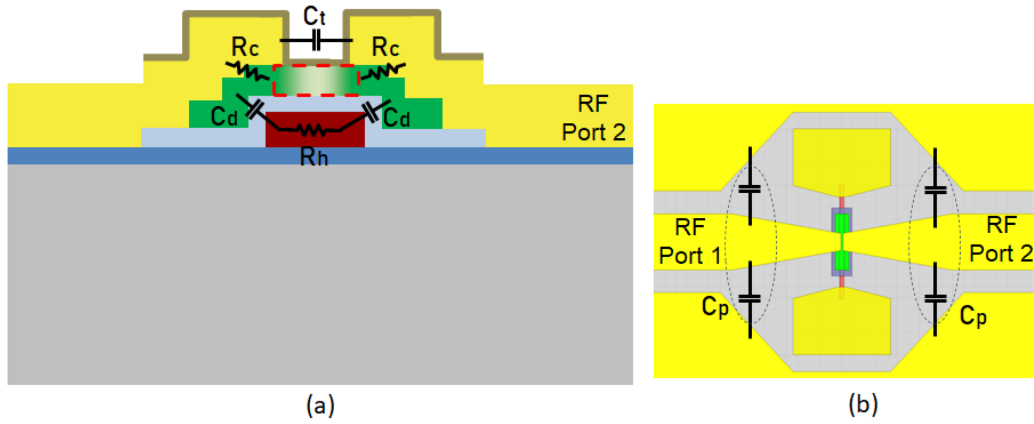

Figure 5.18: Schematic of the GeTe switch and lumped-element model (a) cross-section, (b) top view.

mance, and their effects should be considered. A cross-section and top view of the designed PCM switch are shown in Figure 5.18 (a) and (b), respectively. The parasitic circuit elements that contribute the most to the equivalent lumped-element model are labeled in this figure, and a red dashed square displays the GeTe via. In Figure 5.18 (a), R_c represents the contact resistance between the metal electrodes and the GeTe layer as well as the RF electrodes' resistance. R_h denotes the resistance from the heater itself. C_d represents the capacitance between each RF trace and the heater. The value of this capacitance depends on the dielectric material properties and thickness. C_t displays the capacitance between two RF terminals, and the RF gap defines its value. Finally, C_p in Figure 5.18 (b) is the capacitance between the RF electrodes and ground in the CPW structure. These lumped elements are shown in Figure 5.19 in a circuit configuration. The RF switches behavior was analyzed to determine the GeTe-via model.

Figure 5.19 exhibits the suggested circuit model for the PCM switch in the

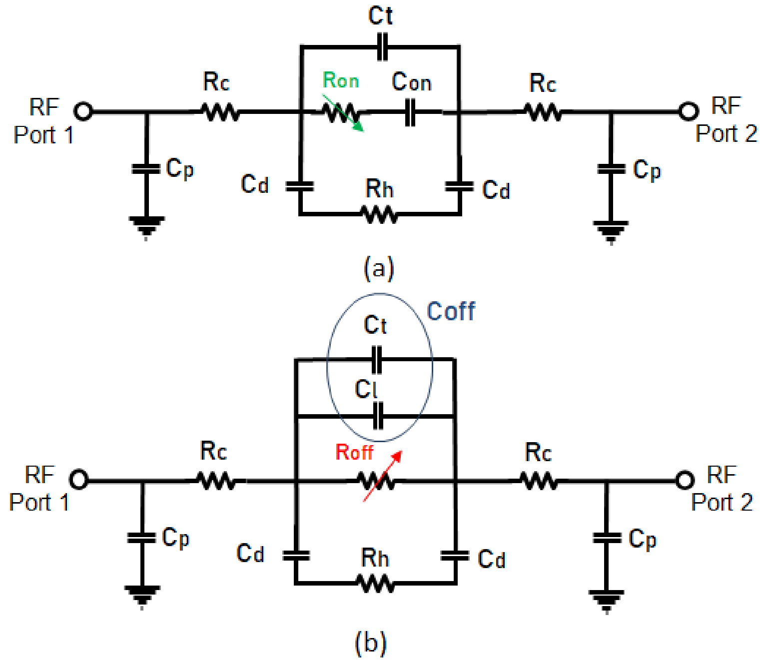

Figure 5.19: Equivalent lumped-element model of a GeTe switch in the (a) ON state, (b) OFF state.

four-terminal, indirect heating structure regarding all parasitic components in both ON and OFF states. The measured RF results of the switch, before de-embedding, which are shown in Figure 5.17 with dashed red lines, are considered to propose the lumped circuit model for the designed GeTe switch. The proposed model was derived based on the switch structure, materials' properties, and geometry. This research's primary area of interest is the GeTe via, which wanted to investigate its circuit model to comprehend its behavior. Therefore, the de-embedded data from Figure 5.17 were considered to extract the GeTe via model.

An ideal switch model is a resistance in parallel with a capacitance. In the ON state (crystalline phase), the resistance is low, and it is the primary

RF signal path; when it switches to the OFF state, the resistance increases, and the parallel capacitance becomes the RF path between two terminals. Figure 5.19 (a) demonstrates the switch model in the ON state, and the resistivity of the PCM (GeTe) specifies the R_{on}. The obtained switch performance in the ON state suggests that the GeTe via does not perform like just a resistance. The higher transmission loss in the lower frequency indicates there is a series capacitance in the RF signal path. The effect of this capacitance is dominant in the lower frequencies. By increasing the frequency, Its reactance drops, and the channel behaves like a resistance, as expected. C_{on} is the intrinsic capacitance from the GeTe via. This capacitance is derived from the measured responses of the switch, and it is believed that it comes from the poly-crystalline structure of the GeTe material. As discussed, the GeTe thin film in the switch structure, and on top of the AlN layer, is not fully crystallized and has a poly-crystalline structure. The poly-crystalline GeTe has an intrinsic capacitance (C_{on}) in series with the GeTe via resistance (R_{on}). The effect of this capacitance is negligible in the OFF state, while the series resistor has a large value. However, its effect is significant with the small series resistor in the ON state (Figure 5.19 (a)). Therefore, in Figure 5.19 (a) R_{on} and C_{on} represent the resistance and capacitance of the crystalline GeTe, respectively. Figure 5.20 shows the S-parameters results from the circuit model and compares them to the measured results.

To change the GeTe state to amorphous, a short voltage pulse, as shown in Figure 5.15 (orange line), was applied across the DC terminals. The OFF pulse amplitude should be high enough to produce the required heat to melt GeTe material in the RF gap area. At the same time, this pulse needs to be

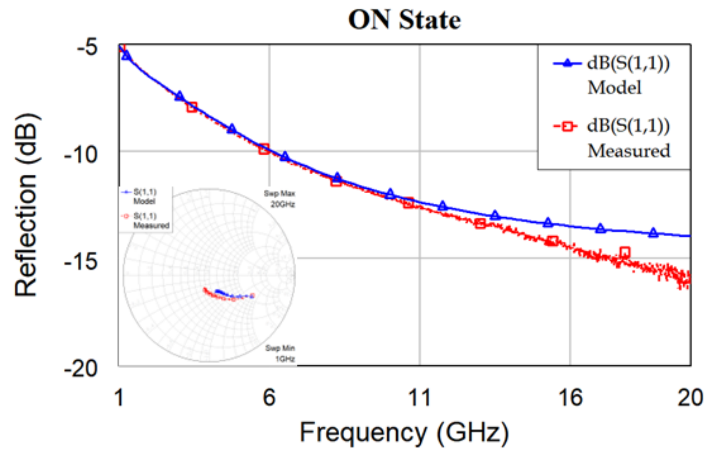

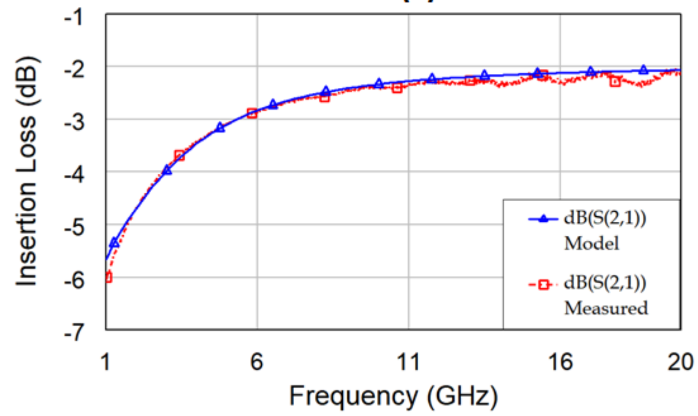

Figure 5.20: Measured and the model RF responses of the GeTe RF switch (a) reflection coefficient (S11) and (b) insertion loss (S21) in the ON state.

short with a very rapid fall time to quench the melted GeTe atoms in a disoriented structure. One of the struggles of this work was the realization of such a pulse. The available equipment did not have such ability, so a circuit with four blocks was designed and realized (Figure 5.15) to achieve the OFF pulse with 11.2 V and 10 ns duration, which was required to change the GeTe phase to amorphous. Applying this OFF pulse increased the transmission loss, as shown in Figure 5.21, and the switch turned OFF. The lumped circuit model of the GeTe switch OFF state was derived from the measured results. As GeTe turned to an amorphous phase, the R_{off} rises, and the parallel C_l, which models the GeTe via capacitance in the amorphous form, becomes the dominant element to specify the RF isolation. The sum of C_l and C_t (capacitance between RF terminals) is the capacitance associated with the OFF state C_{off}. The R_{off} and C_{off} in the Figure 5.19 (b) model the OFF state resistance and capacitance, respectively. The measured and the circuit model S-parameters results are compared in Figure 5.21.

The C_l models the GeTe via capacitance in the amorphous form. The lumped-element model introduced in Figure 5.19 helps to understand the GeTe RF switch behavior in both ON and OFF states. The higher insertion loss in the ON state comes from fabrication limitations, like the lithography minimum feature size, which is more than three times higher than reported by other researchers [101]–[103]. Moreover, the AlN thin film showed that it is not a suitable base layer for GeTe. Although it provides suitable electrical isolation and thermal conductivity, it has a rough surface morphology and poor crystalline quality. The GeTe thin film grown on top of the deposited AlN had around three times higher resistivity than what was achieved on Si. On the

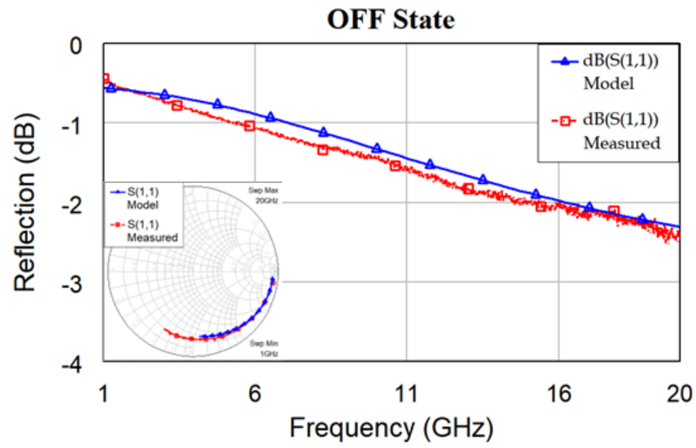

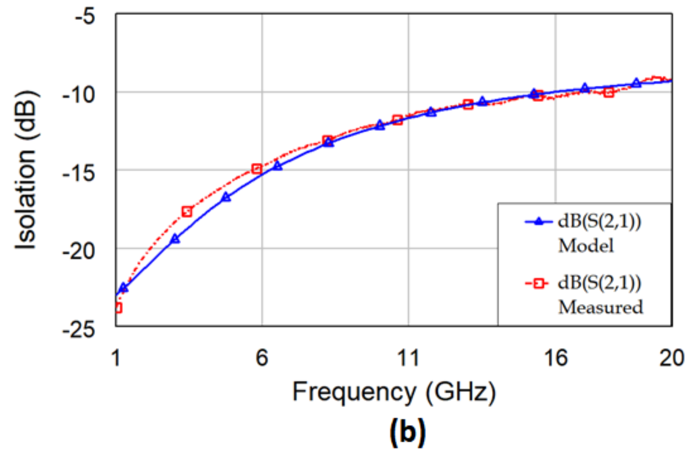

Figure 5.21: Measured and equivalent model RF response of the GeTe RF switch (a) reflection coefficient (S11) and (b) insertion loss (S21) at the OFF-state.

other hand, the AlN layer is a poor choice of seed layer for GeTe. The switch RF results and higher GeTe electrical resistivity shows that the GeTe thin film turned into a poly-crystalline structure by annealing. So, the RF performances of the switch in lower frequencies can be explained by the effect of capacitance in the GeTe-via poly-crystalline structure. Figure 5.22 illustrates a schematic of the switch, emphasizing the GeTe crystalline quality in each state. It is essential to understand that all the materials and structures have crucial effects on the RF switch, and improving the fabrication is the primary key to enhance the RF performance.

Also, some parasitic components affected the RF response in the OFF state. For instance, C_d, the capacitance between the RF terminals and the heater path. This capacitance value depends on the design structure, like the dielectric thickness and how much the heater and RF electrodes overlay. Both of these parameters were optimized for thermal efficiency, a thinner barrier layer, better heat delivery, and wider the heater, lower actuation voltage required. While these are to the benefit of higher parasitic capacitance C_d and resulted in lower signal rejection in the higher frequencies.

5.6 Summary

This chapter demonstrated nonvolatile RF switches based on the chalcogenide material deposited for the first time using a novel method called PED. The designed RF switch was introduced, and the functionality of each feature was discussed. The materials have been chosen based on their electrical and thermal properties to serve a specific role in the phase transition of PCM and

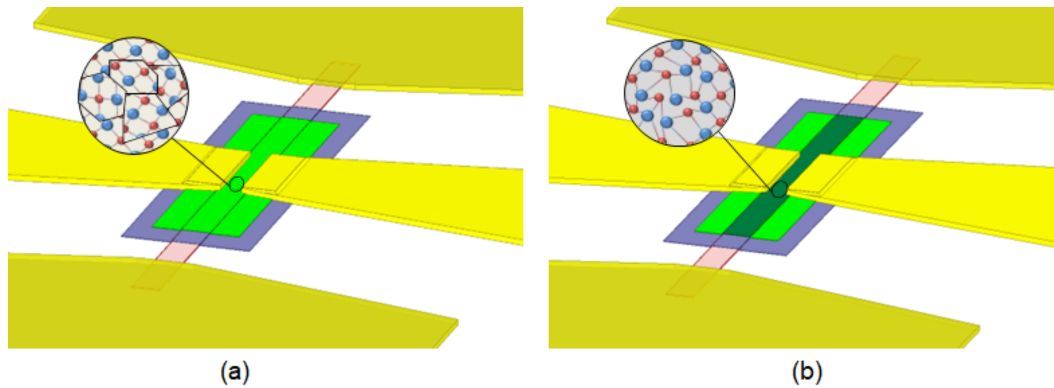

Figure 5.22: Switch schematic in (a) the initial state GeTe poly-crystalline, (b) GeTe amorphous in the RF gap after applying reset pulse.

efficient switching. The designed switches are fabricated using photolithography and lift-off techniques in the university clean room. The fabrication limitations were evaluated, and their effects on the switch RF performance were explained. A four-terminal, indirectly heated PCM switch was successfully fabricated and tested up to 20 GHz. The GeTe material grown and prepared for the first time with the PED technique demonstrated switching between conductor and insulator with 19 dB variation in the S21. The RF switch prepared based on that showed functionality and promising capability for RF reconfigurability.

Chapter 6

Conclusions and Future Directions

6.1 Conclusions

The research has been discussed in this dissertation explored the utilization of phase change material in the RF application. For this purpose, the GeTe has been chosen among different GST compounds as it has some advantages beneficial for RF applications, like fast switching. The GeTe thin film in the amorphous phase is a good insulator and, in the crystalline phase, is a good conductor. PCM has been used in RF switches to take advantage of this feature in the RF application. An RF switch is essential in RF reconfigurability systems, which is vital in today's life. Growing a high-quality thin film of PCM is the first and key step to achieving a reliable RF switch. The goal was to grow a high-quality chalcogenide material with a high $R_{Amorphous}/R_{Crystalline}$ ratio.

The primary contribution achieved during this study was utilizing the PED method, for the first time, to grow GeTe thin films. The pulsed electron-beam deposition has some advantages over other currently used deposition techniques, which makes it a suitable alternative for growing PCM. The growth

parameters have been optimized to obtain GeTe thin films with a smooth surface morphology and adjust the ratio of fundamental elements. The other benefit is a Low-temperature deposition and the ability to use the lift-off method for shaping. The GeTe thin film with a 50:50 elements ratio also has a smooth and uniform surface morphology, which is critical for high-frequency signal loss.

The GeTe deposited by PED is in an amorphous phase. It has been discussed the reason for it is necessary for the PCM section in a switch configuration to be in crystalline format. Crystallization technique by thermal annealer has been characterized, and one of the lowest electrical resistivity of GeTe has been achieved. The lowest crystalline state resistivity that has been reported is $2\ \mu\Omega\cdot$ m [29], which is slightly lower than the accomplished in this research ($2.8\ \mu\Omega\cdot$ m). The resistivity of the conductive phase (crystalline) was almost six orders of magnitude lower than that of the insulating phase (amorphous), which is a huge contrast desired for reliable switching applications.

A 4-terminal PCM-based RF switch was designed, fabricated, and performed successfully. The design's schematic and dimensions and their influences on RF performance have been studied. The switch dimensions and pattern arrangements have been calibrated considering the fabrication limitations. Regarding the material choices in the PCM switch, various materials for each segment have been studied, and the optimum growth and patterning procedure have been examined.

Ultimately, a lumped element model of the switch has been developed, and by comparing its results to the measurements, it was shown that the model

predicts the PCM switch behavior accurately. This circuit model facilitates understanding the PCM switch parts transaction and improves its performance.

6.2 Future Research Directions

The work presented in this dissertation can be expanded in the following areas.

6.2.1 Fabrication Process Improvements

The fabrication approach is one of the biggest challenges to achieving steady and reliable RF switches. As a result, enhancing the fabrication procedure is essential for improving PCM-based RF switches.

Modification of the existing PED system

The PED technique is new and has the potential to improve. Although the deposition parameters have been optimized, the PED chamber itself can alter to upgrade the results.

Improving the AlN thin-film growth for high conductivity purposes

The barrier section in the PCM switch is critical as it is the seed layer for the PCM layer and requires to have specific thermal and electrical properties. AlN material is one of the limited materials that satisfy both requirements. The AlN deposition is challenging and can be improved. Its surface smoothness is critical for switch RF performance as it is the layer underneath the GeTe layer. Also, the crystallinity of AlN is important for the GeTe material adhesion and crystal quality. Post-thermal annealing at very high tempera-

tures (above 1000°C) is necessary, which was missing in this work. Overall, enhancing the AlN thin film will improve the PCM switch performance at high frequencies.

6.2.2 GeTe Atomistic Structure Analysis

Some of the atomistic structures of crystalline GeTe have been studied by high-resolution SEM imaging and X-ray diffraction measurements, but still, the crystalline structures in the thin-film GeTe, and how they form. Further investigation into the exact atomistic structure of the crystalline GeTe films and the formation process of the GeTe crystal would be favorable and improve the GeTe switch performance. Also, the impacts of vacancies in the GeTe thin-film structure and how they can affect the electrical properties in the two phases are not very obvious and require more study in this regard.

6.2.3 PCM RF Switches Enhancement

Future applications of GeTe-based RF switches rely on the progress in their characterization and performance enhancement.

Modeling and further study of materials connections

Still, the material choices and their pattern and dimensions have the potential to study and made better. Investigation of various layer/section materials' properties and modeling them more accurately can help to improve the switch design and get better results. To improve the transmission loss of the switch, the contact resistance between the RF metal contact and GeTe film

should be minimized. The ohmic contact between the Cu RF electrode used in this research and the GeTe layer contributes one-third of the R_{ON}.

Designing of alternative structures to minimize the current limitations

The switch design can be altered to overcome some of the limitations imposed by fabrication. For instance, the heater structure and thickness affect the PCM layer profile and smoothness. One solution can be burying the heater in the substrate to achieve a flat canvas for the PCM layer. Also, the barrier layer material properties and dimensions affect the parasitic capacitances between RF and heater paths. Exploring the structural variations of the insulating section between the heater and the RF signal can minimize the parasitic effects of electrical pulses on the RF performance.

References

[1] A Botula, A Joseph, J Slinkman, *et al.*, “A thin-film SOI 180nm CMOS RF switch technology,” in *Silicon Monolithic Integrated Circuits in RF Systems, 2009. SiRF’09. IEEE Topical Meeting on*, IEEE, 2009, pp. 1–4.

[2] D. Kelly, C. Brindle, C. Kemerling, and M. Stuber, “The state-of-the-art of silicon-on-sapphire CMOS RF switches,” in *Compound Semiconductor Integrated Circuit Symposium, 2005. CSIC’05. IEEE*, IEEE, 2005, 4–pp.

[3] M. Parlak and J. F. Buckwalter, “A 2.5-dB insertion loss, DC-60 GHz CMOS SPDT switch in 45-nm SOI,” in *2011 IEEE Compound Semiconductor Integrated Circuit Symposium (CSICS)*, IEEE, 2011, pp. 1–4.

[4] K Miyatbuji and D. Ueda, “A GaAs high power RF single-pole dual throw switch IC for digital-mobile communication system,” *IEEE Journal of Solid-State Circuits*, vol. 30, no. 9, pp. 979–983, 1995.

[5] H. Lo, “Probe reconfigurable phase change material switches,” Ph.D. dissertation, Carnegie Mellon University, 2009.

[6] P. Grant, M. Denhoff, and R. R. Mansour, “A comparison between RF MEMS switches and semiconductor switches,” in *2004 International Conference on MEMS, NANO and Smart Systems (ICMENS’04)*, IEEE, 2004, pp. 515–521.

[7] P. Hindle, “The state of RF/microwave switches,” *microwave journal*, vol. 53, no. 11, pp. 20–36, 2010.

[8] G. Qin, H.-C. Yuan, G. K. Celler, W. Zhou, and Z. Ma, “Flexible microwave PIN diodes and switches employing transferrable single-crystal Si nanomembranes on plastic substrates,” *Journal of Physics D: Applied Physics*, vol. 42, no. 23, p. 234 006, 2009.

[9] D Teeter, R Wohlert, B Cole, *et al.*, “Ka-band GaAs HBT PIN diode switches and phase shifters,” in *1994 IEEE MTT-S International Microwave Symposium Digest (Cat. No. 94CH3389-4)*, IEEE, 1994, 451 –454.

[10] J.-G. Yang and K Yang, “GaN-based PIN diodes for microwave switching IC applications,” *Electronics letters*, vol. 48, no. 11, pp. 650–652, 2012.

[11] C. A. Liechti, “Microwave field-effect transistors-1976,” *IEEE Transactions on Microwave Theory and Techniques*, vol. 24, no. 6, pp. 279–300, 1976.

[12] P. Bacon, D. Fischer, and R. Lourens, “Overview of RF switch technology and applications,” *Microwave Journal*, vol. 57, no. 7, 2014.

[13] C. Hill, C. S. Levy, H. AlShammary, A. Hamza, and J. F. Buckwalter, “RF watt-level low-insertion-loss high-bandwidth SOI CMOS switches,” *IEEE Transactions on Microwave Theory and Techniques*, vol. 66, no. 12, pp. 5724–5736, 2018.

[14] T.-Y. Lee and S. Lee, “Modeling of soi fet for RF switch applications,” in *2010 IEEE Radio Frequency Integrated Circuits Symposium*, IEEE, 2010, pp. 479–482.

[15] I. J. Bahl, *Control components using Si, GaAs, and GaN technologies*. Artech House, 2014.

[16] C. F. Campbell and D. C. Dumka, “Wideband high power gan on sic spdt switch mmics,” in *2010 IEEE MTT-S International Microwave Symposium*, IEEE, 2010, pp. 145–148.

[17] R. V. Garver, “Microwave semiconductor control devices,” *IEEE Transactions on microwave Theory and Techniques*, vol. 27, no. 5, pp. 523–529, 1979.

[18] R. H. Caverly, “Distortion in off-state arsenide MESFET switches,” *IEEE transactions on microwave theory and techniques*, vol. 41, no. 8, pp. 1323–1328, 1993.

[19] R. Stefanini, M. Chatras, P. Blondy, and G. M. Rebeiz, “Miniature RF MEMS metal-contact switches for DC-20 GHz applications,” in *2011 IEEE MTT-S International Microwave Symposium*, IEEE, 2011, pp. 1–4.

[20] C. Goldsmith, T.-H. Lin, B. Powers, W.-R. Wu, and B. Norvell, “Micromechanical membrane switches for microwave applications,” in *Proceedings of 1995 IEEE MTT-S International Microwave Symposium*, IEEE, 1995, pp. 91–94.

[21] A. Lucibello, E. Proietti, F. Giacomozzi, R. Marcelli, G. Bartolucci, and G. De Angelis, “RF MEMS switches fabrication by using su-8 technology,” *Microsystem technologies*, vol. 19, no. 6, pp. 929–936, 2013.

[22] J. J. Yao, “RF MEMS from a device perspective,” *Journal of micromechanics and microengineering*, vol. 10, no. 4, R9, 2000.

[23] G. M. Rebeiz and J. B. Muldavin, “RF MEMS switches and switch circuits,” *IEEE Microwave magazine*, vol. 2, no. 4, pp. 59–71, 2001.

[24] S. Pacheco, C. T. Nguyen, and L. P. Katehi, “Micromechanical electrostatic k-band switches,” in *1998 IEEE MTT-S International Microwave Symposium Digest (Cat. No. 98CH36192)*, IEEE, vol. 3, 1998, pp. 1569–1572.

[25] J.-s. Moon, H.-C. Seo, and D. Le, “High linearity 1-ohm RF switches with phase-change materials,” in *2014 IEEE 14th Topical Meeting on Silicon Monolithic Integrated Circuits in RF Systems*, IEEE, 2014, pp. 7–9.

[26] B. Razavi, “Cmos technology characterization for analog and RF design,” *IEEE journal of solid-state circuits*, vol. 34, no. 3, pp. 268–276, 1999.

[27] T. Singh and R. R. Mansour, "Characterization, optimization, and fabrication of phase change material germanium telluride based miniaturized DC–67 ghz RF switches," *IEEE Transactions on Microwave Theory and Techniques*, vol. 67, no. 8, pp. 3237–3250, 2019.

[28] A. Crunteanu, A. Mennai, C. Guines, D. Passerieux, and P. Blondy, "Out-of-plane and inline RF switches based on Ge2Sb2Te5 phase-change material," in *2014 IEEE MTT-S International Microwave Symposium (IMS2014)*, IEEE, 2014, pp. 1–4.

[29] T. Singh, G. Hummel, M. Vaseem, and A. Shamim, "Recent advancements in reconfigurable mmWave devices based on phase-change and metal insulator transition materials," *IEEE Journal of Microwaves*, 2023.

[30] C Hillman, P. Stupar, and Z Griffith, "VO2 switches for millimeter and submillimeter-wave applications," in *2015 IEEE Compound Semiconductor Integrated Circuit Symposium (CSICS)*, IEEE, 2015, pp. 1–4.

[31] J. Givernaud, C. Champeaux, A. Catherinot, A. Pothier, P. Blondy, and A. Crunteanu, "Tunable band stop filters based on metal-insulator transition in vanadium dioxide thin films," in *2008 IEEE MTT-S International Microwave Symposium Digest*, IEEE, 2008, pp. 1103–1106.

[32] D. Bouyge, A. Crunteanu, J.-C. Orlianges, *et al.*, "Reconfigurable bandpass filter based on split ring resonators and vanadium dioxide (VO 2) microwave switches," in *2009 Asia Pacific Microwave Conference*, IEEE, 2009, pp. 2332–2335.

[33] D. E. Anagnostou, D. Torres, T. S. Teeslink, and N. Sepulveda, "Vanadium dioxide for reconfigurable antennas and microwave devices: Enabling rf reconfigurability through smart materials," *IEEE Antennas and Propagation Magazine*, vol. 62, no. 3, pp. 58–73, 2020.

[34] N. El-Hinnawy, P. Borodulin, M. R. King, *et al.*, "Origin and optimization of RF power handling limitations in inline phase-change switches," *IEEE Transactions on Electron Devices*, vol. 64, no. 9, 3934 –3942, 2017.

[35] G Bruns, P Merkelbach, C Schlockermann, *et al.*, "Nanosecond switching in GeTe phase change memory cells," *Applied physics letters*, vol. 95, no. 4, p. 043 108, 2009.

[36] S Raoux, H.-Y. Cheng, M. Caldwell, and H.-S. Wong, "Crystallization times of Ge–Te phase change materials as a function of composition," *Applied physics letters*, vol. 95, no. 7, p. 071 910, 2009.

[37] N. El-Hinnawy, P. Borodulin, B. Wagner, *et al.*, "A four-terminal, inline, chalcogenide phase-change rf switch using an independent resistive heater for thermal actuation," *IEEE Electron Device Letters*, vol. 34, no. 10, pp. 1313–1315, 2013.

[38] Y. Shim, G. Hummel, and M. Rais-Zadeh, "RF switches using phase change materials," in *Micro Electro Mechanical Systems (MEMS), 2013 IEEE 26th International Conference on*, IEEE, 2013, pp. 237–240.

[39] N. Bathaei, B. Weng, and H. Sigmarsson, "Crystallization of GeTe phase change thin films grown by pulsed electron-beam deposition," *Materials Science in Semiconductor Processing*, vol. 148, p. 106 781, 2022.

[40] T. Singh and R. R. Mansour, "Experimental investigation of performance, reliability, and cycle endurance of nonvolatile DC–67 GHz phase-change RF switches," *IEEE Transactions on Microwave Theory and Techniques*, vol. 69, no. 11, pp. 4697–4710, 2021.

[41] H.-Y. Cheng, S. Raoux, and J. L. Jordan-Sweet, "Crystallization properties of materials along the pseudo-binary line between GeTe and Sb," *Journal of Applied Physics*, vol. 115, no. 9, p. 093 101, 2014.

[42] M. R. King, N. El-Hinnawy, P. Borodulin, *et al.*, "Connecting post-pulsing electrical and microstructural features in GeTe-based inline phase change switches," *Journal of Applied Physics*, vol. 124, no. 19, p. 195 103, 2018.

[43] N. Arefin, M. H. Kane, P. R. Larson, *et al.*, "GaN growth on silicon based substrates using pulsed electron beam deposition (PED) process," *MRS Online Proceedings Library Archive*, vol. 1736, 2015.

[44] B Tatar, E. Sam, K Kutlu, and M Ürgen, “Synthesis and optical properties of CeO_2 nanocrystalline films grown by pulsed electron beam deposition,” *Journal of materials science*, vol. 43, no. 15, p. 5102, 2008.

[45] R. Choudhary, S. Ogale, S. Shinde, *et al.*, “Pulsed-electron-beam deposition of transparent conducting SnO_2 films and study of their properties,” *Applied physics letters*, vol. 84, no. 9, pp. 1483–1485, 2004.

[46] H. Porter, C Mion, A. Cai, X Zhang, and J. Muth, “Growth of ZnO films on c-plane (0 0 0 1) sapphire by pulsed electron deposition (PED),” *Materials Science and Engineering: B*, vol. 119, no. 2, pp. 210–212, 2005.

[47] R. Comes, M. Gu, M. Khokhlov, H. Liu, J. Lu, and S. A. Wolf, “Electron molecular beam epitaxy: Layer-by-layer growth of complex oxides via pulsed electron-beam deposition,” *Journal of Applied Physics*, vol. 113, no. 2, p. 023 303, 2013.

[48] S. Ovshinsky, “Reversible electrical switching phenomena in disordered structures,” *Physical Review Letters*, vol. 21, no. 20, p. 1450, 1968.

[49] N. Yamada, E. Ohno, N. Akahira, K. Nishiuchi, K. Nagata, and M. Takao, “High speed overwritable phase change optical disk material,” *Japanese Journal of Applied Physics*, vol. 26, no. S4, p. 61, 1987.

[50] N. Yamada, E. Ohno, K. Nishiuchi, N. Akahira, and M. Takao, “Rapid-phase transitions of GeTe-Sb_2Te_3 pseudobinary amorphous thin films for an optical disk memory,” *Journal of Applied Physics*, vol. 69, no. 5, pp. 2849–2856, 1991.

[51] E. Chua, L. Shi, R Zhao, *et al.*, “Low resistance, high dynamic range reconfigurable phase change switch for radio frequency applications,” *Applied Physics Letters*, vol. 97, no. 18, p. 183 506, 2010.

[52] S. Bahl and K. Chopra, “Amorphous versus crystalline GeTe films. iii. electrical properties and band structure,” *Journal of Applied Physics*, vol. 41, no. 5, pp. 2196–2212, 1970.

[53] N. Yamada, M. Takao, and M. Takenaga, "Te-ge-sn-au phase change recording film for optical disk," in *Optical Mass Data Storage II*, International Society for Optics and Photonics, vol. 695, 1987, pp. 79–85.

[54] H.-S. P. Wong, S. Raoux, S. Kim, *et al.*, "Phase change memory," *Proceedings of the IEEE*, vol. 98, no. 12, pp. 2201–2227, 2010.

[55] T Ohta, "Phase-change optical memory promotes the dvd optical disk," *Journal of Optoelectronics and Advanced Materials*, vol. 3, no. 3, 609
–626, 2001.

[56] M. Wang and M. Rais-Zadeh, "Directly heated four-terminal phase change switches," in *2014 IEEE MTT-S International Microwave Symposium (IMS2014)*, IEEE, 2014, pp. 1–4.

[57] M. Wang, Y. Shim, and M. Rais-Zadeh, "A low-loss directly heated two-port RF phase change switch," *IEEE Electron Device Letters*, vol. 35, no. 4, pp. 491–493, 2014.

[58] M. R. King, B. P. Wagner, E. B. Jones, *et al.*, "Development of cap-free sputtered GeTe films for inline phase change switch based RF circuits," *Journal of Vacuum Science & Technology B, Nanotechnology and Microelectronics: Materials, Processing, Measurement, and Phenomena*, vol. 32, no. 4, p. 041 204, 2014.

[59] J. E. Boschker and R. Calarco, "Growth of crystalline phase change materials by physical deposition methods," *Advances in Physics: X*, vol. 2, no. 3, pp. 675–694, 2017.

[60] X. Sun, E. Thelander, P. Lorenz, J. W. Gerlach, U. Decker, and B. Rauschenbach, "Nanosecond laser-induced phase transitions in pulsed laser deposition-deposited GeTe films," *Journal of Applied Physics*, vol.
116, no. 13, p. 133 501, 2014.

[61] X. Sun, U. Roß, J. W. Gerlach, A. Lotnyk, and B. Rauschenbach, "Nanoscale bipolar electrical switching of Ge2Sb2Te5 phase-change material thin films," *Advanced Electronic Materials*, vol. 3, no. 12, p. 1 700 283, 2017.

[62] I. Hilmi, A. Lotnyk, J. W. Gerlach, P. Schumacher, and B. Rauschenbach, “Epitaxial formation of cubic and trigonal Ge-Sb-Te thin films with heterogeneous vacancy structures,” *Materials & Design*, vol. 115, pp. 138–146, 2017.

[63] *Ped systems for thin film deposition*. [Online]. Available: `http://neocera.com/product-category/ped-systems/`.

[64] N. Arefin, “Growth of wide bandgap semiconductors using pulsed electron beam deposition (PED) process,” 2015.

[65] M. Rashidian Vaziri, F Hajiesmaeilbaigi, and M. Maleki, “Microscopic description of the thermalization process during pulsed laser deposition of aluminium in the presence of argon background gas,” *Journal of Physics D Applied Physics*, vol. 43, 2010.

[66] M. Ohring, *Materials science of thin films*. Elsevier, 2001.

[67] M Nistor, N. Mandache, and J Perrière, “Pulsed electron beam deposition of oxide thin films,” *Journal of Physics D: Applied Physics*, vol. 41, no. 16, p. 165 205, 2008.

[68] O Guillot-Noël, R Gomez-San Roman, J Perriere, *et al.*, “Growth of apatite films by laser ablation: Reduction of the droplet areal density,” *Journal of applied physics*, vol. 80, no. 3, pp. 1803–1808, 1996.

[69] J. Perrière, C. Boulmer-Leborgne, R. Benzerga, and S. Tricot, “Nanoparticle formation by femtosecond laser ablation,” *Journal of Physics D: Applied Physics*, vol. 40, no. 22, p. 7069, 2007.

[70] M. Strikovski and K. Harshavardhan, “Parameters that control pulsed electron beam ablation of materials and film deposition processes,” *Applied physics letters*, vol. 82, no. 6, pp. 853–855, 2003.

[71] G. Dhanaraj, K. Byrappa, V. Prasad, and M. Dudley, *Springer handbook of crystal growth*. Springer Science & Business Media, 2010.

[72] M. Wang, F. Lin, and M. Rais-Zadeh, “Need a change? Try GeTe: A reconfigurable filter using germanium telluride phase change RF

switches," *IEEE Microwave Magazine*, vol. 17, no. 12, pp. 70–79, 2016.

[73] G Navarro, V Sousa, A Persico, *et al.*, "Material engineering of Ge_xTe $_{100-x}$ compounds to improve phase-change memory performances," *Solid-State Electronics*, vol. 89, pp. 93–100, 2013.

[74] A. Giussani, K. Perumal, M. Hanke, P. Rodenbach, H. Riechert, and R. Calarco, "On the epitaxy of germanium telluride thin films on silicon substrates," *physica status solidi (b)*, vol. 249, no. 10, pp. 1939–1944, 2012.

[75] Y. Saito, K. V. Mitrofanov, K. Makino, *et al.*, "Sputter growth of chalcogenide superlattice films for future phase change memory applications," *ECS Transactions*, vol.
86, no. 3, pp. 49–54, 2018.

[76] H. Jiang, K. Guo, H. Xu, *et al.*, "Preparation and characterization of $GeTe_4$ thin films as a candidate for phase change memory applications," *Journal of Applied Physics*, vol. 109, no. 6, p. 066 104, 2011.

[77] V Bragaglia, B Jenichen, A Giussani, K Perumal, H Riechert, and R Calarco, "Structural change upon annealing of amorphous GeSbTe grown on Si (111)," *Journal of Applied Physics*, vol. 116, no. 5, 05491 3, 2014.

[78] X. Sun, E. Thelander, J. W. Gerlach, U. Decker, and B. Rauschenbach, "Crystallization kinetics of GeTe phase-change thin films grown by pulsed laser deposition," *Journal of Physics D: Applied Physics*, vol. 48, no. 29, p. 295 304, 2015.

[79] N. Bathaei, B. Weng, and H. Sigmarsson, "Growth study of GeTe phase change material using pulsed electron-beam deposition," *Materials Science in Semiconductor Processing*, vol. 96, pp. 73–77, 2019.

[80] P. Scherrer, "Bestimmung der größe und der inneren struktur von kolloidteilchen mittels röntgenstrahlen," *Nachrichten von der Gesellschaft der Wissenschaften zu Göttingen, Mathematisch-Physikalische Klasse*, vol. 1918, pp. 98–100, 1918. [Online]. Available: `http://eudml.org/doc/59018`.

[81] K. Chopra and S. Bahl, “Amorphous versus crystalline GeTe films. i. growth and structural behavior,” *Journal of Applied Physics*, vol. 40, no. 10, pp. 4171–4178, 1969.

[82] P Borodulin, N El-Hinnawy, A. Graninger, *et al.*, “Operation of a latching, low-loss, wideband microwave phase-change switch below 1 k,” *Journal of Low Temperature Physics*, vol. 194, no. 3, pp. 273–284, 2019.

[83] B. B. Yahia, M. Amara, M Gallard, *et al.*, “In situ monitoring of stress change in GeTe thin films during thermal annealing and crystallization,” *Micro and Nano Engineering*, vol. 1, pp. 63–67, 2018.

[84] P. Noé, C. Sabbione, N. Bernier, N. Castellani, F. Fillot, and F. Hippert, “Impact of interfaces on scenario of crystallization of phase change materials,” *Acta Materialia*, vol. 110, pp. 142–148, 2016.

[85] L. Yashina, S. Kobeleva, T. Shatalova, V. Zlomanov, and V. Shtanov, “Xps study of fresh and oxidized GeTe and (Ge, Sn) te surface,” *Solid State Ionics*, vol. 141, pp. 513–522, 2001.

[86] R Berthier, N Bernier, D Cooper, C Sabbione, F Hippert, and P Noé, “In situ observation of the impact of surface oxidation on the crystallization mechanism of GeTe phase-change thin films by scanning transmission electron microscopy,” *Journal of Applied Physics*, vol. 122, no. 11, p. 115 304, 2017.

[87] L. Yashina, R Püttner, V. Neudachina, T. Zyubina, V. Shtanov, and M. Poygin, “X-ray photoelectron studies of clean and oxidized α-GeTe (111) surfaces,” *Journal of Applied Physics*, vol. 103, no. 9, p. 094 909, 2008.

[88] E Gourvest, B Pelissier, C. Vallée, A Roule, S Lhostis, and S Maitrejean, “Impact of oxidation on Ge2Sb2Te5 and GeTe phase-change properties,” *Journal of The Electrochemical Society*, vol. 159, no. 4, H373, 2012.

[89] T. Karabacak, P.-I. Wang, G.-C. Wang, and T.-M. Lu, “Phase transformation of single crystal β-tungsten nanorods at elevated temperatures,” *Thin solid films*, vol. 493, no. 1-2, pp. 293–296, 2005.

[90] S. M. Rossnagel, I. C. Noyan, and C. Cabral Jr, “Phase transformation of thin sputter-deposited tungsten films at room temperature,” *Journal of Vacuum Science & Technology B: Microelectronics and Nanometer Structures Processing, Measurement, and Phenomena*, vol. 20, no. 5, pp. 2047–2051, 2002.

[91] N. Verbrugghe, D. Fasquelle, B. Duponchel, and S. Députier, “Study of tungsten films deposited by DC sputtering dedicated to integrated heaters,” *Journal of Vacuum Science & Technology B, Nanotechnology and Microelectronics: Materials, Processing, Measurement, and Phenomena*, vol. 35, no. 3, p. 031 204, 2017.

[92] G. A. Slack, R. A. Tanzilli, R. Pohl, and J. Vandersande, “The intrinsic thermal conductivity of AlN,” *Journal of Physics and Chemistry of Solids*, vol. 48, no. 7, pp. 641–647, 1987.

[93] V Moraes, H Riedl, R Rachbauer, *et al.*, “Thermal conductivity and mechanical properties of AlN-based thin films,” *Journal of Applied Physics*, vol. 119, no. 22, p. 225 304, 2016.

[94] B. Belkerk, A Soussou, M. Carette, M. Djouadi, and Y Scudeller, “Structural-dependent thermal conductivity of aluminium nitride produced by reactive direct current magnetron sputtering,” *Applied Physics Letters*, vol. 101, no. 15, p. 151 908, 2012.

[95] C Duquenne, M.-P. Besland, P. Tessier, E Gautron, Y Scudeller, and D Averty, “Thermal conductivity of aluminium nitride thin films prepared by reactive magnetron sputtering,” *Journal of Physics D: Applied Physics*, vol. 45, no. 1, p. 015 301, 2011.

[96] R. Yoshizawa, H. Miyake, and K. Hiramatsu, “Effect of thermal annealing on AlN films grown on sputtered AlN templates by metalorganic vapor phase epitaxy,” *Japanese Journal of Applied Physics*, vol. 57, no. 1S, 01AD05, 2017.

[97] S. Xiao, R. Suzuki, H. Miyake, S. Harada, and T. Ujihara, “Improvement mechanism of sputtered AlN films by high-temperature annealing,” *Journal of Crystal Growth*, vol. 502, pp. 41–44, 2018.

[98] M. Wang, “Phase change material based ohmic switches for reconfigurable RF applications,” Ph.D. dissertation, 2017.

[99] J. Siegel, J Solis, and C. N. Afonso, “Slow interfacial reamorphization of ge films melted by ps laser pulses,” *Journal of applied physics*, vol. 84, no. 10, pp. 5531–5537, 1998.

[100] S. J. Park, H. Park, M. H. Jang, *et al.*, “Laser irradiation-induced modification of the amorphous phase in GeTe films: The role of intermediate ge–te bonding in the crystallization mechanism,” *Journal of Materials Chemistry C*, vol. 3, no. 36, pp. 9393–9402, 2015.

[101] T. Singh and R. R. Mansour, “Investigation into self actuation limitation and current carrying capacity of chalcogenide phase change GeTe-based RF switches,” *IEEE Transactions on Electron Devices*, vol. 6-7, no. 12, pp. 5717–5722, 2020.

[102] A. Leon, B. Reig, E. Perret, *et al.*, “RF power-handling performance for direct actuation of germanium telluride switches,” *IEEE Transactions on Microwave Theory and Techniques*, vol. 68, no. 1, pp. 60–73, 2019.

[103] T. Singh and R. R. Mansour, “Chalcogenide GeTe-based non-volatile switched k-band tunable reflective load for reconfigurable RF circuits,” in *2022 IEEE/MTT-S International Microwave Symposium-IMS 2022*, IEEE, 2022, pp. 967–970.

Appendix A

Direct Heating Switch

Direct heating RF switch involves four terminals, two for RF signal and two for heat bias, and each pair is connected through GeTe via. The GeTe via is sandwiched laterally between RF electrodes and vertically between bias electrodes. Figure A.1 (a) and (b) illustrate the schematic top and cross-section view of the direct heating switch, respectively. The idea behind this design is the heater terminals are connected through the GeTe layer (orange arrow in Figure A.1 (b)). The RF terminals are also connected through the GeTe layer but laterally (blue arrow in Figure A.1 (b)). To prevent the heater and RF electrodes from making direct contact with each other, the GeTe layer was deposited in two steps before and after the electrode deposition. Many lithography attempts were conducted to find the optimal direct heating RF switch design parameters. The final fabricated direct heating switch is shown in Figure A.1 (d).

This design was fabricated and tested with an amorphous GeTe layer. As a result, the primary state of the switches was OFF. Figure A.2 shows the schematic of the ON pulse used to change the GeTe phase from amorphous to crystalline. The measured transmission of the fabricated switch in the

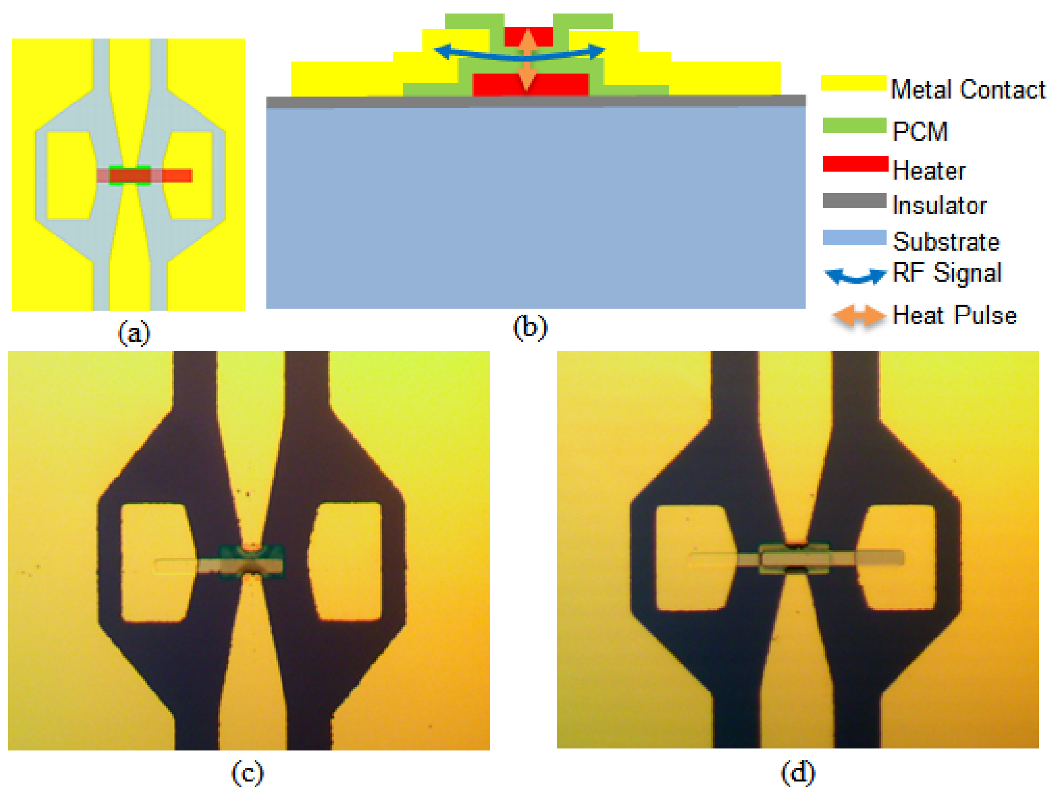

Figure A.1: Direct heating switch design (a) top view, (b) cross-section, and fabricated switch (c) after RF electrodes fab, and (d) finished fab.

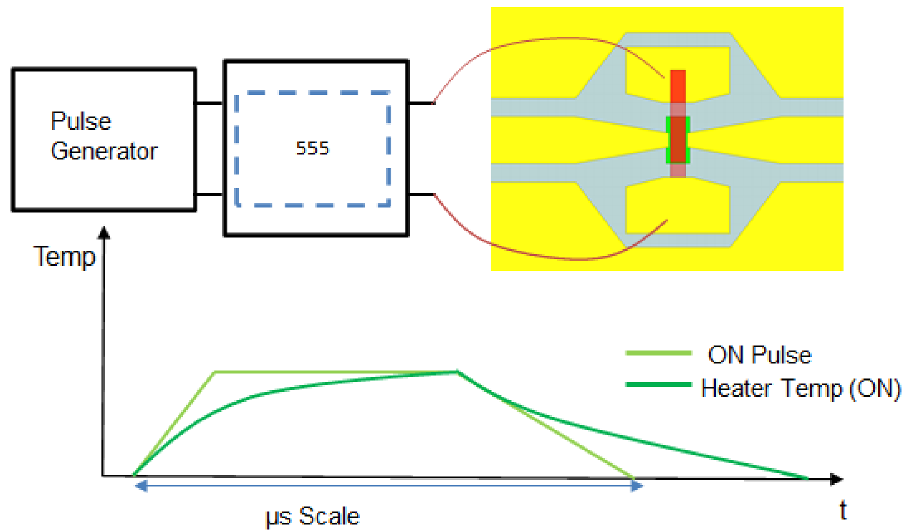

Figure A.2: Direct heating switch actuation circuit.

direct heating structure is shown in Figure A.3. The ON pulse lowered the insertion loss, but the switch was still very high to consider the switch in the ON state. generally, its results were unsatisfactory, and considering all the complications associated with the direct heating structure, it has not been investigated more.

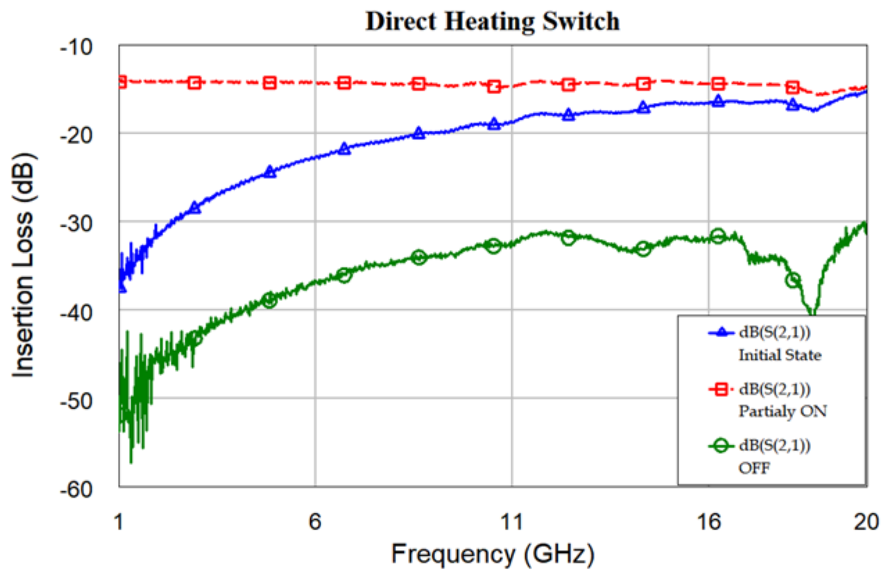

Figure A.3: Direct heating switch RF results.

Appendix B

List of Acronyms and Abbreviations

ACP	Air Coplanar
AlN	Aluminum Nitride
$CMOS$	Complementary Metal Oxide Semiconductor
CPW	Coplanar Waveguide
DUT	Device Under Test
EDX	Energy Dispersive X-ray
$FESEM$	Field Emission Scanning Electron Microscope
FET	Field-effect Transistors
$FWHM$	Full Width at Half Maximum
$GaAs$	Gallium Arsenide
GaN	Gallium Nitride
Ge	Germanium

$GeTe$	Germanium Telluride
GSG	Ground-Signal-Ground
$GST/GeSbTe$	Germanium Antimony Telluride
$HEMT$	High Electron Mobility Transistor
IC	Integrated Circuit
In	Indium
MBE	Molecular Beam Epitaxy
$MEMS$	Microelectromechanical System
$MESFET$	Metal Semiconductor Field Effect Transistor
MIT	Metal-Insulator Transition
$MMIC$	Monolithic Microwave Integrated Circuit
$MMIC$	Monolithic Microwave-Integrated Circuit
$mmWave$	Millimeter Wave
$MOSFET$	Metal Oxide Semiconductor Field Effect Transistor
N_2	Nitrogen
$NiCr$	Nickel Chrome
PCM	Phase Change Material
$PEBS$	Pulsed Electron-Beam Source

PED	Pulse Electron-beam Deposition
$pHEMT$	High Electron Mobility Transistor
PLD	Pulsed Laser Deposition
PR	Photo Resist
PVD	Physical Vapor Deposition
RF	Radio Frequency
RTA	Rapid Thermal Annealer
Sb	Antimony
Se	Selenium
Si	Silicon
SiO_2	Silicon Dioxide
SOI	Silicon on Insulator
$SOLT$	Short-Open-Load-Through
SOS	Silicon on Oxide
$T - Line$	Transmission Line
Te	Telluride
UHV	Ultra-High Vacuum
VNA	Vector Network Analyzers

VO_2	Vanadium Dioxide
XRD	X-ray Diffractometry